GEORGIA INSTITUTE OF TECHNOLOGY   OFFICE OF CONTRACT ADMINISTRATION

PROJECT ADMINISTRATION DATA SHEET

[x] ORIGINAL   [ ] REVISION NO. _____

Project No. __E-20-691__   GTRI/GIT   DATE __5 / 9 / 83__

Project Director: __Dr. S. N. Atluri__   School/Lab __CE__

Sponsor: __Wright Patterson Air Force Base__

Type Agreement: __SFRC F33615-83-K-3205__

Award Period: From __5/1/83__ To __4/30/85__ (Performance) __4/30/85__ (Reports)

Sponsor Amount: This Change   Total to Date

     Estimated: $ __47,134__ $ __47,134__

     Funded: $ __14,668__ $ __14,668__

Cost Sharing Amount: $_____   Cost Sharing No: _____

Title: __Effects of Local Instability on Global Behavior and Instability of Structures__

ADMINISTRATIVE DATA   OCA Contact __Faith G. Costello__

1) Sponsor Technical Contact:

    Dr. Narendra S. Khot

    AFWAL/FIBRA

    Wright-Patterson AFB, OH 45433

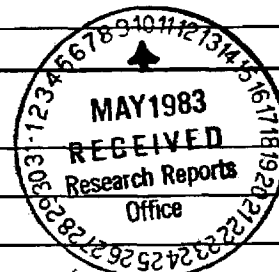   A/C (413) 255-6992

2) Sponsor Admin/Contractual Matters:

    Tom Bryant

    ONR RR

    Georgia Institute of Technology

    206 O'Keefe Building

    Atlanta, GA 30332

Defense Priority Rating: _____   Military Security Classification: __None__

              (or) Company/Industrial Proprietary: _____

RESTRICTIONS

See Attached __Gov't__ Supplemental Information Sheet for Additional Requirements.

Travel: Foreign travel must have prior approval — Contact OCA in each case. Domestic travel requires sponsor

     approval where total will exceed greater of $500 or 125% of approved proposal budget category.

Equipment: Title vests with __GIT__

COMMENTS:

MAY 1983 RECEIVED Research Reports Office

COPIES TO:

Project Director	Procurement/EES Supply Services	GTRI
Research Administrative Network	Research Security Services	Library
Research Property Management	✓Reports Coordinator (OCA)	Project File
Accounting	Research Communications (2)	Other _____

FORM OCA 4:383

GEORGIA INSTITUTE TECHNOLOGY   OFFICE OF CONTRACT ADMINISTRATION

SPONSORED PROJECT TERMINATION/CLOSEOUT SHEET

Date_____6/28/85_____

Project No.___E-20-691____(R-5620-0A0)_____   School/~~XXX~~ CE_____

Includes Subproject No.(s)___N/A_____

Project Director(s)___S. Atluri_____ GTRC ~~XGXX~~

Sponsor_____Wright Patterson AFB, OH_____

Title_____Effects of Local Instability on Global Behavior and Instability of Structures___

Effective Completion Date:___4/30/85_____ (Performance)___6/25/85_____(Reports)

Grant/Contract Closeout Actions Remaining:

- [ ] None

- [X] Final Invoice or Final Fiscal Report

- [X] Closing Documents

- [X] Final Report of Inventions

- [X] Govt. Property Inventory & Related Certificate

- [ ] Classified Material Certificate

- [ ] Other_____

Continues Project No.___N/A_____   Continued by Project No.___N/A_____

COPIES TO:

Project Director
Research Administrative Network
Research Property Management
Accounting
Procurement/GTRI Supply Services
Research Security Services
Reports Coordinator (OCA)
Legal Services

Library
GTRC
Research Communications (2)
Project File
Other____A. Jones; M. Heyser_____

FORM OCA 69.285

E-20-691

REPORT DOCUMENTATION PAGE

1a. REPORT SECURITY CLASSIFICATION		1b. RESTRICTIVE MARKINGS
UNCLASSIFIED		—

2a. SECURITY CLASSIFICATION AUTHORITY	3. DISTRIBUTION/AVAILABILITY OF REPORT
	APPROVED FOR PUBLIC RELEASE
2b. DECLASSIFICATION/DOWNGRADING SCHEDULE	DISTRIBUTION UNLIMITED

4. PERFORMING ORGANIZATION REPORT NUMBER(S)	5. MONITORING ORGANIZATION REPORT NUMBER(S)
GIT-CACM-SNA-14	

6a. NAME OF PERFORMING ORGANIZATION	6b. OFFICE SYMBOL (If applicable)	7a. NAME OF MONITORING ORGANIZATION
Georgia Institute of Technology		

6c. ADDRESS (City, State and ZIP Code)	7b. ADDRESS (City, State and ZIP Code)
Center for the Adv. of Comp. Mechanics School of Civil Engineering Atlanta, GA 30332	Air Force Wright Aeronautical Labs Wright-Patterson AFB, Ohio 45433

8a. NAME OF FUNDING/SPONSORING ORGANIZATION	8b. OFFICE SYMBOL (If applicable)	9. PROCUREMENT INSTRUMENT IDENTIFICATION NUMBER
WPAFB, Ohio		F33615-83-K-3205

8c. ADDRESS (City, State and ZIP Code)	10. SOURCE OF FUNDING NOS.			
	PROGRAM ELEMENT NO.	PROJECT NO.	TASK NO.	WORK UNIT NO.

11. TITLE (Include Security Classification)
LSS-NLAP: A Program for Simplified Nonlinear.

12. PERSONAL AUTHOR(S)
K. Kondoh, K. Tanaka, and S.N. Atluri

13a. TYPE OF REPORT	13b. TIME COVERED	14. DATE OF REPORT (Yr., Mo., Day)	15. PAGE COUNT
Final	FROM 5/1/83 TO 4/30/85	June 1985	171

16. SUPPLEMENTARY NOTATION
Parts of this report were published in two papers – one in Computers & Structures and the other in Int. Jrl. for Num Meth. in Engg.

17. COSATI CODES			18. SUBJECT TERMS (Continue on reverse if necessary and identify by block number)
FIELD	GROUP	SUB. GR.	Large Space Structures, Space Trusses, Space Frames, Post-Buckling Behaviour, Arc-Length Method, Explicit Tangent Stiffness, Local Buckling, Member Buckling, Reduced Order

19. ABSTRACT (Continue on reverse if necessary and identify by block number)

Simplified finite element methodologies for finite deformation, post-buckling analysis of large space trusses and space frames are presented. Arbitrarily large rigid translations and rigid rotations of each member are accounted for. Each 3-D truss member is assumed to withstand an axial force, while each 3-D frame member is assumed to withstand two bending moments, a twisbing moment, and transvers and axial forces at each node. The influence of local (member) buckling on global instability is systematically examined. For both 3-D turss and frame members, explicit tangent stiffness matrices are derived. By explicit, it is meant that no element-wise basis functions are assumed and that no element-wise numerical integrations are involved. These explicit tangent stiffness matrices are very simply evaluated at any point in the load-deformation history of a space truss, or space frame, undergoing large deformations, as well as in the post-buckled region of behaviour of these structures. An arc-length method is implemented to trace the post-buckling behaviour of these large space structures. A large number of examples are included to: (i) bring out

20. DISTRIBUTION/AVAILABILITY OF ABSTRACT	21. ABSTRACT SECURITY CLASSIFICATION
UNCLASSIFIED/UNLIMITED ☒ SAME AS RPT. ☐ DTIC USERS ☐	UNCLASSIFIED

22a. NAME OF RESPONSIBLE INDIVIDUAL	22b. TELEPHONE NUMBER (Include Area Code)	22c. OFFICE SYMBOL
N.S. Khot	513/255-6992	AFWAL/FIBR

DD FORM 1473, 83 APR   EDITION OF 1 JAN 73 IS OBSOLETE.

LSS-NLAP: A PROGRAM FOR SIMPLIFIED NONLINEAR
ANALYSIS OF LARGE SPACE-TRUSSES AND -FRAMES,
USING EXPLICITLY DERIVED TANGENT STIFFNESSES,
AND ACCOUNTING FOR LOCAL BUCKLING

K. Kondoh, K. Tanaka, and S.N. Atluri

Center for the Advancement of Computational Mechanics
School of Civil Engineering
Georgia Institute of Technology, Atlanta, Georgia   30332

June 1985

Prepared for

Flight Dynamics Laboratory
Air Force Wright Aeronautical Laboratories
Air Force Systems Command
Wright-Patterson Air Force Base, Ohio   45433

TABLE OF CONTENTS

LIST OF TABLES

LIST OF ILLUSTRATIONS

CHAPTER I

INTRODUCTION

In the past few years, there has been a renewed interest in the analysis of large frame- and truss-type structures, due to the current dreams of many to deploy very large structures in outerspace. One of the primary topics of current interest is to analyze parts of such structures, that may be subject to large local disturbances, with the ultimate goal of <u>controlling</u> the dynamic deformations through active or passive mechanisms. The research reported herein, however, is limited, as a first step, to considerations of simple, yet highly accurate, methods of nonlinear analyses of space-trusses and space-frames under quasi-static loads.

The phenomena of structural instability are generally classfied as:

(1) bifurcation phenomenon, such as the response of elastic columns and plates subject to compressive loads in the axial and the inplane directions, respectively, or the response of an elastic-plastic bar in tension (also often referred to as the necking phenomenon).

(2) limit phenomenon, such as the response of laterally loaded shallow arches and shells. This may result in a dynamic snap-through or snap-back phenomenon depending on whether load control or displacement control exists in the system. A detailed discussion of the classification of these instability phenomena may be found, for instance, in Refs. [1,2,28].

1

An extensive literature exists concerning computational methods for analyzing structural stability [3-7]. In a majority of these works dealing with elastic stability, the onset of instability is treated as a linear or nonlinear eigenvalue problem.

Large deformation and post-buckling analyses of structures have also been the subjects of extensive research in the past decade [8-10].

In all these studies, an incremental approach, either of the "total Lagrangean type" or of the "updated Lagrangean type", is employed. Also, a number of incremental solution methods, to find the response in the "post-buckling" range, i.e., beyond a bifurcation or a limit point, have been proposed. These include:

(1) the standard load control method

(2) the displacement control method [11,12]

(3) the artificial spring method [13]

(4) the perturbation method [2]

(5) the current-stiffness parameter method [14,15]

(6) the arc-length method [13,16-20]

In calculating the non-linear pre-buckling as well as post-buckling response, an incremental finite element approach, which results in a "tangent stiffness matrix" (which includes all the non-linear geometric as well as mechanical effects) is often employed. In all the literature, including, for instance, Refs. [8-10], the derivation of the "tangent-stiffness matrix" of an element (which may be based, alternatively, on potential energy, complementary energy, or general mixed-hybrid formulations) is, in general, quite a complicated task and involves:

2

(1) Simple polynomial basis functions for displacements and/or stress and moment resultants in each element;

(2) Numerical integration of matrices (dependent on the assumed basis functions and their spatial derivatives) over the domain of the element.

It is now well recognized that the key factors that determine the economic feasibility of the routine use of the above non-linear analysis methods are:

(1) The computational time involved in forming the tangent-stiffness matrix of each element, and of the entire structure, at each increment of external loading;

(2) The degree of refinement of the finite element grid, when elements with simple polynomial basis functions are used;

(3) The techniques for solution of the system stiffness equations especially at or beyond the critical (buckling) points in the load-path.

It can easily be seen that the above "incremental" finite element methods [8-10] (wherein, in each element, a tangent stiffness matrix for each member, and thus for the whole structure, may be routinely evaluated from appropriate variational principles or weak forms, using simple basis functions for the element variables) become prohibitively expensive to treat realistic structures. Examples of such structures of current interest include the very large space-structures and antennae that may be deployed in outer space.

A majority of nonlinear analyses of typical engineering structures, and especially the truss- and frame-type large space-structures, can be vastly simplified if an explicit expression (i.e., without

3

involving assumed basis functions for displacement/stress, and without involving element-wise numerical integrations) for the tangent stiffness matrix of an element (incorporating the effects of initial displacements on the current stiffness) can be derived.

Thus, the primary objective of the work reported herein is to derive explicit expressions for the tangent stiffness matrices of each of the members of either three-dimensional (space) truss- or frame-type structures. Such explicit expressions are derived in both the pre-buckling as well as post-buckling regimes of behavior of each of the members. Further, the derived stiffness matrices are exact even when each member undergoes arbitrarily large rigid motions. Such derivations for planary truss- and frame-type structures were initially given by Kondoh and Atluri [21,22], who also demonstrated that the resultant procedures were not only very inexpensive but also highly accurate in a wide variety of problems involving very large deformations and highly nonlinear pre- and post-buckling responses. The extension of the concepts in [21,22] to three-dimensional cases is a further major step and is presented in the subsequent chapters in this report.

Each member of a space-truss type structure is assumed to undergo an axial stretching deformation and to carry only an axial load. On the other hand, each member of a space-frame type structure is assumed to undergo bending deformations in two mutually independent planes, stretching (which is coupled to bending), as well as torsional deformations, and thus carry two bending moments, an axial load as well as a torsional moment. Explicit expressions for the coefficients of the tangent stiffness matrix of an element (applicable over a wide

4

range of deformations) are derived. Here, "explicit" means that the procedure does not involve assumptions of basis functions for the element nor of numerical integrations over each element.

The derivation of an explicit tangent stiffness matrix for a three-dimensional (space) frame is a rather complicated task. A reason for this is that a general three-dimensional non-linear formulation for a member of a space-frame is not a simple extension of a two-dimensional formulation because the three-dimensional large rotations defy a simple mathematical description. In this context, the concept of "semi-tangential" rotations is introduced to express arbitrary three-dimensional rotations [24,25]. Also, the concept of a "polar-decomposition" of the deformation [26,27] is employed to decompose the arbitrary deformation of the element into rigid rotations and pure stretches.

The present derivation of the explicit expression for the stiffness matrix of an element is based on the assumptions:

(1) Arbitrarily large, rigid translations and rotations of each member/element of a space-structure (both truss- and frame-type) are accounted for.

(2) For a member of a space-frame, the local relative (non-rigid) rotations of a differential segment of a member/element are moderately small, and that only their squares enter into the expression for axial stretch, in a manner analogous to that in the well-known Von Karman theory for plates.

5

(3) The non-linear coupling between the bending and stretching

   motions of the member/element of a space-frame is inherently

   accounted for.

The ranges of validity of these approximations are critically

examined. This simplified procedure of forming the stiffness matrix,

in conjunction with the arc length method [13,16-20], which is

appropriately modified herein to account for an individual member's

buckling, is used to study the post-buckling behavior.

In a structural assembly such as a truss, frame, stiffened plate,

etc., the response may involve both local buckling as well as global

buckling. In present context, local buckling implies the buckling of a

discrete member in the structure under consideration. The local

buckling is often of the bifurcation type. The influence of local

buckling on subsequent load transfer in the structure and on the

overall response of the structure is another subject of prime concern

in this report. However, the literature that deals with the effect of

local instability (or instability of one or a few members of the

structure) on the overall buckling and post-buckling response of the

structure, is rather sparse. Reference [23] presents an interesting

study of such phenomena. However, the study of Ref. [23] pertains to

the effects of interaction of local and global imperfections on the

overall response of the structure. Further, the methodology employed

in Ref. [23] makes it difficult to compute the post-buckling response

of the structure.

Several numerical examples dealing with the non-linear pre- and

post-buckling responses of space-trusses and -frames are presented.

All these examples also serve to effectively bring out the ranges of

6

applicability and the advantages of the presently proposed simplified procedures for forming the tangent stiffness of the members as well ass that of the structure. It is demonstrated that in most of the cases a single element, with the presently derived explicit stiffness matrix, is adequate to model each member. It is also demonstrated that the methodology presented herein is not only very inexpensive but is also highly accurate even for ranges of deformations that are well beyond those likely to be encountered in practice.

The remainder of this report is organized as follows: Chapters II and III give detailed accounts of the present procedures for explicit evaluations of the tangent stiffness matrices of a member of a space-truss and space-frame, respectively, at any point in the non-linear load-deformation path. Chapter IV is devoted to a brief account of the "arc length" method employed to solve the system stiffness equations in the pre- and post-buckled range. Several numerical examples are presented and discussed in Chapter V, to bring out the advantageous features of economy as well as accuracy of the present methodology. Some concluding comments are made in Chapter VI.

CHAPTER II

DERIVATION OF AN EXPLICIT TANGENT STIFFNESS MATRIX
FOR FINITE-DEFORMATION, POST-BUCKLING ANALYSIS OF SPACE TRUSSES

The space truss structures discussed herein are assumed to remain elastic. Also, only a conservative system of concentrated loads at the nodes of the space truss structures is considered.

II.1 Relation Between Stretch and Axial Force in a Truss Member

Consider a typical slender truss member spanning between nodes 1 and 2 as shown in Fig. 1. This member is considered to have a uniform cross section, and its length before deformation is ℓ. The coordinates x_1, x_2, and x_3 are the member's local coordinates; while u_1, u_2, and u_3 denote the displacements at the centroidal axis of a member along the coordinate directions x_1, x_2, and x_3, respectively.

From the polar decomposition theorem, the relation between the total axial stretch and displacements of the member is (see Appendix A):

$$\delta = [(\tilde{u}_1)^2 + (\tilde{u}_2)^2 + (\ell + \tilde{u}_3)^2]^{1/2} - \ell \qquad (2.1)$$

where δ: Total axial stretch

$$\tilde{u}_1 = {}^2u_1 - {}^1u_1$$

8

$$\bar{u}_2 = {}^2u_2 - {}^1u_2$$

$$\bar{u}_3 = {}^2u_3 - {}^1u_3$$

Equation (2.1) holds for both the pre- and post-buckled states of the member.

The incremental relation between the incremental total stretch and the incremental axial force in the member is written as:

$$\Delta N = k \cdot \Delta \delta \qquad (2.2)$$

where ΔN: Incremental axial force in the member

$\Delta \delta$: Incremental total axial stretch in the member

$k = EA/\ell$ in the pre-buckled state   (2.3a)

$= \pi^2 \cdot EI/2\ell^3$ in the post-buckled state (for the
range of deformations considered)   (2.3b)

E : Young's modulus

A : Cross section area of the member

I : Moment of inertia

Equation (2.3a) simply follows from the linear-elastic (isotropic) stress-strain law of the material of the member.[1] On the other hand, Eq. (2.3b) for the post-buckled state of the member is derived in the Appendix B by simplifying and modifying the governing

---

[1]While the material is assumed to be linear elastic in the present, the subsequent derivations of the tangent stiffness matrix remain valid, with straight forward modifications, even when the material stress-strain law is of a Ramberg-Osgood type: $\sigma = E\varepsilon + B\varepsilon^n$.

equations of the problem of the elastica, which is treated as a simply supported beam.

Here, one should note that N is in the direction of the straight line connecting node 1 and node 2 of the member after its deformation (see Fig. 1), and δ is calculated from Eq. (2.1). Hence, Eq. (2.2) holds even when the rigid motion of the member is very large. Also, note that the stiffness-coefficient k is a __constant__ in each of the two states, such as pre-buckled and post-buckled, of each member, of a space-truss.

The condition for the buckling of a member, treated as a simply supported beam, is given by the following well-known equation.

$$N = {}^{cr}N \tag{2.4}$$

where
$$ {}^{cr}N = -\pi^2 EI/\ell^2 , \tag{2.5}$$

the negative sign being used to denote the compressive axial force.

II.2 Tangent Stiffness Matrix of a Member for Arbitrarily Large Deformation

The only force acting on a truss-member is considered to be the axial force. Hence, the strain energy of the member, U, in either the pre- or post-buckled states of the member, is given by:

$$U = \frac{1}{2} \int_0^{\ell} \left(EA \cdot \varepsilon^2 + EI \cdot \kappa^2 \right) dx_3 \tag{2.6}$$

$$= \int_0^{\delta} N \, d\delta$$

where ε: Point-wise axial stretch

    κ: Curvature

    $= 0$ for the pre-buckled state

    $\neq 0$ for the post-buckled state

The incremental form of Eq. (2.6) is represented, using Eq. (2.2), as:

$$\Delta U = N \cdot \Delta \delta + \frac{k}{2} \left(\Delta \delta \right)^2 \tag{2.7}$$

The incremental form of Eq. (2.1) is given by:

$$\Delta \delta = a \cdot \Delta \bar{u}_1 + b \cdot \Delta \bar{u}_2 + c \cdot \Delta \bar{u}_3 \tag{2.8}$$

$$+ \frac{1}{2\ell^*} \left[\left(b^2 + c^2 \right) \cdot \Delta \bar{u}_1^2 + \left(c^2 + a^2 \right) \cdot \Delta \bar{u}_2^2 + \left(a^2 + b^2 \right) \cdot \Delta \bar{u}_3^2 \right]$$

$$- \frac{1}{\ell^*} \left[(a \cdot b) \cdot \Delta \bar{u}_1 \Delta \bar{u}_2 + (b \cdot c) \Delta \bar{u}_2 \Delta \bar{u}_3 + (c \cdot a) \Delta \bar{u}_3 \Delta \bar{u}_1 \right]$$

    + Higher order terms

11

where $\quad \ell^* = \left[(\bar{u}_1)^2 + (\bar{u}_2)^2 + (\ell + \bar{u}_3)^2 \right]^{1/2}$

$\qquad a \quad = \bar{u}_1 / \ell^*$

$\qquad b \quad = \bar{u}_2 / \ell^*$

$\qquad c \quad = (\ell + \bar{u}_3) / \ell^*$

$\Delta\bar{u}_1$, $\Delta\bar{u}_2$, and $\Delta\bar{u}_3$ represent the increments
of $\bar{u}_1$, $\bar{u}_2$, and $\bar{u}_3$, respectively.

Substituting Eq. (2.8) into Eq. (2.7), one finds that:

$$\Delta U = N \left(a \cdot \Delta\bar{u}_1 + b \cdot \Delta\bar{u}_2 + c \cdot \Delta\bar{u}_3 \right) \qquad\qquad (2.9)$$

$$+ \frac{1}{2} \left[(b^2 + c^2) \cdot \frac{N}{\ell^*} + k \cdot a^2 \right] \Delta\bar{u}_1^2$$

$$+ \frac{1}{2} \left[(c^2 + a^2) \cdot \frac{N}{\ell^*} + k \cdot b^2 \right] \Delta\bar{u}_2^2$$

$$+ \frac{1}{2} \left[(a^2 + b^2) \cdot \frac{N}{\ell^*} + k \cdot c^2 \right] \Delta\bar{u}_3^2$$

$$+ \left(k - \frac{N}{\ell^*}\right)\left[(a \cdot b)\Delta \bar{u}_1 \Delta \bar{u}_2 + (b \cdot c)\Delta \bar{u}_2 \Delta \bar{u}_3 + (c \cdot a)\Delta \bar{u}_3 \Delta \bar{u}_1\right]$$

+ High order terms

Furthermore, neglecting terms of higher than the second order, the variation in the incremental strain-energy may be derived from Eq. (2.9) as:

$$\delta(\Delta U) = \delta \Delta \bar{u}_1 (N \cdot a) + \delta \Delta \bar{u}_2 (N \cdot b) + \delta \Delta \bar{u}_3 (N \cdot c) \tag{2.10}$$

$$+ \delta \Delta \bar{u}_1 \left\{ \left[(b^2 + c^2) \cdot \frac{N}{\ell^*} + k \cdot a^2 \right] \Delta \bar{u}_1 + \left(k - \frac{N}{\ell^*} \right) \cdot a \cdot b \cdot \Delta \bar{u}_2 \right.$$

$$\left. + \left(k - \frac{N}{\ell^*} \right) \cdot c \cdot a \cdot \Delta \bar{u}_3 \right\}$$

$$+ \delta \Delta \bar{u}_2 \left\{ \left[(c^2 + a^2) \cdot \frac{N}{\ell^*} + k \cdot b^2 \right] \Delta \bar{u}_2 + \left(k - \frac{N}{\ell^*} \right) \cdot b \cdot c \cdot \Delta \bar{u}_3 \right.$$

$$\left. + \left(k - \frac{N}{\ell^*} \right) \cdot a \cdot b \cdot \Delta \bar{u}_1 \right\}$$

$$+ \delta \Delta \bar{u}_3 \left\{ \left[(a^2 + b^2) \cdot \frac{N}{\ell^*} + k \cdot c^2 \right] \Delta \bar{u}_3 + \left(k - \frac{N}{\ell^*} \right) \cdot c \cdot a \cdot \Delta \bar{u}_1 \right.$$

$$+ \left(k - \frac{N}{\ell*}\right) \cdot b \cdot c \cdot \Delta \bar{u}_2 \Big\}$$

$$\equiv \delta \Delta \underline{d}^{m^t} \cdot \underline{R}^m + \delta \Delta \underline{d}^{m^t} \cdot \underline{K}^m \cdot \Delta \underline{d}^m$$

where
$\underline{d}^m$: Vector of generalized nodal displacements

$\underline{R}^m$: Vector of internal forces

$\underline{K}^m$: Stiffness matrix of the element

$$\Delta d^{m^t} = \lfloor \Delta^1 u_1 ; \Delta^2 u_1 ; \Delta^1 u_2 ; \Delta^2 u_2 ; \Delta^1 u_3 ; \Delta^2 u_3 \rfloor$$

$$R^m = \begin{Bmatrix} (N \cdot a) \cdot \{I\} \\ (N \cdot b) \cdot \{I\} \\ (N \cdot c) \cdot \{I\} \end{Bmatrix}$$

$$K^m = \begin{bmatrix} C_1[E] & C_4[E] & C_6[E] \\ C_4[E] & C_2[E] & C_5[E] \\ C_6[E] & C_5[E] & C_3[E] \end{bmatrix}$$

$$C_1 = (b^2 + c^2) \cdot \frac{N}{\ell*} + k \cdot a^2$$

$$C_2 = (c^2 + a^2) \cdot \frac{N}{\ell*} + k \cdot b^2$$

$$C_3 = (a^2 + b^2) \cdot \frac{N}{\ell*} + k \cdot c^2$$

14

$$C_4 = \left(k - \frac{N}{\ell^*}\right) \cdot a \cdot b$$

$$C_5 = \left(k - \frac{N}{\ell^*}\right) \cdot b \cdot c$$

$$C_6 = \left(k - \frac{N}{\ell^*}\right) \cdot c \cdot a$$

$$\{I\} = \begin{Bmatrix} -1 \\ 1 \end{Bmatrix} \quad , \quad [E] = \begin{bmatrix} 1 & -1 \\ -1 & 1 \end{bmatrix} \tag{2.11}$$

One should note that Eqs. (2.10) and (2.11) are written in the local coordinate system, so that it is necessary to transform the displacement vector from the local coordinate system to the global coordinate system in the usual fashion.

It should be emphasized again that Eqs. (2.10) and (2.11) (and thus the tangent-stiffness matrix and the load vector) are applicable for both the pre- and post-buckled states of the member, and that k has a constant value in each of the two states as given in Eq. (2.3). Consequently, if a member buckles, it is only necessary for the value of k to be changed. In view of this, it is seen that it is very simple to derive the tangent stiffness of the member.

CHAPTER III

DERIVATION OF AN EXPLICIT TANGENT STIFFNESS MATRIX
FOR FINITE-DEFORMATION, POST-BUCKLING ANALYSIS OF SPACE FRAMES

The frame-type structures discussed herein are assumed to remain elastic, and only a conservative system of concentrated loads are assumed to act at the nodes of the frame.

III.1 Three-Dimensional Kinematics of Deformation
of a Member/Element of a Space-Frame

Consider a typical frame member, modeled here as a beam element, that spans between nodes 1 and 2 as shown in Fig. 2. The element is considered to have a uniform cross section and to be of length ℓ before deformation. The coordinates $^j x_i$ are the local coordinates at the node j (j = 1,2) of an undeformed element. Likewise, $^j u_i$ (i = 1,2,3) denote the displacements at the centroidal axis of the element along the coordinate directions x_i, i = 1,2,3, respectively. Also, as shown in Fig. 2, $^j \theta_i$ are the angles of rotation about the axes of x_i. After a deformation of the element, two coordinate systems are introduced to represent the rigid and relative (non-rigid) rotations of the element. One is the coordinate system x_i^* which is locally "tangential" and "normal" to the deformed centroidal axis; another is $\hat{x}_i$ which characterizes the rigid translations and rotations of the member (see Fig. 2).

Considering each rotation as a semi-tangential rotation, we can treat rotations as vectors. Thus, the relation among the total, rigid, and relative rotation vectors is given by:

$$^i\underline{\gamma} = \underline{\beta} + {}^i\underline{\alpha} \qquad (i = 1,2) \qquad\qquad (3.1)$$

where $\quad {}^i\underline{\gamma}$: Total rotation vector at the node i

$\underline{\beta}$: Rigid rotation vector of the element

$^i\underline{\alpha}$: Relative rotation vector at the node i

Using Eq. (3.1), the total rotation vector at the node 2, $^2\underline{\gamma}$, is represented as:

$$^2\underline{\gamma} = \underline{\beta} + {}^1\underline{\alpha} + \underline{\alpha}' \qquad\qquad (3.2)$$

where

$$\underline{\alpha}' = {}^2\underline{\gamma} - {}^1\underline{\gamma} \qquad\qquad (3.3)$$

Therefore, the relative rotation vector at the node 2 can be defined using Eqs. (3.1) and (3.2) as:

$$^2\underline{\alpha} = {}^1\underline{\alpha} + \underline{\alpha}' \qquad\qquad (3.4)$$

On the other hand, the expressions of the rotation vectors may be written, by using their components in any coordinate system, as follows [24,25]. Using the local coordinate system, the total rotation vector at the node i may be written [24,25] as:

$$^i\underline{\gamma} = \tan\frac{^i\theta_j}{2} \cdot \underline{e}_j \qquad \begin{array}{l}(i = 1,2)\\(j = 1,2,3)\end{array} \qquad (3.5)$$

The relative rotation vector at the node i in the coordinate system $\hat{x}_i$ is given by:

$$^i\underline{\alpha} = \tan\frac{^i\hat{\theta}_j}{2} \cdot \hat{\underline{e}}_j \qquad \begin{array}{l}(i = 1,2)\\(j = 1,2,3)\end{array} \qquad (3.6)$$

Substituting Eq. (3.5) into Eq. (3.3), the difference between the rotation vectors at nodes 1 and 2 is given by:

$$\underline{\alpha}' = (\tan\frac{^2\theta_j}{2} - \tan\frac{^1\theta_j}{2}) \cdot \underline{e}_j \qquad (3.7)$$

$$= (\underline{\alpha}' \cdot \hat{\underline{e}}_j) \cdot \hat{\underline{e}}_j$$

$$\equiv \tan\frac{\hat{\theta}_j{}'}{2} \cdot \hat{\underline{e}}_j \qquad (3.8)$$

Also substituting Eqs. (3.6) and (3.8) into Eq. (3.4), the relative rotation at node 2 is represented as:

$$^2\underline{\alpha} \equiv \tan\frac{^2\hat{\theta}_j}{2} \cdot \hat{\underline{e}}_j \qquad (3.9)$$

$$= (\tan\frac{^1\hat{\theta}_j}{2} + \tan\frac{\hat{\theta}_j{}'}{2}) \cdot \hat{\underline{e}}_j \qquad (3.10)$$

18

Furthermore, the action of a rotation R, which transforms a vector $d\underset{\sim}{X}$ to $d\underset{\sim}{X}^R$, is represented by the relation [24,25]:

$$d\underset{\sim}{X}^R = \frac{1}{1 + \underline{R} \cdot \underline{R}} \left[(1 - \underline{R} \cdot \underline{R}) \cdot d\underline{X} + 2(\underline{R} \cdot d\underline{X}) \cdot \underline{R} + 2\underline{R} \times d\underline{X} \right] \qquad (3.11)$$

Substituting the unit vectors $\underset{\sim}{e}_i^*$ and the total rotation vector, $^i\underset{\sim}{\gamma}$ at the node i not Eq. (3.11), one obtains the following equations:

$$^i\underset{\sim}{e}_j^* = {}^i\underline{T}_{jk} \cdot \underset{\sim}{e}_k \qquad (i = 1,2) \qquad (3.12)$$

where

$$^iT_{jk} = \begin{bmatrix} ^iA & ^iB & ^iC \\ ^iD & ^iE & ^iF \\ ^iG & ^iH & ^iI \end{bmatrix} \qquad (3.13)$$

$$^iA = \frac{1}{1 + {}^i\theta^2} \left[1 + \tan\frac{2 {}^i\theta_1}{2} - \tan\frac{2 {}^i\theta_2}{2} - \tan\frac{2 {}^i\theta_3}{2} \right] \qquad (3.14a)$$

$$^iB = \frac{2}{1 + {}^i\theta^2} \left[\tan\frac{{}^i\theta_1}{2} \tan\frac{{}^i\theta_2}{2} + \tan\frac{{}^i\theta_3}{2} \right] \qquad (3.14b)$$

$$^iC = \frac{2}{1 + {}^i\theta^2} \left[\tan\frac{{}^i\theta_3}{2} \tan\frac{{}^i\theta_1}{2} - \tan\frac{{}^1\theta_2}{2} \right] \qquad (3.14c)$$

$$^iD = \frac{2}{1 + {}^i\theta^2} \left[\tan\frac{{}^i\theta_1}{2} \tan\frac{{}^i\theta_2}{2} - \tan\frac{{}^i\theta_3}{2} \right] \qquad (3.14d)$$

19

$$ {}^i E = \frac{1}{1 + {}^i \theta^2} \left[1 - \tan\frac{2{}^i\theta_1}{2} + \tan\frac{2{}^i\theta_2}{2} - \tan\frac{2{}^i\theta_3}{3} \right] \qquad (3.14e) $$

$$ {}^i F = \frac{2}{1 + {}^i \theta^2} \left[\tan\frac{{}^i\theta_2}{2} \tan\frac{{}^i\theta_3}{2} + \tan\frac{{}^i\theta_1}{2} \right] \qquad (3.14f) $$

$$ {}^i G = \frac{2}{1 + {}^i \theta^2} \left[\tan\frac{{}^i\theta_3}{2} \tan\frac{{}^i\theta_1}{2} + \tan\frac{{}^i\theta_2}{2} \right] \qquad (3.14g) $$

$$ {}^i H = \frac{2}{1 + {}^i \theta^2} \left[\tan\frac{{}^i\theta_2}{2} \tan\frac{{}^i\theta_3}{2} - \tan\frac{{}^i\theta_1}{2} \right] \qquad (3.14h) $$

$$ {}^i I = \frac{1}{1 + {}^i \theta^2} \left[1 - \tan\frac{2{}^i\theta_1}{2} - \tan\frac{2{}^i\theta_2}{2} + \tan\frac{2{}^i\theta_3}{3} \right] \qquad (3.14i) $$

$$ {}^i \theta^2 = \tan\frac{2{}^i\theta_1}{2} + \tan\frac{2{}^i\theta_2}{2} + \tan\frac{2{}^i\theta_3}{2} \qquad (3.15) $$

On the other hand, $\hat{\underline{e}}_3$, as a unit vector in the direction of the line joining node 1 to 2 in the deformed configuration, may be represented as:

$$ \hat{\underline{e}}_3 = r \cdot \underline{e}_1 + s \cdot \underline{e}_2 + t \cdot \underline{e}_3 \qquad (3.16) $$

where

20

$$r = \frac{\bar{u}_1}{\ell^*} , \quad s = \frac{\bar{u}_2}{\ell^*} \qquad (3.17a,b)$$

$$t = \frac{\ell + \bar{u}_3}{\ell^*} \qquad (3.18)$$

and
$$\bar{u}_i = {}^2u_i - {}^1u_i \qquad (3.19)$$

Other unit vectors, $\hat{\underline{e}}_1$, $\hat{\underline{e}}_2$, corresponding to the coordinate system, $\hat{x}_i$, may be written, using Eq. (3.11) and the rotation vector, $^1\underline{w}$, at node 1, shown in Fig. 3, as:

$$\hat{\underline{e}}_i = \frac{1}{1 + {}^1\underline{w} \cdot {}^1\underline{w}} [(1 - {}^1\underline{w} \cdot {}^1\underline{w}) \cdot {}^1\underline{e}_i^* + 2({}^1\underline{w} \cdot {}^1\underline{e}_i^*) \cdot {}^1\underline{w} + 2({}^1\underline{w} \times {}^1\underline{e}_i^*)] \qquad (3.20)$$
$$(i = 1,2)$$

where

$$^1\underline{w} = \tan \frac{w}{2} \cdot \frac{{}^1\underline{e}_3^* \times \hat{\underline{e}}_3}{|{}^1\underline{e}_3^* \times \underline{e}_3|} \qquad (3.21)$$

$$w = \cos^{-1}({}^1\underline{e}_3^* \cdot \hat{\underline{e}}_3) \qquad (3.22)$$

$$^1\underline{w} \cdot \hat{\underline{e}}_3 = 0 \qquad (3.23a)$$

$$^1\underline{w} \cdot [({}^1\underline{e}_3^* \times \hat{\underline{e}}_3) \times ({}^1\underline{e}_3^* + \hat{\underline{e}}_3)] = 0 \qquad (3.23b)$$

From Eqs. (3.12) to (3.19) and Eqs. (3.21) to (3.22), the relative rotation vector at node 1 is represented as:

21

$$^1\underline{w} = h\cdot\underline{e}_1 + \ell\cdot\underline{e}_2 + m\cdot\underline{e}_3 \qquad (3.23)$$

where

$$h = \frac{^1H\cdot t - {}^1I\cdot s}{1 + {}^1G\cdot r + {}^1H\cdot s + {}^1I\cdot t} \qquad (3.24a)$$

$$\ell = \frac{^1I\cdot r - {}^1G\cdot t}{1 + {}^1G\cdot r + {}^1H\cdot S + {}^1I\cdot t} \qquad (3.24b)$$

$$m = \frac{^1G\cdot s - {}^1H\cdot r}{1 + {}^1G\cdot r + {}^1H\cdot S + {}^1I\cdot t} \qquad (3.24c)$$

Substituting Eqs. (3.12) to (3.15) and Eqs. (3.23) to (3.24) into Eq. (3.20), the following equations are obtained:

$$\hat{\underline{e}}_1 = o\cdot\underline{e}_1 + p\cdot\underline{e}_2 + q\cdot\underline{e}_3 \qquad (3.25)$$

$$\hat{\underline{e}}_2 = u\cdot\underline{e}_1 + v\cdot\underline{e}_2 + w\cdot\underline{e}_3 \qquad (3.26)$$

where

$$o = [C_1\cdot{}^1A + 2h\cdot C_2 + 2(\ell\cdot{}^1C - m\cdot{}^1B)]/C_3 \qquad (3.27a)$$

$$p = [C_1\cdot{}^1B + 2\ell\cdot C_2 + 2(m\cdot{}^1A - h\cdot{}^1C)]/C_3 \qquad (3.27b)$$

$$q = [C_1\cdot{}^1C + 2m\cdot C_2 + 2(h\cdot{}^1B - \ell\cdot{}^1A)]/C_3 \qquad (3.27c)$$

$$u = [C_1 \cdot {}^1D + 2h \cdot C_4 + 2(\ell \cdot {}^1F - m \cdot {}^1E)]/C_3 \qquad (3.27d)$$

$$v = [C_1 \cdot {}^1E + 2\ell \cdot C_4 + 2(m \cdot {}^1D - h \cdot {}^1F)]/C_3 \qquad (3.27e)$$

$$w = [C_1 \cdot {}^1F + 2m \cdot C_4 + 2(h \cdot {}^1E - \ell \cdot {}^1D)]/C_3 \qquad (3.27f)$$

$$C_1 = 1 - h^2 - \ell^2 - m^2 \qquad (3.28a)$$

$$C_2 = h \cdot {}^1A + \ell \cdot {}^1B + m \cdot {}^1C \qquad (3.28b)$$

$$C_3 = 1 + h^2 + \ell^2 + m^2 \qquad (3.28c)$$

$$C_4 = h \cdot {}^1D + \ell \cdot {}^1E + m \cdot {}^1F \qquad (3.28d)$$

We denote by ${}^1\underset{\sim}{\alpha}$ the relative rotation at node 1. Thus, ${}^1\underset{\sim}{\alpha}$ characterizes the transformation of the coordinate system $\hat{x}_i$ to x_i^* at node 1. From Eq. (3.23), one obtains:

$$ {}^1\underset{\sim}{\alpha} = - {}^1\underset{\sim}{w} = - (h \cdot {}^1\underset{\sim}{e}_1 + \ell \cdot {}^1\underset{\sim}{e}_2 + m \, {}^1\underset{\sim}{e}_3) \qquad (3.29)$$

Also, using Eqs. (3.16), (3.25), and (3.26),

$$ {}^1\underset{\sim}{\alpha} = ({}^1\underset{\sim}{\alpha} \cdot \hat{\underset{\sim}{e}}_1) \cdot \hat{\underset{\sim}{e}}_1 + ({}^1\underset{\sim}{\alpha} \cdot \hat{\underset{\sim}{e}}_2) \cdot \hat{\underset{\sim}{e}}_2 + ({}^1\underset{\sim}{\alpha} \cdot \hat{\underset{\sim}{e}}_3) \cdot \hat{\underset{\sim}{e}}_3 \qquad (3.30)$$

23

Therefore, the components of the relative rotation at node 1, i.e., $^1\underset{\sim}{\alpha}$, are obtained from Eqs. (3.6), (3.16), (3.25), (3.26), and (3.29) to (3.30), as:

$$\tan\frac{^1\hat{\theta}_1}{2} = -\,(h\cdot o + \ell\cdot p + m\cdot q) \tag{3.31a}$$

$$\tan\frac{^1\hat{\theta}_2}{2} = -\,(h\cdot u + \ell\cdot v + m\cdot w) \tag{3.31b}$$

$$\tan\frac{^1\hat{\theta}_3}{2} = -\,(h\cdot r + \ell\cdot s + m\cdot t) \tag{3.31c}$$

Also, the components of the relative rotation at node 2, $^2\underset{\sim}{\alpha}$, are obtained from Eqs. (3.7) to (3.10), (3.16), (3.25), and (3.26), as:

$$\tan\frac{^2\hat{\theta}_1}{2} = \tan\frac{^1\hat{\theta}_1}{2} + \left(\tan\frac{^2\theta_1}{2} - \tan\frac{^1\theta_1}{2}\right)\cdot o + \left(\tan\frac{^2\theta_2}{2} - \tan\frac{^1\theta_2}{2}\right)\cdot p$$

$$+ \left(\tan\frac{^2\theta_3}{2} - \tan\frac{^1\theta_3}{2}\right)\cdot q \tag{3.32a}$$

$$\tan\frac{^2\hat{\theta}_2}{2} = \tan\frac{^1\hat{\theta}_2}{2} + \left(\tan\frac{^2\theta_1}{2} - \tan\frac{^1\theta_1}{2}\right)\cdot u + \left(\tan\frac{^2\theta_2}{2} - \tan\frac{^1\theta_2}{2}\right)\cdot v$$

$$+ \left(\tan\frac{{}^2\theta_3}{2} - \tan\frac{{}^1\theta_3}{2}\right)\cdot w \qquad\qquad (3.32b)$$

$$\tan\frac{{}^2\hat{\theta}_3}{2} = \tan\frac{{}^1\hat{\theta}_3}{2} + \left(\tan\frac{{}^2\theta_1}{2} - \tan\frac{{}^1\theta_1}{2}\right)\cdot r + \left(\tan\frac{{}^2\theta_2}{2} - \tan\frac{{}^1\theta_2}{2}\right)\cdot s$$

$$+ \left(\tan\frac{{}^2\theta_3}{2} - \tan\frac{{}^1\theta_3}{2}\right)\cdot t \qquad\qquad (3.32c)$$

It should be noted that the component ${}^1\hat{\theta}_3$ of the relative rotation at node 1 is zero due to the rotation ${}^1\underset{\sim}{w}$ being as in Eq. (3.21).

Finally, as shown in Chapter II, the relation between the total axial stretch and displacements of the member is:

$$\delta = [\bar{u}_1^2 + \bar{u}_2^2 + (\ell + \bar{u}_3)^2]^{1/2} - \ell \qquad\qquad (3.33)$$

where δ: Total axial stretch

$$\bar{u}_i = {}^2u_i - {}^1u_i \qquad (i = 1,2, \text{ and } 3)$$

III.2 Relations Between the "Stretch and Relative Rotations" and the "Axial Force and Bending Moments" for a Frame Member

In preparation for the task of deriving an explicit expression for the tangent stiffness matrix that is valid for a wide range of

deformations of a frame member, in this section, certain explicit relations are derived between the kinematic variables of stretch and relative rotations, on the one hand the mechanical variables of axial force and bending moments on the other, of an individual frame member (or of a finite element if more than one finite element is contemplated for modeling an individual member). These "generalized" force-displacement relations for an individual member/element are also intended to be valid over a range of deformations that may be considered as "large".

To achieve the above purpose, a beam-column, as shown in Fig. 4, is considered. It should be noted that all of the rotations are semitangential rotations [24,25], and $^1\hat{\theta}_3$ at node 1 is zero. Using the relative rotations, $\hat{\theta}_1$, $\hat{\theta}_2$, and $\hat{\theta}_3$, and the relative rotation vector, $^1\underset{\sim}{\alpha}$ which is given by Eq. (3.6), the relation between unit vectors $\underset{\sim}{e}_i^*$ and $\underset{\sim}{\hat{e}}_i$ is written, using Eq. (3.11), as:

$$\underset{\sim}{e}_i^* = \underset{\sim}{S}_{ij} \cdot \underset{\sim}{\hat{e}}_j \qquad (3.34)$$

where

$$S_{ij} = \begin{bmatrix} S_{11} & S_{12} & S_{13} \\ S_{21} & S_{22} & S_{23} \\ S_{31} & S_{32} & S_{33} \end{bmatrix} \qquad (3.35)$$

$$S_{11} = \frac{1}{1 + \hat{\theta}^2}[1 + \tan\frac{^2\hat{\theta}_1}{2} - \tan\frac{^2\hat{\theta}_2}{2} - \tan\frac{^2\hat{\theta}_3}{2}] \qquad (3.36a)$$

26

$$S_{12} = \frac{2}{1 + \hat{\theta}^2}[\tan\frac{\hat{\theta}_1}{2}\cdot\tan\frac{\hat{\theta}_2}{2} + \tan\frac{\hat{\theta}_3}{2}] \qquad (3.36b)$$

$$S_{13} = \frac{2}{1 + \hat{\theta}^2}[\tan\frac{\hat{\theta}_3}{2}\cdot\tan\frac{\hat{\theta}_1}{2} - \tan\frac{\hat{\theta}_2}{2}] \qquad (3.36c)$$

$$S_{21} = \frac{2}{1 + \hat{\theta}^2}[\tan\frac{\hat{\theta}_1}{2}\cdot\tan\frac{\hat{\theta}_2}{2} - \tan\frac{\hat{\theta}_3}{2}] \qquad (3.36d)$$

$$S_{22} = \frac{1}{1 + \hat{\theta}^2}[1 - \tan^2\frac{\hat{\theta}_1}{2} + \tan^2\frac{\hat{\theta}_2}{2} - \tan^2\frac{\hat{\theta}_3}{2}] \qquad (3.36e)$$

$$S_{23} = \frac{2}{1 + \hat{\theta}^2}[\tan\frac{\hat{\theta}_2}{2}\cdot\tan\frac{\hat{\theta}_3}{2} + \tan\frac{\hat{\theta}_1}{2}] \qquad (3.36f)$$

$$S_{31} = \frac{2}{1 + \hat{\theta}^2}[\tan\frac{\hat{\theta}_3}{2}\cdot\tan\frac{\hat{\theta}_1}{2} + \tan\frac{\hat{\theta}_2}{2}] \qquad (3.36g)$$

$$S_{32} = \frac{2}{1 + \hat{\theta}^2}[\tan\frac{\hat{\theta}_2}{2}\cdot\tan\frac{\hat{\theta}_3}{2} - \tan\frac{\hat{\theta}_1}{2}] \qquad (3.36h)$$

$$S_{33} = \frac{1}{1 + \hat{\theta}^2}[1 - \tan^2\frac{\hat{\theta}_1}{2} - \tan^2\frac{\hat{\theta}_2}{2} + \tan^2\frac{\hat{\theta}_3}{2}] \qquad (3.36i)$$

$$\hat{\theta}^2 = \tan\frac{2\hat{\theta}_1}{2} + \tan\frac{2\hat{\theta}_2}{2} + \tan\frac{2\hat{\theta}_3}{2}] \qquad (3.37)$$

The curvatures along a centroidal axis of a deformed member are given by:

$$K_1^* = \frac{d\underline{e}_1^*}{dx_3^*} \cdot \underline{e}_3^* \qquad (3.38a)$$

$$K_2^* = \frac{d\underline{e}_2^*}{dx_3^*} \cdot \underline{e}_3^* \qquad (3.38b)$$

$$K_{12}^* = \frac{d\underline{e}_1^*}{dx_3^*} \cdot \underline{e}_2^* \quad \text{or} \quad - \frac{d\underline{e}_2^*}{dx_3^*} \cdot \underline{e}_1^* \qquad (3.38c)$$

Substituting Eqs. (3.34) and (3.35) into Eq. (3.38), the following equations are obtained:

$$K_1^* = \frac{dS_{11}}{dx_3^*} \cdot S_{31} + \frac{dS_{12}}{dx_3^*} \cdot S_{32} + \frac{dS_{13}}{dx_3^*} \cdot S_{33} \qquad (3.39a)$$

$$K_2^* = \frac{dS_{21}}{dx_3^*} \cdot S_{31} + \frac{dS_{22}}{dx_3^*} \cdot S_{32} + \frac{dS_{23}}{dx_3^*} \cdot S_{33} \qquad (3.39b)$$

28

$$K^*_{12} = \frac{dS_{11}}{dx^*_3} \cdot S_{21} + \frac{dS_{12}}{dx^*_3} \cdot S_{22} + \frac{dS_{13}}{dx^*_3} \cdot S_{23} \qquad (3.39c)$$

Also, the moments along a centroidal axis of a deformed member are given by:

$$M^*_1 = EI_1 \cdot K^*_1 \qquad (3.40a)$$

$$M^*_2 = EI_2 \cdot K^*_2 \qquad (3.40b)$$

$$M^*_{12} = GJ \cdot K^*_{12} \qquad (3.40c)$$

where EI_1 : Bending stiffness about $\hat{x}_2$ axis

EI_2 : Bending stiffness about $\hat{x}_1$ axis

GJ : Torsional stiffness

As shown in Fig. 5, the moments $\hat{M}_1$, $\hat{M}_2$, and $\hat{M}_3$ are represented, in terms of M^*, M^*, M^* , and S_{ij}, as:

$$\hat{M}_1 = - S_{12} \cdot M^*_2 + S_{22} \cdot M^*_1 - S_{32} \cdot M^*_{12} \qquad (3.41a)$$

29

$$\hat{M}_2 = S_{11} \cdot M_2^* - S_{21} \cdot M_1^* + S_{31} \cdot M_{12}^* \tag{3.41b}$$

$$\hat{M}_3 = S_{13} \cdot M_2^* - S_{23} \cdot M_1^* + S_{33} \cdot M_{12}^* \tag{3.41c}$$

The equation of equilibrium in the two transverse directions of the beam may be witten [29,30,36] as:

$$-\frac{d\hat{M}_1}{dx_3^*} + \hat{Q}_1 \cdot (\underline{e}_3^* \cdot \hat{\underline{e}}_3) - \hat{N} \cdot (\underline{e}_3^* \cdot \hat{\underline{e}}_1) = 0 \tag{3.42a}$$

$$-\frac{d\hat{M}_2}{dx_3^*} + \hat{Q}_2 \cdot (\underline{e}_3^* \cdot \hat{\underline{e}}_3) - \hat{N} \cdot (\underline{e}_3^* \cdot \hat{\underline{e}}_2) = 0 \tag{3.42b}$$

Also

$$-\frac{d\hat{M}_3}{dx_3^*} = 0 \tag{3.42c}$$

where

$$\hat{Q}_1 = -\frac{1}{\ell + \delta} \left({}^1\hat{M}_1 - {}^2\hat{M}_1 \right) \tag{3.43a}$$

$$\hat{Q}_2 = -\frac{1}{\ell + \delta} \left({}^1\hat{M}_2 - {}^2\hat{M}_2 \right) \tag{3.43b}$$

Substituting Eqs. (3.34) to (3.36) and (3.39) to (3.41) into Eq. (3.42), the following equilibrium equations are obtained:

30

$$EI_2 \frac{d}{dx_3^*} [S_{12}(\frac{dS_{21}}{dx_3^*} \cdot S_{31} + \frac{dS_{22}}{dx_3^*} \cdot S_{32} + \frac{dS_{23}}{dx_3^*} \cdot S_{33})]$$

$$- EI_1 \frac{d}{dx_3^*} [S_{22}(\frac{dS_{11}}{dx_3^*} \cdot S_{31} + \frac{dS_{12}}{dx_3^*} \cdot S_{32} + \frac{dS_{13}}{dx_3^*} \cdot S_{33})]$$

$$+ GJ \frac{d}{dx_3^*} [S_{32}(\frac{dS_{11}}{dx_3^*} \cdot S_{21} + \frac{dS_{12}}{dx_3^*} \cdot S_{22} + \frac{dS_{13}}{dx_3^*} \cdot S_{23})]$$

$$+ \hat{Q}_1 \cdot S_{33} - \hat{N} \cdot S_{31} = 0 \qquad\qquad (3.44a)$$

$$- EI_2 \cdot \frac{d}{dx_3^*} [S_{11}(\frac{dS_{21}}{dx_3^*} \cdot S_{31} + \frac{dS_{22}}{dx_3^*} \cdot S_{32} + \frac{dS_{23}}{dx_3^*} \cdot S_{33})]$$

$$+ EI_1 \cdot \frac{d}{dx_3^*} [S_{21}(\frac{dS_{11}}{dx_3^*} \cdot S_{31} + \frac{dS_{12}}{dx_3^*} \cdot S_{32} + \frac{dS_{13}}{dx_3^*} \cdot S_{33})]$$

$$- GJ \cdot \frac{d}{dx_3^*} [S_{31}(\frac{dS_{11}}{dx_3^*} \cdot S_{21} + \frac{dS_{12}}{dx_3^*} \cdot S_{22} + \frac{dS_{13}}{dx_3^*} \cdot S_{23})]$$

$$+ \hat{Q}_2 \cdot S_{33} - \hat{N} \cdot S_{32} = 0 \qquad\qquad (3.44b)$$

31

and
$$- EI_2 \cdot \frac{d}{dx_3^*} \left[S_{13} \left(\frac{dS_{21}}{dx_3^*} \cdot S_{31} + \frac{dS_{22}}{dx_3^*} \cdot S_{32} + \frac{dS_{23}}{dx_3^*} \cdot S_{33} \right) \right]$$

$$+ EI_1 \cdot \frac{d}{dx_3^*} \left[S_{23} \left(\frac{dS_{11}}{dx_3^*} \cdot S_{31} + \frac{dS_{12}}{dx_3^*} \cdot S_{32} + \frac{dS_{13}}{dx_3^*} \cdot S_{33} \right) \right]$$

$$- GJ \cdot \frac{d}{dx_3^*} \left[S_{33} \left(\frac{dS_{11}}{dx_3^*} \cdot S_{21} + \frac{dS_{12}}{dx_3^*} \cdot S_{22} + \frac{dS_{13}}{dx_3^*} \cdot S_{23} \right) \right]$$

$$= 0 \qquad\qquad\qquad (3.44c)$$

On the other hand, the expression for the total axial stretch, δ, of the beam may be written [29,30] as:

$$\delta = \int_0^\ell \left\{ 1 + \frac{1}{EA} \cdot \left[\hat{N} \cdot (\underline{e}_3^* \cdot \hat{\underline{e}}_3) + \hat{Q}_1 \cdot (\underline{e}_3^* \cdot \hat{\underline{e}}_1) \right.\right.$$

$$\left.\left. + \hat{Q}_2 \cdot (\underline{e}_3^* \cdot \hat{\underline{e}}_2) \right] \right\} \cdot (\underline{e}_3^* \cdot \hat{\underline{e}}_3) \cdot dx_3^* - \ell \qquad\qquad (3.45)$$

where   A: Cross-sectional area of the member

            E: Young's modulus

Using Eq. (3.34), it is seen that:

32

$$\delta = \int_0^{\ell} \{1 + \frac{1}{EA} \cdot [\hat{N} \cdot s_{33} + \hat{Q}_1 \cdot s_{31} + \hat{Q}_2 \cdot s_{32}]\} \cdot s_{33} \cdot dx_3^* - \ell \qquad (3.46)$$

For the type of problems contemplated, we assume that the deformation of the frame as a whole is such that the relative rotations, $\hat{\theta}_1$, $\hat{\theta}_2$, and $\hat{\theta}_3$ (non-rigid rotations) in each individual member/its elements of the frame may be considered as being small. Under this assumption, Eqs. (3.43), (3.44), and (3.46) may be approximated as follows:

$$EI_1 \frac{d^2\hat{\theta}_2}{dx_3^{*2}} - \frac{{}^1\hat{M}_1 - {}^2\hat{M}_1}{\ell} - \hat{N} \cdot \hat{\theta}_2 = 0 \qquad (3.47a)$$

$$- EI_2 \frac{d^2\hat{\theta}_1}{dx_3^{*2}} - \frac{{}^1\hat{M}_2 - {}^2\hat{M}_2}{\ell} + \hat{N} \cdot \hat{\theta}_1 = 0 \qquad (3.47b)$$

$$- GJ \frac{d^2\hat{\theta}_3}{dx_3^{*2}} = 0 \qquad (3.47c)$$

Also, the boundary conditions are given by:

33

$$- EI_1 \left.\frac{d\hat{\theta}_2}{dx_3^*}\right|_{x_3^*=0} = {}^1\hat{M}_1 \quad , \quad - EI_1 \left.\frac{d\hat{\theta}_2}{dx_3^*}\right|_{x_3^*=\ell} = {}^2\hat{M}_1 \qquad (3.48a,b)$$

$$EI_2 \left.\frac{d\hat{\theta}_1}{dx_3^*}\right|_{x_3^*=0} = {}^1\hat{M}_2 \quad , \qquad EI_2 \left.\frac{d\hat{\theta}_1}{dx_3^*}\right|_{x_3^*=\ell} = {}^2\hat{M}_2 \qquad (3.48c,d)$$

$$\hat{\theta}_3 \Big|_{x_3^*=0} = 0 \quad , \quad GJ \left.\frac{d\hat{\theta}_3}{dx_3^*}\right|_{x_3^*=\ell} = {}^2\hat{M}_3 \qquad (3.48e,f)$$

The total axial stretch becomes:

$$\delta = -\frac{1}{2}\int_0^\ell (\hat{\theta}_1^2 + \hat{\theta}_2^2) dx_3^* + \frac{\ell\hat{N}}{EA} \qquad (3.49)$$

Thus, the non-linear terms, $\hat{\theta}_1^2$ and $\hat{\theta}_2^2$, are retained in the axial stretch relation as, for instance, in the Von Karman plate theory. Eqs. (3.47) to (3.49) form the basis of the present derivation of the relations between the generalized displacements and forces in the element.

The non-dimensional axial forces and bending moments, denoted as n_1, n_2, m_1, and m_2 may be defined, respectively, through the relations:

34

$$n_1 = \frac{\hat{N}\ell^2}{EI_1} \;,\quad m_1 = \frac{\hat{M}_1 \ell}{EI_1} \tag{3.50a,b}$$

$$n_2 = \frac{\hat{N}\ell^2}{EI_2} \;,\quad m_2 = \frac{\hat{M}_2 \ell}{EI_2} \tag{3.50c,d}$$

The solutions of Eqs. (3.47a) and (3.48a,b) are given by:

(1) for $n_1 < 0$

$$\hat{\theta}_2 = {}^1m_1 \cdot \left[\frac{1}{d^2} - \frac{1}{d}\sin\frac{d \cdot x_3^*}{\ell} - \frac{1}{d}\cdot\cot d \cdot \cos\frac{d \cdot x_3^*}{\ell}\right] \tag{3.51}$$

$$+ {}^2m_1 \cdot \left[-\frac{1}{d^2} + \frac{1}{d}\cdot\csc d \cdot \cos\frac{d \cdot x_3^*}{\ell}\right]$$

where
$$d = \sqrt{-n_1} \tag{3.52}$$

(2) for $n_1 > 0$

$$\hat{\theta}_2 = {}^1m_1 \cdot \left[-\frac{1}{e^2} - \frac{1}{e}\sinh\frac{e \cdot x_3^*}{\ell} + \frac{1}{e}\cdot\coth e \cdot \cosh\frac{e \cdot x_3^*}{\ell}\right] \tag{3.53}$$

35

$$+ {}^2m_1 \cdot \left[\frac{1}{e^2} - \frac{1}{e} \cdot \text{cosech } e \cdot \cosh \frac{e \cdot x_3^*}{\ell}\right]$$

where
$$e = \sqrt{n_1} \qquad\qquad (3.54)$$

The solutions of Eqs. (3.47b) and (3.48c,d) are given by:

(3)   for $n_2 < 0$

$$\hat{\theta}_1 = - {}^1m_2 \cdot \left\{\frac{1}{f^2} - \frac{1}{f} \sin \frac{f \cdot x_3^*}{\ell} - \frac{1}{f} \cdot \cot f \cdot \cos \frac{f \cdot x_3^*}{\ell}\right\} \qquad (3.55)$$

$$- {}^2m_2 \cdot \left\{-\frac{1}{f^2} + \frac{1}{f} \cdot \text{cosec } f \cdot \cos \frac{f \cdot x_3^*}{\ell}\right\}$$

where
$$f = \sqrt{-n_2} \qquad\qquad (3.56)$$

(4)   for $n_2 > 0$

$$\hat{\theta}_1 = - {}^1m_2 \cdot \left\{-\frac{1}{g^2} - \frac{1}{g} \sinh \frac{g \cdot x_3^*}{\ell} + \frac{1}{g} \cdot \coth g \cdot \cos \frac{g \cdot x_3^*}{\ell}\right\} \qquad (3.57)$$

36

$$- {}^2m_2 \cdot \left\{ \frac{1}{g^2} - \frac{1}{g} \cdot \text{cosech } g \cdot \cosh \frac{g \cdot x_3^*}{\ell} \right\}$$

where
$$g = \sqrt{n_2} \qquad\qquad (3.58)$$

Equation (3.51) through Eq. (3.58) lead to the following relations between the relative rotations, ${}^1\hat{\theta}_1$, ${}^2\hat{\theta}_1$, ${}^1\hat{\theta}_2$, and ${}^2\hat{\theta}_2$, at the ends of the member and the corresponding bending moments, ${}^1m_1$, ${}^2m_1$, ${}^1m_2$, and ${}^2m_2$:

(1) for $n_1 < 0$

$$ {}^1\hat{\theta}_2 = {}^1m_1 \cdot \left[\frac{1}{d^2} - \frac{\cot d}{d} \right] + {}^2m_1 \cdot \left[- \frac{1}{d^2} + \frac{\csc d}{d} \right] \qquad (3.59a)$$

$$ {}^2\hat{\theta}_2 = {}^1m_1 \cdot \left[\frac{1}{d^2} - \frac{\csc d}{d} \right] + {}^2m_1 \cdot \left[- \frac{1}{d^2} + \frac{\cot d}{d} \right] \qquad (3.59b)$$

(2) for $n_1 > 0$

$$ {}^1\hat{\theta}_2 = {}^1m_1 \cdot \left[- \frac{1}{e^2} + \frac{\coth e}{e} \right] + {}^2m_1 \cdot \left[\frac{1}{e^2} - \frac{\text{cosech } e}{e} \right] \qquad (3.60a)$$

$$ {}^2\hat{\theta}_2 = {}^1m_1 \cdot \left[- \frac{1}{e^2} + \frac{\text{cosech } e}{e} \right] + {}^2m_1 \cdot \left[\frac{1}{e^2} - \frac{\coth e}{e} \right] \qquad (3.60b)$$

(3) for $n_2 < 0$

$$^1\hat{\theta}_1 = -\,^1m_2 \cdot [\frac{1}{f^2} - \frac{\cot f}{f}] - \,^2m_2 \cdot [-\frac{1}{f^2} + \frac{\cosec f}{f}] \qquad (3.61a)$$

$$^2\hat{\theta}_1 = -\,^1m_2 \cdot [\frac{1}{f^2} - \frac{\cosec f}{f}] - \,^2m_2 \cdot [-\frac{1}{f^2} + \frac{\cot f}{f}] \qquad (3.61b)$$

(4) for $n_2 > 0$

$$^1\hat{\theta}_1 = -\,^1m_2 \cdot [-\frac{1}{g^2} + \frac{\coth g}{g}] - \,^2m_2 \cdot [\frac{1}{g^2} - \frac{\cosech g}{g}] \qquad (3.62a)$$

$$^2\hat{\theta}_1 = -\,^1m_2 \cdot [-\frac{1}{g^2} + \frac{\cosech g}{g}] - \,^2m_2 \cdot [\frac{1}{g^2} - \frac{\coth g}{g}] \qquad (3.62b)$$

Also, using Eqs. (3.49) and Eq. (3.51) through (3.58), the following expressions concerning the total axial stretch, δ, are obtained as:

(1) for the case in which $n_i < 0$ (i = 1,2)

$$\frac{\delta}{\ell} = \sum_{i=1}^{2} \{[\frac{1}{2(-n_i)^2} - \frac{\cosec^2\sqrt{-n_i}}{4(-n_i)} - \frac{\cot\sqrt{-n_i}}{4(-n_i)\sqrt{-n_i}}](^1m_i^2 + \,^2m_i^2) \qquad (3.63a)$$

38

$$+ \left[- \frac{1}{(-n_i)^2} + \frac{\cot\sqrt{-n_i} \cdot \mathrm{cosec}\sqrt{-n_i}}{2(-n_i)} + \frac{\mathrm{cosec}\sqrt{-n_i}}{2(-n_i)\sqrt{-n_i}} \right]{}^1m_i\,{}^2m_i \Big\}$$

$$+ \frac{\hat{N}}{EA}$$

(2) for the case in which $n_i > 0$ $(i = 1,2)$

$$\frac{\delta}{\ell} = \sum_{i=1}^{2} \left\{ \left[\frac{1}{2n_i^2} - \frac{\mathrm{cosech}^2\sqrt{n_i}}{4n_i} - \frac{\coth\sqrt{n_i}}{4n_i\sqrt{n_i}} \right]\left({}^1m_i^2 + {}^2m_i^2\right) \right.$$ (3.63b)

$$+ \left[- \frac{1}{n_i^2} + \frac{\coth\sqrt{n_i} \cdot \mathrm{cosech}\sqrt{n_i}}{2n_i} + \frac{\mathrm{cosech}\sqrt{n_i}}{2n_i\sqrt{n_i}} \right]{}^1m_i\,{}^2m_i \Big\}$$

$$+ \frac{\hat{N}}{EA}$$

The set of Eqs. (3.59) to (3.63) may be written in a more convenient form by decomposing the kinematic and mechanical variables of the beam into "symmetric" and "antisymmetric" parts, as:

$$^a\hat{\theta}_i = \tfrac{1}{2}\left({}^1\hat{\theta}_i + {}^2\hat{\theta}_i\right), \quad {}^s\hat{\theta}_i = \tfrac{1}{2}\left({}^1\hat{\theta}_i - {}^2\hat{\theta}_i\right) \qquad \text{(3.64a,b)}$$

also $\quad {}^am_i = {}^1m_i - {}^2m_i, \quad {}^sm_i = {}^1m_i + {}^2m_i \quad (i = 1,2) \qquad \text{(3.65a,b)}$

where the subscripts "a" and "s" refer to "antisymmetric" and "symmetric" parts, respectively.

39

Therefore, in terms of the variables, $^a\hat\theta_i$, $^s\hat\theta_i$, $^a m_i$, and $^s m_i$, Eqs. (3.59) to (3.62) may be written as:

$$^a\hat\theta_1 = {}^a h_2 \cdot {}^a m_2 \, , \qquad ^s\hat\theta_1 = {}^s h_2 \cdot {}^s m_2 \qquad\qquad (3.66a,b)$$

$$^a\hat\theta_2 = {}^a h_1 \cdot {}^a m_1 \, , \qquad ^s\hat\theta_2 = {}^s h_1 \cdot {}^s m_1 \qquad\qquad (3.67a,b)$$

wherein

(1) for $n_1 < 0$

$$^a h_1 = \frac{1}{(-n_1)} - \frac{1}{2\sqrt{-n_1}} \cdot \cot\frac{\sqrt{-n_1}}{2} \qquad\qquad (3.68a)$$

$$^s h_1 = \frac{1}{2\sqrt{-n_1}} \cdot \tan\frac{\sqrt{-n_1}}{2} \qquad\qquad (3.68b)$$

(2) for $n_1 > 0$

$$^a h_1 = -\frac{1}{n_1} + \frac{1}{2\sqrt{n_1}} \cdot \coth\frac{\sqrt{n_1}}{2} \qquad\qquad (3.69a)$$

$$^s h_1 = \frac{1}{2\sqrt{n_1}} \cdot \tanh\frac{\sqrt{n_1}}{2} \qquad\qquad (3.69b)$$

(3) for $n_2 < 0$

$$^a h_2 = -\frac{1}{(-n_2)} + \frac{1}{2\sqrt{-n_2}} \cot\frac{\sqrt{-n_2}}{2} \qquad\qquad (3.70a)$$

40

$$s_{n_2} = -\frac{1}{2\sqrt{-n_2}}\tan\frac{\sqrt{-n_2}}{2} \qquad (3.70b)$$

(4) for $n_2 > 0$

$$a_{n_2} = \frac{1}{n_2} - \frac{1}{2\sqrt{n_2}}\coth\frac{\sqrt{n_2}}{2} \qquad (3.71a)$$

$$s_{n_2} = -\frac{1}{2\sqrt{n_2}}\tanh\frac{\sqrt{n_2}}{2} \qquad (3.71b)$$

Also, in terms of the new variables, Eqs. (3.63a,b) may be rewritten in a unified form as follows:

$$\frac{\delta}{\ell} = \sum_{i=1}^{2}\left[\frac{a_{m_i}^2}{2}\frac{d^a h_i}{dn_i} + \frac{s_{m_i}^2}{2}\frac{d^s h_i}{dn_i}\right] + \frac{\hat{N}}{EA} \qquad (3.72a)$$

$$\equiv \frac{a_{\hat{\theta}_2}^2}{2^a h_1^2}\cdot\frac{d^a h_1}{dn_1} + \frac{s_{\hat{\theta}_2}^2}{2^s h_1^2}\cdot\frac{d^s h_1}{dn_1} + \frac{a_{\hat{\theta}_1}^2}{2^a h_2^2}\cdot\frac{d^a h_2}{dn_2} + \frac{s_{\hat{\theta}_1}^2}{2^s h_2^2}\cdot\frac{d^s h_2}{dn_2} + \frac{\hat{N}}{EA} \qquad (3.72b)$$

where

(1) for $n_1 < 0$

$$\frac{d^a h_1}{dn_1} = \frac{1}{(-n_1)^2} - \frac{1}{4(-n_1)\sqrt{-n_1}}\cdot\cot\frac{\sqrt{-n_1}}{2} - \frac{1}{8(-n_1)}\cdot\csc^2\frac{\sqrt{-n_1}}{2} \qquad (3.73a)$$

$$\frac{\cdot d^s h_1}{dn_1} = \frac{1}{4(-n_1)\sqrt{-n_1}}\cdot\tan\frac{\sqrt{-n_1}}{2} - \frac{1}{8(-n_1)}\cdot\sec^2\frac{\sqrt{-n_1}}{2} \qquad (3.73b)$$

(2) for $n_1 > 0$

$$\frac{d^a h_1}{dn_1} = \frac{1}{n_1^2} - \frac{1}{4n_1\sqrt{n_1}}\cdot\coth\frac{\sqrt{n_1}}{2} - \frac{1}{8n_1}\cdot\operatorname{cosech}^2\frac{\sqrt{n_1}}{2} \quad (3.74a)$$

$$\frac{d^s h_1}{dn_1} = -\frac{1}{4n_1\sqrt{n_1}}\cdot\tanh\frac{\sqrt{n_1}}{2} + \frac{1}{8n_1}\cdot\operatorname{sech}^2\frac{\sqrt{n_1}}{2} \qquad (3.74b)$$

(3) for $n_2 < 0$

$$\frac{d^a h_2}{dn_2} = -\frac{1}{(-n_2)^2} + \frac{1}{4(-n_2)\sqrt{-n_2}}\cdot\cot\frac{\sqrt{-n_2}}{2} + \frac{1}{8(-n_2)}\cdot\operatorname{cosec}^2\frac{\sqrt{-n_2}}{2} \quad (3.75a)$$

$$\frac{d^s h_2}{dn_2} = -\frac{1}{4(-n_2)\sqrt{-n_2}}\cdot\tan\frac{\sqrt{-n_2}}{2} + \frac{1}{8(-n_2)}\cdot\sec^2\frac{\sqrt{-n_2}}{2} \qquad (3.75b)$$

(4) for $n_2 > 0$

$$\frac{d^a h_2}{dn_2} = -\frac{1}{n_2^2} + \frac{1}{4n_2\sqrt{n_2}}\cdot\coth\frac{\sqrt{n_2}}{2} + \frac{1}{8n_2}\cdot\operatorname{cosech}^2\frac{\sqrt{n_2}}{2} \quad (3.76a)$$

$$\frac{d^s h_2}{dn_2} = \frac{1}{4n_2\sqrt{n_2}}\cdot\tanh\frac{\sqrt{n_2}}{2} - \frac{1}{8n_2}\cdot\operatorname{sech}^2\frac{\sqrt{n_2}}{2} \qquad (3.76b)$$

Equations (3.66), (3.67), and (3.72) are the sought-after

42

relations between the generalized displacements and forces at the nodes of an individual frame member, for the range of deformations considered. In connection with Eqs. (3.66), (3.67), and (3.72), it is worthwhile to recall that:

(1) $\hat{N}$ is in the direction of the straight line connecting the nodes of the frame member after its deformation.

(2) The parameters δ, $^1\hat{\theta}_1$, $^2\hat{\theta}_1$, $^1\hat{\theta}_2$, and $^2\hat{\theta}_2$ are calculated from Eqs. (3.31) to (3.33), which are valid in the presence of arbitrarily large rigid motions (translations and rotations) of the individual member.

Thus, while the local stretch (pure strain) and relative rotation (non-rigid) of a differential element of an individual frame-member may be small, the individual member as a whole (and as a part of the overall frame) may undergo arbitrarily large rigid motion. Hence, the generalized force-displacement relations embodied in Eqs. (3.66), (3.67), and (3.72) remain valid in the presence of arbitrarily large rigid motions of the individual member of the frame. Also, it is important to note that the present relations for each element account, as in the Von Karman plate theory, the non-linear coupling between the bending and stretching deformations, as seen from Eqs. (3.66), (3.67), and (3.72).

III.3 Tangent Stiffness Matrix of a Space Frame Member/Element

Recall that, for the most part of the previous subsection, each member of the frame is treated as a beam column; but in extreme cases, i.e., of "pathological" deformations, it may be modeled by two or three elements utmost.

Now we consider the strain energy due to axial stretch of the member. Since the total axial stretch, δ, is related in a highly non-linear fashion to the axial force, $\hat{N}$, as well as the bending moments, $^a m_i$ and $^s m_i$, ($i = 1,2$), from Eq. (3.72), the inversion of this relation in an explicit form, which expresses the axial force $\hat{N}$ as a function of δ, appears impossible. With a view towards carrying out this inversion of the δ vs. $\hat{N}$ relation incrementally, the strain energy due to stretching, which is denoted as π_s, needs to be expressed in a "mixed" form using the well-known concept of a Legendre contact transformation [31] as:

$$\pi_s = \hat{N} \cdot \delta - \frac{\ell \cdot \hat{N}^2}{2EA} \qquad (3.77)$$

On the other hand, the strain energy due to bending is introduced as follows. The "flexibility" coefficients, $^a h_i$ and $^s h_i$ ($i = 1,2$), are highly non-linear functions of the axial force in Eqs. (3.66) to (3.71). However, unless the flexibility coeffients are equal to zero, one may invert Eqs. (3.66) and (3.67) to write the "force-displacement" relations as:

$$^a m_1 = \frac{^a \hat{\theta}_2}{^a h_1} , \quad ^s m_1 = \frac{^s \hat{\theta}_2}{^s h_1} \qquad (3.78a,b)$$

$$^a m_2 = \frac{^a \hat{\theta}_1}{^a h_2} , \quad ^s m_2 = \frac{^s \hat{\theta}_1}{^s h_2} \qquad (3.79a,b)$$

44

Using the definition of non-dimensional moments as in Eq. (3.50), one may express the strain energy due to bending, which is denoted as π_b, as:

$$\pi_b = \frac{EI_1}{2\ell} \cdot \left[\frac{{}^a\hat{\theta}_2^2}{{}^a h_1} + \frac{{}^s\hat{\theta}_2^2}{{}^s h_1}\right] + \frac{EI_2}{2\ell} \cdot \left[\frac{{}^a\hat{\theta}_1^2}{{}^a h_2} + \frac{{}^s\hat{\theta}_1^2}{{}^s h_2}\right] \qquad (3.80)$$

However, when in the limit as $\hat{N}$ tends to $(-4\pi^2 EI_i/\ell^2)$, as explained in [22], ${}^s h_i$ $(i = 1,2)$ tend to zero; thus, the inversions of Eqs. (3.66) and (3.67) to obtain Eqs. (3.78) and (3.79) are not meaningful. In such a case, one may use a mixed form for the bending energy of the symmetric mode, treating both ${}^s m_i$ and ${}^s\hat{\theta}_i$ $(i = 1,2)$ as variables, as:

$$\frac{EI_1}{2\ell} \cdot \frac{{}^s\hat{\theta}_2^2}{{}^s h_1} \equiv \frac{EI_1}{\ell} \cdot \left[{}^s m_1 \cdot {}^s\hat{\theta}_2 - \frac{{}^s h_1 \cdot {}^s m_1^2}{2}\right] \qquad (3.80a)$$

$$\frac{EI_2}{2\ell} \cdot \frac{{}^s\hat{\theta}_1^2}{{}^s h_2} \equiv \frac{EI_2}{\ell} \cdot \left[{}^s m_2 \cdot {}^s\hat{\theta}_1 - \frac{{}^s h_2 \cdot {}^s m_2^2}{2}\right] \qquad (3.80b)$$

However, as explained in [22], without loss of generality for a practical frame-structure, we may consider the strain energy in the form of Eq. (3.80). It should be noted that in the view of the dependence of ${}^a h_i$ and ${}^a h_i$ on n_i $(i = 1,2)$ as in Eqs. (3.68) to (3.71), there is coupling between "bending" and "stretching" variables.

The strain energy due to torsion, which is denoted as π_t, may be written as:

$$\pi_t = \frac{GJ}{2\ell} \cdot \hat{\theta}_3^2 \qquad\qquad (3.81)$$

The internal energy in the member due to combined bending, stretching, and torsion is represented as:

$$\pi = \frac{EI_1}{2\ell} \cdot \left[\frac{{}^a\hat{\theta}_2^2}{{}^a h_1} + \frac{{}^s\hat{\theta}_2^2}{{}^s h_1}\right] + \frac{EI_2}{2\ell} \cdot \left[\frac{{}^a\hat{\theta}_1^2}{{}^a h_2} + \frac{{}^s\hat{\theta}_1^2}{{}^s h_2}\right] \qquad (3.82)$$

$$+ \frac{GJ}{2\ell} \cdot \hat{\theta}_3^2 + \hat{N} \cdot \delta - \frac{\ell \cdot \hat{N}^2}{2EA}$$

The condition of vanishing of the first variation of π, which is denoted here as π^*, in Eq. (3.82) due to a variation in $\hat{N}$, which is denoted here as $\hat{N}^*$, is given by:

$$\frac{\pi^*}{\ell} = 0 = -\frac{1}{2}\left[\left(\frac{{}^a\hat{\theta}_2}{{}^a h_1}\right)^2 \cdot \frac{d\,{}^a h_1}{dn_1} + \left(\frac{{}^s\hat{\theta}_2}{{}^s h_1}\right)^2 \cdot \frac{d\,{}^s h_1}{dn_1} + \left(\frac{{}^a\hat{\theta}_1}{{}^a h_2}\right)^2 \cdot \frac{d\,{}^a h_2}{dn_2}\right. \qquad (3.83)$$

$$\left. + \left(\frac{{}^s\hat{\theta}_1}{{}^s h_2}\right)^2 \cdot \frac{d\,{}^s h_2}{dn_2}\right] \cdot \hat{N}^* + \left(\frac{\delta}{\ell} - \frac{\hat{N}}{EA}\right) \cdot \hat{N}^*$$

Equation (3.83) leads clearly to the relation between δ and the generalized forces as given in Eq. (3.72).

The reason for using the "mixed" form for the stretching energy in Eq. (3.77) is now clear from the above result. By using a similar mixed form for the increment of stretching energy, the incremental

46

axial stretch vs. incremental generalized force relation can be derived

in a manner analogous to that used in obtaining Eq. (3.83) from Eq.

(3.82). This incremental relation, which is, by definition, piecewise

linear, may easily be inverted, as demonstrated in the following.

Also, it is shown in the following that Eq. (3.82) froms the basis for

generating an explicit form for the "tangent-stiffness" of the member.

The increment of the internal energy of the member, which is

denoted as $\Delta\pi$, involving terms up to second order in the "incremental"

variables, $\Delta^a\hat{\theta}_1$, $\Delta^s\hat{\theta}_1$, $\Delta^a\hat{\theta}_2$, $\Delta^s\hat{\theta}_2$, $\Delta\hat{N}$, and $\Delta\delta$ can be seen from Eq.

(3.82) as:

$$\Delta\pi = \frac{EI_1}{\ell}\cdot\left[\frac{{}^a\hat{\theta}_2}{{}^a h_1}\cdot\Delta^a\hat{\theta}_2 + \frac{\Delta^a\hat{\theta}_2^2}{2\,{}^a h_1} + \frac{{}^a\hat{\theta}_2^2}{2}\cdot\Delta\left(\frac{1}{{}^a h_1}\right) + {}^a\hat{\theta}_2\cdot\Delta^a\hat{\theta}_2\cdot\Delta\left(\frac{1}{{}^a h_1}\right)\right. \quad (3.84)$$

$$\left. + \frac{{}^s\hat{\theta}_2}{{}^s h_1}\cdot\Delta^s\hat{\theta}_2 + \frac{\Delta^s\hat{\theta}_2^2}{2\,{}^s h_1} + \frac{{}^s\hat{\theta}_2^2}{2}\cdot\Delta\left(\frac{1}{{}^s h_1}\right) + {}^s\hat{\theta}_2\cdot\Delta^s\hat{\theta}_2\cdot\Delta\left(\frac{1}{{}^s h_1}\right)\right]$$

$$+ \frac{EI_2}{\ell}\cdot\left[\frac{{}^a\hat{\theta}_1}{{}^a h_2}\cdot\Delta^a\hat{\theta}_1 + \frac{\Delta^a\hat{\theta}_1^2}{2\,{}^a h_2} + \frac{{}^a\hat{\theta}_1^2}{2}\cdot\Delta\left(\frac{1}{{}^a h_2}\right) + {}^a\hat{\theta}_1\cdot\Delta^a\hat{\theta}_1\cdot\Delta\left(\frac{1}{{}^a h_2}\right)\right.$$

$$\left. + \frac{{}^s\hat{\theta}_1}{{}^s h_2}\cdot\Delta^s\hat{\theta}_1 + \frac{\Delta^s\hat{\theta}_1^2}{2\,{}^s h_2} + \frac{{}^s\hat{\theta}_1^2}{2}\cdot\Delta\left(\frac{1}{{}^s h_2}\right) + {}^s\hat{\theta}_1\cdot\Delta^s\hat{\theta}_1\cdot\Delta\left(\frac{1}{{}^s h_2}\right)\right]$$

$$+ \frac{GJ}{2\ell}\cdot\left[2\hat{\theta}_3\cdot\Delta\hat{\theta}_3 + \Delta\hat{\theta}_3^2\right]$$

$$+ \left(\delta - \frac{\ell \cdot \hat{N}}{EA}\right) \cdot \Delta\hat{N} - \frac{\ell \cdot \Delta\hat{N}^2}{2EA} + \Delta\delta \cdot \Delta\hat{N} + \hat{N} \cdot \Delta\delta$$

In the above equation, it should be recalled that $^a h_i$ and $^s h_i$ ($i = 1,2$) are functions of $\hat{N}$.

Now, using Eqs. (3.31) to (3.33), (3.66), and (3.67), the incremental quantities, $\Delta^a \hat{\theta}_1$, $\Delta^s \hat{\theta}_1$, $\Delta^a \hat{\theta}_2$, $\Delta^s \hat{\theta}_2$, and $\Delta\delta$ may be expressed in terms of $^j u_i$ and $^j \theta_i$ ($i = 1,2,3$, $j = 1,2$) and/or their increments. Henceforth, we use the notation for the vector $\underline{d}^m$ that:

$$\underline{d}^{mt} = \lfloor {}^1u_1; {}^2u_1; {}^1u_2; {}^2u_2; {}^1u_3; {}^2u_3; {}^1\theta_1; {}^2\theta_1; {}^1\theta_2; {}^2\theta_2; {}^1\theta_3; {}^2\theta_3 \rfloor \quad (3.85)$$

as shown in Fig. 2.

In terms of the increment $\Delta\underline{d}^m$, Eq. (3.84) may be written as:

$$\Delta\pi = \tfrac{1}{2} \Delta\underline{d}^{m^t} \cdot \underline{A}_{dd} \cdot \Delta\underline{d}^m + \Delta\hat{N} \cdot \underline{A}_{nd}^t \cdot \Delta\underline{d}^m \quad (3.86)$$

$$+ \frac{A_{nn}}{2} \cdot \Delta\hat{N}^2 + \underline{B}_d^t \cdot \Delta\underline{d}^m + B_n \cdot \Delta\hat{N}$$

The details of $\underline{A}_{dd}$, $\underline{A}_{nd}$, A_{nn}, $\underline{B}_d$, and B_n are as shown in Appendix D.

By setting to zero the variation of $\Delta\pi$ in Eq. (3.86) with respect to $\Delta\hat{N}$, one obtains the following relation as:

$$\underline{A}_{nd}^t \cdot \Delta\underline{d}^m + B_n = -A_{nn} \cdot \Delta\hat{N} \quad (3.87)$$

Thus, the above equation is the incremental counterpart of δ vs.

48

the generalized force relation obtained in Eq. (3.83). Unlike the non-linear relation in Eq. (3.83), the piecewise linear relation, Eq. (3.87), can be inverted to express $\hat{N}$ in terms of the generalized displacements as:

$$\Delta\hat{N} = -\frac{1}{A_{nn}}[\underline{A}_{nd}^{t} \cdot \Delta\underline{d}^{m} + B_{n}]$$

(3.88)

Substituting Eq. (3.88) into Eq. (3.86), one obtains the internal energy expression as:

$$\Delta\pi = \frac{1}{2}\Delta\underline{d}^{m^{t}} \cdot \underline{K}^{m} \cdot \Delta\underline{d}^{m} + \Delta\underline{d}^{m^{t}} \cdot \underline{R}^{m} - \frac{B_{n}^{2}}{2A_{nn}}$$

(3.89)

where

$\underline{K}^{m}$: Tangent stiffness matrix of member/element

$$= \underline{A}_{dd} - \frac{1}{A_{nn}} \cdot \underline{A}_{nd} \cdot \underline{A}_{nd}^{t}$$

(3.90)

$\underline{R}^{m}$: Internal generalized force vector for member/element

$$= \underline{B}_{d} - \frac{B_{n}}{A_{nn}} \cdot \underline{A}_{nd}$$

(3.91)

Recall that the tangent stiffness matrix and the internal force vector are written in the member coordinate system as shown in Fig. 2.

49

Thus, it is necessary to transform $\underset{\sim}{d}^m$ from a member coordinate system to a global coordinate system as shown in Appendix E.

It should be emphasized once again that the tangent stiffness matrix $\underset{\sim}{K}^m$ of Eq. (3.90) is given an explicit expression, as in Appendix D; and likewise, the internal generalized force vector $\underset{\sim}{R}^m$ is also given explicitly. No member-wise numerical integrations are involved. During the course of deformation of the frame, once the nodal displacements of the frame at stage C_N are known, the tangent stiffness of each of the members and hence of the frame structure, which governs the deformation of the frame from stage C_N to an incrementally close neighboring stage C_{N+1}, can easily be evaluated from Eq. (3.90). This distinguishing feature of the present formulation renders the large deformation analysis of framed structures much more computationally inexpensive than the standard incremental (updated or total Lagrangean) finite element formulations reported in current literature [3]. Numerical examples illustrating this are given later.

CHAPTER IV

SOLUTION STRATEGY

Although a number of solution procedures are available for non-linear structural analyses, a reliable approach to trace the structural response near limit points, and in a post-buckled range, is the arc-length method which was proposed by Riks [16] and Wempner [18] and modified by Chrisfield [19,20] and Ramm [13]. This method is the incremental/iterative procedure which represents a generalization of the displacement control approach. The arc length method, in which the Euclidian norm of the increment in the displacement and load space is adopted as the prescribed increment, allows one to trace the equilibrium path beyond limit points such as in snap-through and snap-back phenomena.

The i-th iteration in any incremental stiffness equation may be written, as shown in Fig. 6, as:

$$p_{i-1} \cdot \underline{P} - \underline{R}^{(i-1)} + \Delta p \cdot \underline{P} = \underline{K}^{(i)} \cdot \Delta \underline{d} \tag{4.1}$$

where

$\underline{P}$: Standard load vector

p_{i-1} : Total load parameter after the (i-1)th iteration

$\underline{R}^{(i-1)}$: Internal force vector after the (i-1)th iteration

Δp : Iterative load parameter during this iteration

51

$\underline{K}^{(i)}$: Stiffness matrix during this iteration

$\Delta\underline{d}$: Iterative displacement vector during this iteration

In the numerical implementation of Eq. (4.1), the standard Newton-Raphson procedure or the modified Newton-Raphson procedure may be employed.

We decompose $\Delta\underline{d}$ into two parts,

$$\Delta\underline{d} = \Delta\underline{d}^* + \Delta p \cdot \Delta\underline{d}^{**} \tag{4.2}$$

where

$\Delta\underline{d}^*$: Displacement vector due to the unbalanced force

$$= \underline{K}^{(i)^{-1}} \cdot (p_{i-1} \cdot \underline{P} - \underline{R}^{(i-1)}) \tag{4.3a}$$

$\Delta\underline{d}^{**}$: Displacement vector to the external load

$$= \underline{K}^{(i)^{-1}} \cdot \underline{P} \tag{4.3b}$$

Also it is seen that:

$$\Delta\underline{d}^{(i)} = \Delta\underline{d}^{(i-1)} + \Delta\underline{d}^* + \Delta p \cdot \Delta\underline{d}^{**} \tag{4.4}$$

52

where $\Delta\underline{d}^{(i)}$: Incremental displacement vector after the i-th iteration during the current increment

$$\Delta\underline{d}^{(i)} = \Delta\underline{d}^{(i-1)} + \Delta\underline{d}$$

The incremental arc length, Δn_i, after the i-th iteration during the current increment is defined as [20]:

$$\Delta n_i = \left[\Delta\underline{d}^{(i)^t}\cdot\Delta\underline{d}^{(i)} + \gamma\cdot\Delta p^2 \cdot\underline{P}^t\cdot\underline{P}\right]^{1/2} \qquad (4.5)$$

where Δp_i: Incremental load parameter after the i-th iteration during this increment

γ : Scaling parameter which represents the contribution of the load term

Numerical experience has shown that it is preferable to ignore the contribution of the load term [13,19-20]. Consequently, using Eq. (4.4), Eq. (4.5) may be written as:

$$\Delta n_i = \left[\Delta\underline{d}^{(i)^t}\cdot\Delta\underline{du}\right]^{1/2} \qquad (4.6)$$

$$= \left[\Delta\underline{d}^{**^t}\cdot\Delta\underline{d}^{**}\cdot\Delta p^2 + 2\Delta\underline{d}^{**^t}\cdot\left(\Delta\underline{d}^{(i-1)} + \Delta\underline{d}^{*}\right)\cdot\Delta p\right.$$

$$\left. + \left(\Delta\underline{d}^{(i-1)^t} + \Delta\underline{d}^{*^t}\right)\cdot\left(\Delta\underline{d}^{(i-1)} + \Delta\underline{d}^{*}\right)\right]^{1/2}$$

53

In order to decide the incremental/iterative displacement $\Delta \underset{\sim}{d}$, it is needed to compute Δp. In the case of a truss structure, two procedures, such as by the prescribed incremental arc length and by the criterion of member buckling, are used.

As for the procedure of the prescribed incremental arc length which is used for both truss and frame structures, Δp is decided by Eq. (4.6) and the following equation.

$$\Delta \eta_i = \Delta \bar{\eta} \tag{4.7}$$

where $\quad \Delta \bar{\eta}$: Prescribed incremental arc length

Substituting Eq. (4.7) into Eq. (4.6), it is seen that:

$$a \cdot \Delta p^2 + b \cdot \Delta p + c = 0 \tag{4.8}$$

where

$$a = \Delta \underline{d}^{**t} \cdot \Delta \underline{d}^{**} \tag{4.9}$$

$$b = 2 \cdot \Delta \underline{d}^{**t} \cdot \left(\Delta \underline{d}^{(i-1)} + \Delta \underline{d}^{*} \right)$$

$$c = \left(\Delta \underline{d}^{(i-1)t} + \Delta \underline{d}^{*} \right) \cdot \left(\Delta \underline{d}^{(i-1)} + \Delta \underline{d}^{*} \right) - \left(\Delta \bar{\eta} \right)^2$$

54

Then, the following conditions are imposed on the incremental displacements to avoid "doubling back" [19].

$$\Delta \underline{d}^{(i)^t} \cdot \Delta \underline{\hat{d}} \quad > \quad 0 \qquad (i = 1) \tag{4.10a}$$

$$\Delta \underline{d}^{(i)^t} \cdot \Delta \underline{d}^{(i-1)} \quad > \quad 0 \qquad (i > 1) \tag{4.10b}$$

where $\Delta \underline{\hat{d}}$: Incremental displacement vector of the previous increment

It should be noted that in Eq. (4.10), $i = 1$ represents the incremental process and $i > 1$ the iterative process.

Another procedure to decide Δp, which is used only for truss structures, can be developed based on the criterion for member buckling. According to Eqs. (2.1) and (4.4), the total axial stretch of the member after the i-th iteration prior to its buckling, δ_i, at any point in the load history is given by:

$$\delta_i = [(\bar{u}_1^{(i-1)} + \bar{u}_1^* + \Delta p \cdot \Delta \bar{u}^{**})^2 + (\bar{u}_2^{(i-1)} + \Delta \bar{u}_2^* + \Delta p \cdot \Delta \bar{u}_2^{**})^2 \tag{4.11}$$

$$+ (\ell + \bar{u}_3^{(i-1)} + \Delta \bar{u}_3^* + \Delta p \cdot \Delta \bar{u}_3^{**})^{\frac{1}{2}} - \ell$$

The axial force after the i-th iteration, N_i, is also given by:

$$N_i = k \cdot \delta_i \tag{4.12}$$

55

Substituting Eqs. (4.11) and (4.12) into the buckling condition for the member Eqs. (2.4) and (2.5), it is seen that:

$$r \cdot \Delta p^2 + s \cdot \Delta p + t = 0 \qquad (4.13)$$

where

$$r = \overline{\Delta u}_1^{**2} + \overline{\Delta u}_2^{**2} + \overline{\Delta u}_3^{**2} \qquad (4.14)$$

$$s = 2 \cdot \overline{\Delta u}_1^{**} \cdot (\overline{u}_1^{(i-1)} + \overline{\Delta u}_1^{*}) + 2 \cdot \overline{\Delta u}_2^{**} \cdot (\overline{u}_2^{(i-1)} + \overline{\Delta u}_2^{*})$$

$$+ 2 \cdot \overline{\Delta u}_3^{**} \cdot (\ell + \overline{u}_3^{(i-1)} + \overline{\Delta u}_3^{*})$$

$$t = (\overline{u}_1^{(i-1)} + \overline{\Delta u}_1^{*})^2 + (\overline{u}_2^{(i-1)} + \overline{\Delta u}_2^{*})^2 + (\ell + \overline{u}_3^{(i-1)} + \overline{\Delta u}_3^{*})^2$$

$$- (^{cr}N/k + \ell)^2$$

In order to avoid "doubling back", the constraint equations, Eq. (4.10), are imposed on Δp; and in addition, the following condition for $i > 1$ is imposed:

$$\Delta \delta_i \cdot \Delta \delta_{i-1} > 0 \qquad (4.15)$$

56

where $\Delta\delta_i$:   Incremental total axial stretch after the
                  i-th iteration

Finally, in the load parameter ΔP computed by Eqs. (4.8) and (4.13), the value for ΔP which satisfies the constraint equations, Eqs. (4.10) and (4.15) and gives the minimum value for $\Delta\eta_i$ is employed.

Moreover, an additional precaution is necessary in certain cases in using the constraint Eq. (4.10a) to avoid "doubling back". In the case that any member had undergone bifurcation buckling in the previous increment, the incremental deformation of the member during the current increment may change significantly due to the abrupt change in the tangent stiffness. Therefore, in this case, the following constraint condition is employed instead of Eq. (4.10a):

$$\Delta\delta_i < 0 \qquad (i = 1) \qquad\qquad (4.16)$$

So far, the situation of the progressive buckling of an individual member has been discussed. It might happen that the member might be forced to undergo a "restraightening" after the member has buckled during the continued deformation of the structure. In this case, the numerical procedure is similar to the one treated above, wherein a member begins to undergo buckling. Instead of Eqs. (4.12) and (4.16), the following equations are used:

$$N_i = k\hat{\delta}_i + {}^{cr}N \qquad\qquad (4.17)$$

57

$$\Delta \delta_i \; > \; 0 \qquad (i = 1) \qquad\qquad (4.18)$$

where $\quad \hat{\delta}_i$: Total stretch in the post-buckled state
after the i-th iteration

$\quad k$: Stiffness in the post-buckled state

Equation (4.8) usually provides two roots for (Δp), one of which usually satisfies Eqs. (4.10) and the other does not. It it happens that both of the roots of Eq. (4.8) satisfy Eqs. (4.10), the appropriate value of (Δp) is the closest to the solution of the following linear equation [19,20]:

$$b(\Delta p) + c = 0 \qquad\qquad (4.19)$$

Finally, it should be noted that, in Eq. (4.5), if a large value for γ is adopted, $\Delta \eta_i$ tends to be proportional to the incremental load; and the method tends toward the standard load control method. On the other hand, for a small value of γ, the arc length method may be interpreted as a generalized displacement control method, wherein the Euclidian norm of the increment in the displacement space is prescribed, instead of the increment of a specific displacement.

CHAPTER V

NUMERICAL EXAMPLES

Several numerical examples are considered in this chapter, to demonstrate the validity of the present study.

As a criterion for the convergence of the iteration in solving the incremental equations, the following equation using the modified Euclidean norm is employed.

$$\frac{[\frac{1}{n}\Delta\underline{d}^t \cdot \Delta\underline{d}]^{1/2}}{[\frac{1}{n}\Delta\underline{d}^{(i)^t} \cdot \Delta\underline{d}^{(i)}]^{1/2}} < \varepsilon$$

where   n: Total number of degrees of freedom

$\varepsilon = 1.0 \times 10^{-3}$ for all the numerical examples

V.1   Truss Structures

In subsection V.1.1, we present several examples of plane trusses; while in subsection V.1.2, we treat examples of space (three-dimensional) trusses.

V.1.1. Plane Trusses

Examples 1 and 2 are those of simple truss structures, for which theoretical solutions for the buckling load and the initial slope of the post-buckling load-displacement curve are given by Britvec [36]. For these structures, experiments were also carried out by Britvec, who

59

found good correlation between his theoretical and experimental solutions.

These structures are composed of two and three member, respectively. All the members have a rectangular cross-section of width 2.54(cm), depth of 0.16(cm), and each has a length of 38.1(cm). Also, the buckling loads of the individual members are 13.26(kg) for Example 1, 13.15(kg) for Example 2, respectively.

The schematics of the structures and the results obtained are summarized in Fig. 7. Both of these structures have a special type of structural behavior in which the global buckling is caused by the buckling of one of the members. The present solutions agree excellently with Britvec's theoretical solutions concerning the buckling load and the initial slope of the post-buckling curve. However, the present solutions develop the tendencies that the stiffnesses of the structure gradually increase as the post-buckling deformations progress. This phenomenon is brought out by the effect of the geometrical nonlinearity, and the result of Britvec's experiments also show the same tendencies in the post-buckling range. Thus, the present results appear to be reasonably accurate.

Example 3 is that of a simple structural model [see Fig. 8(a)], which exhibits a snap-through phenomenon and is chosen here to study the effect of member buckling on such phenomena. In this example, the range of deformations is much larger than in the earlier examples. The structure is composed of two identical members, which have a solid circular cross section of area 96.77(cm^2), a length of 38.1(cm), and a Young's modulus of 7.03 x 10^5(kg/cm^2). To study the influence of the member's buckling, three different cases are investigated. In Case 1

60

the buckling of both the members is ignored, in Case 2 the buckling of only one of the members is considered, and in Case 3 the buckling of both the members is considered.

Figure 8(b) shows the relations between the applied load and the vertical displacement of the center. Case 1 exhibits a typical snap-through phenomenon and reaches the limit point at a load of 3.76×10^6(kg). In Cases 2 and 3, the individual members buckle at a load of 2.93×10^6(kg) and cause the structure to be in the unstable region just after this load. There is little difference to be found between Cases 2 and 3.

The fourth example is that of a strut structure, which was first suggested by Thompson and Hunt [37] and later analyzed by Rosen and Schmit [23] to study the influence of local as well as global geometric imperfections on global stability.

The outline of this structure is shown in Fig. 9(a) and Table 1. The structure is composed of 35 members, all of which have a solid circular cross section and an identical Young's modulus of 7.03×10^5(kg.cm^2). As in the case of Example 3, four different cases are dealt with in this example also, to investigate the influence of the member's buckling and of a slight difference of the cross-sectional area of individual members on global buckling. The cross-sectional areas of the members for each ases are shown in Table 1. Note that the structure of this example is not strictly symmetric about the z axis, and this unsymmetry causes the effective neutral axis of the strut to be slightly above the z axis for Cases 1-3 or slightly below the z axis for Case 4. In Case 1, the buckling of all of the members is ignored. In the other cases, the buckling of all of the members is considered;

61

however, the cross-sectional area of the members is slightly different for each case, as shown in Table 1. The results obtained are shown in Figs. 9(b)-(d).

Case 1 exhibits an entirely stable equilibrium path in the load-displacement space. At a load of about 7.2×10^5(kg), the global buckling occurs; and the stiffness of the structure goes down and tends to zero after that. However, the equilibrium path is still stable.

The difference between Cases 1 and 2 is that member buckling is considered only in the latter, while the cross-sectional areas of the members are the same in both the cases. Thus, the structure of Case 2 exhibits exactly the same behavior as that of Case 1 until a load of 6.916×10^5(kg), when the member of no. 15 buckles.

In Case 3, the cross-sectional area of the member with no. 15 is set to be about 5.89 percent smaller than the corresponding area in Case 2. However, the structural behavior is almost the same as that in Case 2. With this slight reduction in cross-sectional area of one member, the stiffness of the structure as well as the load level when the member of no. 15 buckles are reduced as compared with Case 2.

In Case 4, the cross-sectional areas of the members 14 and 16 are set to be 94.11 percent of the corresponding areas of Case 1. This reduction of the cross-sectional areas causes the effective neutral axis of the strut to be slightly below the z axis. Also, the members 14 and 16 buckle at an external load P of 6.323 (kg).

It is interesting to see that even in a fairly complicated structure such as in Fig. 9(a), the buckling of only one or a few members renders the structure to be unstable. It is also noted that even a slight difference of the cross-sectional area of the members has

62

a great influence on the overall behavior of the structure. In Fig. 9(c), the z-displacement of node 19 [see Fig. 9(a)] is shown as a function of the load P for each of the four cases. The variations of axial forces (directed along the undeformed axes of the members) in members 14 and 15 as a function of the external load P are shown in Fig. 9(d) for each of the four cases. It is instructive, while examining Fig. 9(d), to remember that Case 1 precludes buckling of any member; in Cases 2 and 3, member 15 buckles (this load is lower in Case 3 than in Case 2); and in Case 4, member 14 buckles first. Figure 9(d) indicates that the load transfer mechanism in a structure after the buckling of an individual member is rather complicated.

Example 5 is an idealized model of a truss of the plane arch shape. This structure was also analyzed by Rosen and Schmit [22] to investigate the influence of geometric imperfections. This thin, shallow arch is made up of 35 truss members, all of which have a solid circular cross section and a Young modulus of $7.03 \times 10^6 (\text{kg/cm}^2)$. It is shown schematically in Fig. 10(a) and in Tables 2(a,b). Again, three cases are considred for this example. In Case 1, the buckling of any member is entirely ignored, while it is considered in Cases 2 and 3. The difference between Cases 2 and 3 is only that the cross-sectional areas of members 27 and 28 in Case 3 are 25.00 percent smaller than the corresponding areas in Case 2. The results obtained are given in Figs. 10(b-d).

Case 1 indicates the snap-through phenomenon similar to that of the behavior of thin shallow arches made of homogeneous isotropic elastic materials. The limit point is reached at a load of about $2.64 \times 10^3 (\text{kg})$.

In Case 2, members 11 and 12 buckle slightly after the whole structure passes the limit point. As seen from Fig. 10(b), the global structural response in Case 2 is markedly different from that in Case 1. In Case 3, the cross-sectional areas of two members (i.e., nos. 27, 28) are smaller than the corresponding areas in the other cases. Thus, the overall response in Case 3 is slightly different form the other two cases, until buckling occurs first in members 27 and 28, after passing the limit point of the structure as a whole. However, in spite of the buckling of members 27 and 28, there is little change in the overall behavior of the structure as compared with the former cases. However, when the deformation progresses further, the members 21 and 22 buckle; and this alters the load-carrying capacity of the structure more decisively.

The sixth and final example of plane-truss structures deals with the interactive effects of imperfections of the structure at the global level and the possibility of local buckling of individual members. The structure considered is identical to that in Example 4 and shown in Fig. 9(a). While Example 4 treated a perfect structure, now two cases of global imperfections are considered. The imperfection is of a half-sine-wave form. Two different values of the amplitude of this imperfection mode, 1.32(cm) and 2.64(cm), respectively, are considered. In both the cases of imperfection, individual member buckling is considered; and the cross-sectional areas of members are identical to those in Cases 1 and 2 of Example 4, as shown in Table 1. The present example is summarized in Table 3. The results are shown in Figs. 11(a-c). Cases 1 and 2 as marked in Fig. 11(a) are identical to Cases 1 and 2 as marked in Fig. 9(b) for a perfect structure. Comparing

64

these cases with Cases 3 and 4 in Fig. 11(a), the dramatic combined effects of small global imperfections of the structure, and of the buckling of individual members, on global response, may be noted. The variation of z-displacement, at node 19, with the external load, is shown in Fig. 11(b). The complicated nature of load-transfer in the structure after an individual member's buckling, in an imperfect structure, may be seen from Fig. 11(c).

The present numerical examples thus delineate: (i) the effect of buckling of an individual member or members on the response of the structure as a whole and on the subsequent load-distribution in the structure, (ii) the effects of even minor variations in the cross-sectional areas of individual members, and (iii) the effects of imperfections at the global level, while imperfections at the local level, in each member, may be expected to have similar effects. The present numerical examples also serve to point out the relative efficiency of simple procedures adopted in the present work for obtaining tangent stiffnesses.

V.1.2 Space (Three-Dimensional) Trusses

The first example considered in this category is the shallow geodesic dome shown in Fig. 12. This structure, which exhibits a snap-through phenomenon, is subjected to one concentrated load at the central node. Two initial configurations of the structure, one geometrically perfect and the other with slight imperfections, as specified in Table 4, are considered. This example was also analyzed, using a perturbation method by Hangai [2] to study global stability. In the present study, however, the influence of local buckling on global stability is also examined.

65

Figures 13 and 14, for the case of perfect geometry, show a typical snap-through phenomenon wherein the first limit point is reached at a load of 3.15×10^{-4} EA (Kg). The present results are seen to be in good agreement with those of Hangai [2].

The influence of local buckling on global instability is illustrated in Figs. 15, 16, and 19, which indicate that a global behavior strongly depends on the local buckling of a single member. In a practical design of a three-dimensional truss structure, this understanding is very essential and useful. Also, the effects of slight geometric imperfection are illustrated in Figs. 17 and 18, wherein the comparison results of Hangai [2] are also included.

Example 2 is also that of a shallow geodesic dome, analyzed earlier by Noor [32] and shown in Fig. 20. Two types of loading systems are considered: the first loading system consists of lateral concentrated loads P_1 over the entire dome; the second one, P_2, consists of concentrated lateral loads only over a quarter of the dome. An important difference between the present analysis and that of Noor [32] should be mentioned. Noor [32] ignores local buckling and assumes each member of the truss to remain straight and stable. On the other hand, in the present analysis, local buckling of each member is allowed; and only for comparison purposes, results are also obtained using the present procedure with local buckling being intentionally suppressed.

Figure 21 provides a comparison of the vertical displacement of the central node in the present and Noor's solutions for various conbinations of P_1 and P_2, when local member buckling is ignored. The present results agree well with those of Noor [32] except beyond the

66

limit point of $P_1 = -5.132 \times 10^{-5}$. The stability boundary, i.e., the combinations load parameters P_1 and P_2 which render the structure unstable when local member buckling is ignored, is shown in Fig. 22, from which an excellent correlation of the present results (with member-buckling being suppressed) with those of Noor [32] may also be noted.

Figures 23 to 26 show the present results when local buckling is considered. Figure 23 shows the variation of vertical displacement of the central node; Fig. 24 shows the stability boundary under the various conbinations of P_1 and P_2; Fig. 25 shows the equilibrium path under the load system $P_2 = 0$ and $P_1 \neq 0$.

From this numerical example (especially Fig. 24), it is clear that the decrease in the magnitude of critical loads for the structure, due to buckling of an individual member or members, i.e., the influence of local buckling on the response of the structure as a whole, is quite remarkable.

The third example of space trusses is that of a beam-like space truss (PACOSS Truss) subjected to axial and bending loads. The structure is that of a twelve-bay truss whose member properties are shown in Figs. 27 and 29. In order to trigger the coupling between the axial and transverse displacements, which is characteristic of the buckling mode, in the case of only axial-load application, a "load imperfection" equal to P/1000 is added in the transverse direction at one of the end nodes, as shown in Fig. 27.

For the above predominantly axial-load case, Fig. 28 shows the relation between the magnitudes of the axial load and that of the transverse displacement at the loaded end, for two scenarios: (i) when

local (member) buckling is suppressed and each member is assumed to remain straight and stable and (ii) when each member is allowed to undergo local buckling. Fig. 28 clearly demonstrates the advantageous effects of controlling the local buckling deformations of individual members and forcing them to remain straight and stable. This leads one to the concept of active/passive control of member deformations.

Figure 29 shows the schematic of the PACOSS Truss subject to predominantly bending loads. Fig. 30 shows the relation between the magnitudes of transverse (bending) load and transverse displacement, respectively, once again for two scenarios: (i) when local member buckling is suppressed and (ii) when member buckling is allowed. Figure 30 again demonstrates the beneficial effects of control of deformations of each member. Figure 31 shows a computer plot of the deformed shape of the PACOSS Truss under bending loads.

It should be noted that in Figs. 28 and 30, the letters A, B, C, etc. indicate the stages at which the respective members, whose numbers are identified in Figs. 28 and 30 respectively, undergo local buckling.

V.2   Frame Structures

In subsection V.2.1, we present several examples of plane frames, while in subsection V.2.2, we treat examples of space (three-dimensional) frames.

V.2.1 Plane Frames

We first examine the ranges of deformation of a frame element, for which the presently developed tangent-stiffness matrices are valid.

Recall that the principal assumptions underlying the present development of an explicit expression for the tangent-stiffness matrix of an element are as follows: (i) arbitrarily large rigid translations

68

and rigid rotations of the element are accounted for; (ii) however, the local (non-rigid) rotations $\hat{\theta}_i$ (i = 1,2) are restricted to be small such that $\sin\hat{\theta}_i \approx \hat{\theta}_i$ amd $\cos\hat{\theta}_i = 1$; (iii) the local axial stretch ε is restricted to be small; (iv) the non-linear coupling between the bending deformation (characterized by $\hat{\theta}_i$) and stretching deformation (characterized by total axial stretch δ) is accounted for.

We consider the problem of an "elastica" - a simply supported (but axially movable beam, of length ℓ, that is subjected to an axial compressive load, with a load eccentricity of ($\ell/1000$) from the undeformed axis of the beam, as shown schematically in Fig. 32a. The beam has a square cross-section of area 1.0 (in^2), ℓ = 100.0 (in), E = 10^7(psi), and I = 0.8333 (in^4). For testing the range of deformations, over which the present explicit expression for tangent stiffness matrix of an element are valid, the beam is idealized, successively, by 1, 2, 4, and 8 elements over its length, respectively. As shown in Fig. 32a, δ_V is the total axial "stretch" of the beam, while δ_H is the transverse displacement at midspan, in the post-buckling range. Figure 32b shows the dependence of (δ_V and δ_H) on the axial load N, for the range of deformations [(δ_V/ℓ) and (δ_H/ℓ)] $\approx$ 0.30. On the other hand, Fig. 32c shows the dependence of (δ_V and δ_H) on the axial load N, for a much wider range of deformations, viz., (δ_V/ℓ) $\approx$ 1.0 and (δ_H/ℓ) $\approx$ 0.5.

From Figs. 32b and 32c, it is seen that, while a "single-element" representation of the entire beam does account for the non-linear coupling between bending and stretching (as seen from the large values of δ_V and δ_H at N $\approx$ N$_E$), the slope of the post-buckling response curve for N vs. (δ_V or δ_H) is not accurately represented. On the other hand, Figs. 32b and 32c clearly indicate that even a two-element

69

representation of the beam yields results for post-buckling response, that are in close agreement with the classical "elastica" solution, even for very large deformations of the order $(\delta_H/\ell) \doteq 0.4$ and $(\delta_V/\ell) \doteq 0.5$. It is also seen from Figs. 32b and 32c that a four-element representation produces solutions that are in exact agreement with the "elastica" solutions for the entire range of deformations considered. The reason for this excellent behavior of the "two-" or "multi-"element models of the elastica is due to the fact that the present element development can account for arbitrarily large rigid motions, even if for element-wise small-strain motions, as discussed under assumptions (i) to (iv) at the beginning of this section.

It is worth pointing out that while arbitrarily large deformaitons (such as the straight beam folding into a circle) have been considered in the present example of a single beam, when a practical frame-structure is considered, it is unlikely that each of its members will undergo such gross deformations. Thus, inasmuch as the present element development accounts for nonlinear bending-stretching coupling, it may be sufficient to model each member of the frame by only one or two of the present elements, whose stiffness matrices are given explicitly in Chapter III. The following five numerical examples illustrate this assertion.

The first example is that of the so-called Wiliams' toggle frame, which was first treated by Williams [38] and later analyzed by Wood and Zienkiewicz [39] and Karamanlidis, Honecker, and Knothe [40]. A schematic of the structure is shown in Fig. 33a. The structure has a semispan of 12.943 (in), a raise of 0.386 (in), and is composed of two identical members, each with a rectangular cross section of width 0.753

(in), depth of 0.243 (in), and E = 1.03 x 10⁷ (psi). Each member of

the frame is modeled by a single element of the type derived in Chapter

III. Figure 33 shows the presently computed relation between the

external load P and the conjugate displacement δ, and also that between

P and the horizontal reaction (R) at the fixed end. Also, shown in

Fig. 33b are the comparison experimental results of Williams [38] as

well as the numerical solutions obtained by Wood and Zienkiewicz [39].

Excellent agreement between all the three sets of results may be noted.

However, the efficiency of the present method is clearly borne out by

the facts that: (a) the present solution uses one element to model

each member, while Ref. [39] uses five elements to model each member;

and (b) no numerical integrations are used, in the present, to derive

the tangent stiffness of the element during each step of deformation,

since an explicit expression for such is given in Chapter III.

The next two examples concern frames, with two and three members,

respectively, which bring out rather fascinating features of responses

of frames. For these examples, experimental results were reported by

Britvec and Chilver [29], while theoretical solutions for the buckling

load and post-buckling responses were also reported in [29,30]. In

these two examples, each of the members has a rectangular cross-section

of width 1.0 (in), depth 0.0625 (in), and ℓ = 20.0 (in). Also, the

buckling load of each member, when considered individually as a

pinned-pinned column, is 8.1 (1b). The schematics of the two examples

are given in Figs. 34 and 35a, respectively. In both these examples,

each member of the frames is modeled by a single element.

Each of the structures shown in Figs. 34a and 35a, respectively,

has two distinctly different post-buckling load-displacement curves,

corresponding to the two types of buckling modes, designated, respectively, as (α) and (β) in the insets of Figs. 34b and 35b. Each of the modes (α) and (β) may be excited by considering a corresponding type of load eccentricity, designated also as cases (α) and (β), respectively, in Figs. 34a and 35a.

Figure 34b shows the presently computed post-buckling P vs. δ relation for the two-member frame of Fig. 34a, along with the experimental and analytical results reported in [29,30]. The present results agree excellently with those in [29,30], except for the Mode (β) deformation, in which case, the present results are close to the analytical results of [29,30], while experiment appears to predict a much stiffer response than either the present results or the analytical results of [29,30]. Similar observations apply to the results given in Fig. 35b for the post-buckling response of the three-member frame of Fig. 35a.

The fourth example is that of a right-angled frame, shown schematically in Fig. 36a. This structure was first studied experimentally and analytically by Roorda [41] and Koiter [42], and later analyzed by Argyris and dunne [43] to demonstrate the imperfection sensitivities of structures. Recently, this problem was also analyzed in Ref. [40]. The dimensions and material properties of the members are identical to those used in Ref. [40] and are indicated in Fig. 36a. Based on the experience with the example of a beam considered in Fig. 32a, each of the members in Fig. 36a is modeled by two elements of the present type, derived in Chapter III. Five different cases of load-eccentricity, with e as marked in Fig. 36a being given the values (e/ℓ) = 0.0001; 0.01; 0.05; -0.001; -0.01,

72

respectively, are considered. Figure 36b shows the presently computed results (for each of the five e values) for the P vs. θ (the rotation at the corner, as defined in Fig. 36a) relations, along with the available numerical results of Karamanlidis, Honecker, and Knothe [40] (i.e., for (e/ℓ) = 0.01 and 0.05) and the analytical results of Koiter [42] for th case of zero eccentricity (e = 0) of the load. From Fig. 36b, it is seen that when the imperfection (e) is very small (i.e., e ≃ ±.001), the present solutions agree excellently with those of Koiter [42] (e = 0), in the range of small deformations (θ ≃ 10 degrees). However, the present numerical results indicate that the structure stiffens gradually, as the post-buckling deformation progresses. This apparent effect of very large deformations is also confirmed by Roorda's [41] experimental results. Thus, the present results appear to be accurate over a wide range of deformations. Moreover, for the values of (e/ℓ) = ≃0.001 and (e/ℓ) = 0.05, the present results are in excellent agreement with those of Karamanlidis et al. [40]. However, it should be remarked that the present solutions are based on using four elements to model this two-member frame, while Ref. [40] uses 18 elements to model the same frame. To provide a further insight into the post-buckling response, and imperfection sensitivity, of this simple frame, the presently computed variations of the displacement δ (see Fig. 36a) with load P, for each of the five values of load eccentricity, e, are shown in Fig. 36c.

The final example concerns a four-member frame subjected to point loads, as sketched in Fig. 37a. The geometric and material data of the members, which are identical, is given in Fig. 37a. Because of symmetry, one-quarter of the frame (the rectangle 1-2-3) alone is

modeled by using four elements (two each in segments 1-2 and 2-3, respectively, as in Fig. 37a). The presently computed variations of displacements δ_1 and δ_3 (as defined in Fig. 37a) with the applied load P are shown in Fig. 37b, along with comparison results of Lee et al. [44] and the theoretical results [45]. The variations of the presently computed moments M_1 and M_2 (at points 1 and 2, respectively) with the applied load are shown in Fig. 37c along with the theoretical results [45]. Figures 37b and 37c illustrate the excellent accuracy of the present sumplified method. Lastly, the profiles of deformation of the frame at various levels of applied load P are sketched in Fig. 37d.

V.2.2 Space (Three-Dimensional) Frames

Prior to consideration of space frames, we consider the case of large-deformation bending response of a single member, through the example of a cantilever beam subject to a transverse load at the tip, as shown in Fig. 38. It is seen that the present results, using just two elements agree excellently with those of Bathe and Bolourchi [33]. The relative rotation at tip, as computed from the present procedure, is shown in Fig. 29 and is found to agree excellently with an independent analytical solution.

We now consider the example of a space frame, whose geometry is identical to that of the space truss shown in Fig. 27. Here, it is assumed that the joint-design in the structure is such that each member can withstand bending moments, twisting moments, and transverse shear forces, in addition to an axial force; and hence, the structure can be modeled as a space frame. The pertinent geometric as well as material parameters of the considered space frame are indicated in Fig. 40.

The results for the case of axial loading are shown in Fig. 41. In this case, to trigger global buckling, a loading imperfection of magnitude (P/1000) is considered in the transvers direction (where 4P is the axial load) as shown in the inset of Fig. 41. Also shown in Fig. 41 is the comparison response of the structure when modeled as a space truss, with local buckling, as also shown in Fig. 28. An examination and comparison of Figs. 28 and 41 shows that the response of the space frame under an axial load system indicated in Fig. 41 is is nearly the same as that predicted when a space-truss-type model is employed and when the local (member) buckling is accounted for. (Note that both the responses, i.e., those predicted by a space-frame modeling as well as a space-truss modeling with member buckling, are considerably more flexible than that predicted by a space-truss modeling without local buckling being considered.) This points to the potential use of space-truss-type modeling with local buckling being accounted for.

The results for the case of transverse (bending) loading are shown in Fig. 42, when the structure is modeled as a space frame. Also included in Fig. 42 are the comparison results, shown earlier in Fig. 30, when the structure was modeled as a space truss and when local buckling was suppressed. A comparison of Figs. 30 and 42 again reveals that the bending response of the structure of Fig. 40, when modeled as a space frame is nearly similar to that of a space truss when local (individual) buckling is properly accounted for.

CHAPTER VI

CLOSURE

In this report, simple and effective procedures of explictly determining the tangent stiffness matrix, and an arc length method, have been presented for analyzing the large deformation and post-buckling response of (three-dimensional) space-truss and frame structures. The influence of local (member) buckling on the global response has been systematically explored. In each category of modeling of a large space structure, i.e., a space truss or a space frame, certain salient features of the present methodology are indicated below.

VI.1 Space-Truss Structures

The salient features of the present methodology are:

(1) The stiffness matrix of an individual member is formed explicitly (without element-numerical integration) in both the pre- and post-buckled ranges of behavior of each individual member.

(2) The range of validity of the invoked approximations, such that the stiffness coefficient, k, for each member has constant values in the pre- and post-buckled states respectively, has been demonstrated to cover most practical situations of space-truss structures.

(3) As the result of (1) and (2), the tangent stiffness matrix of the structure as a whole is evaluated very simply.

(4) The arc length method is efficient to trace the non-linear response of the structure beyond limit points.

(5) The consideration of the local (member) buckling is very

significant for understanding the global instability of

space-truss structures.

Thus, it can be concluded that the methodology proposed in this

report is very useful in analyzing practical space truss-type

structures.

VI.2 Space-Frame Structures

(1)   An explicit expression (i.e. requiring no further

element-numerical integration) is given for the "tangent-stiffness"

matrix of an individual element (which may then be assembled in the

usual fashion to form the "tangent-stiffness matrix" of the frame

structure).   The formulation that is employed accounts for (a)

arbitrarily large rigid rotations and translations of the individual

element, (b) the non-linear coupling between the bending and axial

stretching motions of the element. Each element can withstand bending

moments, a twisting moment, transverse shear forces, and an axial

force.

(2)   The presently proposed siimplified methodology has excellent

accuracy in that only one element may be sufficient, in most cases (of

practical interest in the behavior of structural frames), to model each

member of the frame structure. Inasmuch as the relative (non-rigid)

rotation of a differential segment of the present element is restricted

to be small, a single element alone is not enough to model the

post-buckling response of an entire beam column undergoing excessively

large deformations as in an elastica. However, when considered as a

part of a practical frame structure, the situation of each member of

the frame undergoing abnormally large deformations, as in an elastica, represents a pathological case.

(3)   Because of (1) and (2), the present method is by far the most computationally inexpensive method to analyze three-dimensional (space) frame structures and, therefore, is of considerable potential applicability in analyzing large practical space-structures.

APPENDIX A

DERIVATION OF EQ. (2.1) USING POLAR DECOMPOSITION

Deformation tensor is defined as follow [27]:

$$\underline{F} = \underline{R} \cdot \underline{U} \qquad (A.1)$$

where $\underline{F}$: Deformation tensor

   $\underline{R}$: Rotation tensor

   $\underline{U}$: Pure stretching tensor

$$
\underline{F} =
\begin{bmatrix}
1 + \dfrac{\partial u_1}{\partial x_1} & \dfrac{\partial u_1}{\partial x_2} & \dfrac{\partial u_1}{\partial x_3} \\[2ex]
\dfrac{\partial u_2}{\partial x_1} & 1 + \dfrac{\partial u_2}{\partial x_2} & \dfrac{\partial u_2}{\partial x_3} \\[2ex]
\dfrac{\partial u_3}{\partial x_1} & \dfrac{\partial u_3}{\partial x_2} & 1 + \dfrac{\partial u_3}{\partial x_3}
\end{bmatrix}
\qquad (A.2)
$$

$$
\underline{R} =
\begin{bmatrix}
\cos\theta\cos\psi\cos\phi & \cos\theta\sin\psi\cos\phi & -\sin\theta\cos\phi \\
\quad -\sin\psi\sin\phi & \quad +\cos\psi\sin\phi & \\[1ex]
-\cos\theta\cos\psi\sin\phi & -\cos\theta\sin\psi\sin\phi & \sin\theta\sin\phi \\
\quad -\sin\psi\cos\phi & \quad +\cos\psi\cos\phi & \\[1ex]
\sin\theta\cos\psi & \sin\theta\sin\psi & \cos\theta
\end{bmatrix}
\qquad (A.3)
$$

where the rotations ψ, θ, ϕ are defined as point-wise Euler angles (the order of rotation is $\psi \rightarrow \theta \rightarrow \phi$) [34].

Consider an initially straight one-dimensional member aligned initially along the x_1 axis. Then, it is appropriate to introduce the plausible kinematic assumption that the displacements u_i are functions of x_1 alone. Thus, in this case, F is approximated as:

$$F_{11} = 1 + \frac{\partial u_1}{\partial x_1} \; ; \quad F_{21} = \frac{\partial u_2}{\partial x_1} \; ; \quad F_{31} = \frac{\partial u_3}{\partial x_1} \qquad (A.4)$$

Thus, $F_{i1} \neq 0$ ($i = 1,2,3$) and all other $F_{ij} = 0$. Likewise, the stretch tensor U may be approximated as:

$$U_{11} = (1 + \varepsilon) \; ; \quad U_{22} = 1 \; ; \quad U_{33} = 1 \qquad (A.5)$$

and all other U_{ij} are zero. For the present kinematic assumptions, one obtains:

$$F_{i1} = R_{ik} U_{k1} \qquad [i = 1,2,3; \; k = 1,2,3]$$

or

$$1 + \frac{\partial u_1}{\partial x_1} = (1 + \varepsilon)[\cos\theta\cos\psi\cos\phi - \sin\psi\sin\phi] \qquad (A.5)$$

$$\frac{\partial u_2}{\partial x_1} = (1 + \varepsilon)[-\cos\theta\cos\psi\sin\phi - \sin\psi\cos\phi]$$

80

$$\frac{\partial u_3}{\partial x_1} = (1 + \varepsilon)\sin\theta\cos\psi$$

On the other hand, if the member is initially along x_3 axis, one may introduce the kinematic assumptions:

$$F_{13} = \frac{\partial u_1}{\partial x_3} \; ; \quad F_{23} = \frac{\partial u_2}{\partial x_3} \; ; \quad F_{33} = 1 + \frac{\partial u_3}{\partial x_3} \qquad (A.6)$$

$$U_{11} = 1 \; ; \quad U_{22} = 1 \; ; \quad U_{33} = (1 + \varepsilon)$$

$$\frac{\partial u_1}{\partial x_3} = - (1 + \varepsilon)\sin\theta\cos\phi \; ; \quad \frac{\partial u_2}{\partial x_3} = (1 + \varepsilon)\sin\theta\sin\phi \; ;$$

$$1 + \frac{\partial u_3}{\partial x_3} = (1 + \varepsilon)\cos\theta$$

Thus, in general, from (A.5) and (A.6) one obtains:

$$\delta = [(\bar{u}_1)^2 + (\bar{u}_2)^2 + (\bar{u}_3 + \ell)^2]^{\frac{1}{2}} - \ell$$

81

APPENDIX B

POST-BUCKLING BEHAVIOR OF A TRUSS MEMBER

In this appendix, Eq. (2.3b) for the post-buckled state of the truss member is derived.

Consider the truss member being subjected to the compressive force (-N), as shown in Fig. 1. When N satisfies Eq. (2.4), this member undergoes bifurcation buckling. From the detailed treatment of the elastica problem given in Ref. [28], the post-buckling behavior of this member, treated as a simply-supported beam, is governed by the following equations:

$$\ell = \frac{1}{f} \cdot F(\beta) \tag{B.1a}$$

$$\ell + \hat{\delta} = \frac{2}{f} \cdot E(\beta) - \ell \tag{B.1b}$$

$$\bar{\delta} = \frac{2}{f} \cdot \beta \tag{B.1c}$$

where

$$F(\beta) = \int_{-\frac{\pi}{2}}^{\frac{\pi}{2}} \frac{d\phi}{\sqrt{1 - \beta^2 \sin^2 \phi}}$$

$$E(\beta) = \int_{-\frac{\pi}{2}}^{\frac{\pi}{2}} \sqrt{1 - \beta^2 \sin^2 \phi} \cdot d\phi$$

$$f^2 = -\frac{N}{EI} , \quad \beta = \sin\left(\frac{\alpha}{2}\right)$$

$$\alpha = \left. \hat{\theta} \right|_{u_3=0} = -\left. \hat{\theta} \right|_{u_3=\ell} \tag{B.2}$$

and $F(\beta)$, $E(\beta)$ are the elliptic integrals of the first and the second kind, respectively. Also, $\hat{\delta}$ is the stretch after the buckling of the member; and $\hat{\delta}$ is the lateral deflection at the middle of the centroidal axis of the element. Note that the total stretch δ is given by the sum of $\hat{\delta}$ and the stretch, $^{cr}N \cdot \ell/EA$, before the buckling of the member. Also, it should be noted that in the derivation of Eqs. (B.1), the change in the length of the member due to the compressive force is neglected.

Equations (B.1) give the exact relations between N, $\hat{\delta}$, and $\tilde{\delta}$ in the post-buckled range, except for the assumption concerning the length of the element. We now simplify and modify these relations to a form more useful for the present purposes of evaluating a tangent stiffness matrix. To this end, we start by expanding $F(\beta)$, $E(\beta)$ in terms of β [see Ref. 35].

$$F(\beta) = \pi + \frac{1}{2} \beta^2 \cdot S_2 + \frac{1 \cdot 3}{2 \cdot 4} \cdot \beta^4 \cdot S_4 + \dots \tag{B.3a}$$

83

$$E(\beta) = \pi - \frac{1}{2} \beta^2 \cdot S_2 - \frac{1}{2 \cdot 4} \cdot \beta^4 \cdot S_4 + \ldots \qquad \text{(B.3b)}$$

where

$$S_n = \int_{-\frac{\pi}{2}}^{\frac{\pi}{2}} \sin^n \phi \cdot d\phi \qquad \text{(B.4)}$$

We shall retain the terms of Eqs. (B.3) up to the second order for the approximations of $F(\beta)$, $E(\beta)$:

$$F(\beta) = \pi + \frac{\pi}{4} \cdot \beta^2 \qquad \text{(B.5a)}$$

$$E(\beta) = \pi - \frac{\pi}{4} \cdot \beta^2 \qquad \text{(B.5b)}$$

The range of validity of these approximations will be demonstrated momentarily.

Then, Eqs. (B.1a) and (B.1b), respectively, become:

$$\ell = \frac{1}{f} \left(\pi + \frac{\pi}{4} \beta^2 \right) \qquad \text{(B.6a)}$$

$$\ell + \hat{\delta} = \frac{2}{f} \left(\pi - \frac{\pi}{4} \beta^2 \right) - \ell \qquad \text{(B.6b)}$$

From Eqs. (B.6) one obtains:

84

$$4\ell + \hat{\delta} = \frac{4}{f} \cdot \pi \qquad\qquad (B.7)$$

Noting that $f^2 = (-N/EI)$, one sees from Eq. (B.7):

$$N = N^{(cr)} \frac{1}{(1 + \frac{\hat{\delta}}{4\ell})^2} \qquad\qquad (B.8)$$

where $N^{(cr)}$ is the critical axial force for bifurcation buckling as given in Eq. (2.5).

For small values of $-(\hat{\delta}/\ell)$, Eq. (B.8) may be approximated as:

$$N = N^{(cr)}[1 - \frac{1}{2}(\frac{\hat{\delta}}{\ell})] \qquad\qquad (B.9)$$

The incremental form of Eq. (B.9) results in Eq. (2.3). The linear relation (B.9), and its incremental counterpart, are useful in tangent stiffness evaluations.

We now derive the relation between $\hat{\delta}$ and $\tilde{\delta}$. This relation is not necessary for the construction of the tangent stiffness, but it is useful for the determination of maximum and/or minimum stress in each of the members.

Noting that β is non-negative except for $\alpha > 2\pi$, one obtains from Eq. (B.6a):

$$\beta = 2\sqrt{\frac{1}{\pi} \cdot f \cdot \ell - 1} \qquad\qquad (B.10)$$

Substituting Eq. (B.10) into Eq. (B.1c), it is seen that:

$$\bar{\delta} = \frac{4}{\pi} \cdot \sqrt{\frac{1}{\pi} \cdot f \cdot \ell - 1} \qquad (B.11)$$

Substituting for f in terms of N and using Eq. (B.8), the following relation between $\hat{\delta}$ and $\tilde{\delta}$ is obtained:

$$\frac{\bar{\delta}}{\ell} = \frac{4}{\pi} \cdot \sqrt{-\frac{\hat{\delta}}{4\ell}\left(1 + \frac{\hat{\delta}}{4\ell}\right)} \qquad (B.12)$$

Thus, when the axial contraction $\hat{\delta}$ is solved for from the finite element stiffness equation, Eq. (B.12) may be used to calculate the transverse displacement $\tilde{\delta}$ at midspan of the member; and from it, one may calculate the maximum or minimum stress in the member.

Figure 43 shows the relations between N, $\hat{\delta}$, and $\tilde{\delta}$ as given by Eqs. (B.9) and (B.12) and their comparisons with the exact solutions for the elastica problem. The dotted lines indicate the present solutions and the solid ones indicate the exact. From this figure, it is seen that Eqs. (B.9) and (B.12) are good approximations in the range of values for $-(\hat{\delta}/\ell)$ and $(\tilde{\delta}/\ell)$ being smaller than about 0.15 and 0.25, respectively. It is also seen that this range of values for $-(\hat{\delta}/\ell)$ and $(\tilde{\delta}/\ell)$ is typical in the problem of local (member) buckling in a practical truss structure.

86

APPENDIX C

COORDINATION TRANSFORMATION OF ROTATIONS

The coordinate transformation for semi-tangential rotations from the global to the local system is considered as a usual coordinate transformation, because a rotation vector can be defined, when semi-tangential rotations are used as rotational variables.

Therefore, using a rotation vector $\underset{\sim}{R}$, from Fig. 44, the following equations are obtained:

$$\underset{\sim}{R} = \tan \frac{\overset{\textcircled{H}}{\theta_i}}{2} \underset{\sim}{e}_i \qquad (C.1)$$

$$= \tan \frac{\theta_i}{2} \underset{\sim}{e}'_i \qquad (C.2)$$

From Eq. (C.1) and (C.2),

$$\tan \frac{\theta_i}{2} = c_{ij} \cdot \tan \frac{\overset{\textcircled{H}}{\theta_j}}{2} \qquad (i,j = 1,2,3) \qquad (C.3)$$

where c_{ij}: direction cosines: $c_{ij} = \underset{\sim}{e}_i \cdot \underset{\sim}{e}'_j$

Finally, the following relations are obtained.

$$\theta_i = 2 \cdot \tan^{-1}\left(c_{ij} \cdot \tan \frac{\overset{\textcircled{H}}{\theta_j}}{2} \right) \qquad (C.4)$$

APPENDIX D

REPRESENTATIONS OF MATRICES FORMING TANGENT STIFFNESS MATRIX OF A FRAME MEMBER

The vectors for representing Eq. (3.86), herein, are defined as:

$$\underset{\sim}{M}^t = \lfloor\ {}^a\hat{M}_1 \quad {}^s\hat{M}_1 \quad {}^a\hat{M}_2 \quad {}^s\hat{M}_2 \quad \hat{M}_3\ \rfloor \tag{D.1}$$

$$\underset{\sim}{T}^t = \lfloor\ {}^a\hat{\theta}_2 \quad {}^s\hat{\theta}_2 \quad {}^a\hat{\theta}_1 \quad {}^s\hat{\theta}_1 \quad \hat{\theta}_3\ \rfloor \tag{D.2}$$

$$\underset{\sim}{C}^t = \lfloor\ \frac{EI_1}{\ell\,{}^ah_1} \quad \frac{EI_1}{\ell\,{}^sh_1} \quad \frac{EI_2}{\ell\,{}^ah_2} \quad \frac{EI_2}{\ell\,{}^sh_2} \quad \frac{GJ}{\ell}\ \rfloor \tag{D.3}$$

$$\equiv (\underset{\sim}{A} \cdot \underset{\sim}{J})^t \tag{D.4}$$

$$\underset{\sim}{I}^t = \lfloor\ -1 \quad 1\ \rfloor \tag{D.5}$$

$$\underset{\sim}{E} = \begin{bmatrix} 1 & -1 \\ -1 & 1 \end{bmatrix} \tag{D.6}$$

$$\underline{D}^t = \left\lfloor \ell \frac{d}{dn_1} \left(\frac{1}{{}^a h_1}\right) \quad \ell \frac{d}{dn_1} \left(\frac{1}{{}^s h_1}\right) \quad \ell \frac{d}{dn_2} \left(\frac{1}{{}^a h_2}\right) \quad \ell \frac{d}{dn_2} \left(\frac{1}{{}^s h_2}\right) \quad 0 \right\rfloor \qquad (D.7)$$

$$= \left(\underline{\underline{B}} \cdot \underline{J}\right)^t \qquad (D.8)$$

$$\underline{J} = \text{unit vector} \qquad (5 \times 1) \qquad (D.9)$$

1. $\underline{A}_{dd}$

$\underline{A}_{dd}$ is represented as a (12 × 12) matrix as shown in Table (D.1), which the components F_{ij}, ${}^m G_{ij}$, and ${}^{mn} H_{ij}$ are given by:

$$F_{ij} = M_k \cdot \frac{\partial^2 T_k}{\partial \bar{u}_i \partial \bar{u}_j} + \frac{\partial T_k}{\partial \bar{u}_i} \cdot A_{k\ell} \cdot \frac{\partial T_\ell}{\partial \bar{u}_j} + \hat{N} \frac{\partial^2 \delta}{\partial \bar{u}_i \partial \bar{u}_j} \qquad (D.10)$$

$$^m G_{ij} = M_k \cdot \frac{\partial^2 T_k}{\partial \bar{u}_i \partial ({}^m \theta_j)} + \frac{\partial T_k}{\partial \bar{u}_i} \cdot A_{k\ell} \cdot \frac{\partial T_\ell}{\partial ({}^m \theta_j)} \qquad (D.11)$$

$$^{mn} H_{ij} = M_k \cdot \frac{\partial^2 T_k}{\partial ({}^m \theta_i) \partial ({}^n \theta_j)} + \frac{\partial T_k}{\partial ({}^m \theta_i)} \cdot A_{k\ell} \cdot \frac{\partial T_\ell}{\partial ({}^n \theta_j)} \qquad (D.12)$$

where $i, j = 1, 2, 3$; $m, n = 1, 2$

89

2. $\underline{A}_{nd}$

$\underline{A}_{nd}$ is represented as a (12×1) vector as shown in Table D.2, which the components L_i and ^jN_i are given by:

$$L_i = T_k \cdot B_{k\ell} \cdot \frac{\partial T_\ell}{\partial \bar{u}_i} + \frac{\partial \delta}{\partial \bar{u}_i} \qquad \text{(D.13)}$$

$$^jN_i = T_k \cdot B_{k\ell} \cdot \frac{\partial T_\ell}{\partial (^j\theta_i)} \qquad \text{(D.14)}$$

where $i = 1,2,3 \; ; \; j = 1,2$

3. A_{nn}

A_{nn} is a scalar factor as follows.

$$A_{nn} = \frac{\ell^3}{2EI_1} \cdot \left[\, ^a\hat{\theta}_2^2 \cdot \frac{d^2}{dn_1^2} \left(\frac{1}{^ah_1}\right) + \, ^s\hat{\theta}_2^2 \cdot \frac{d^2}{dn_1^2} \left(\frac{1}{^sh_1}\right) \right] \qquad \text{(D.15)}$$

$$+ \frac{\ell^3}{2EI_2} \cdot \left[\, ^a\hat{\theta}_1^2 \cdot \frac{d^2}{dn_2^2} \left(\frac{1}{^ah_2}\right) + \, ^s\hat{\theta}_1^2 \cdot \frac{d^2}{dn_2^2} \left(\frac{1}{^sh_2}\right) \right]$$

$$- \frac{\ell}{EA}$$

90

4. $\underset{\sim}{B}_d$

$\underset{\sim}{B}_d$ is represented as a (12 × 1) vector as shown in Table D.3, which the components R_i and ^jS_i are given by:

$$R_i = M_k \cdot \frac{\partial T_k}{\partial \tilde{u}_i} + \hat{N} \frac{\partial \delta}{\partial \tilde{u}_i} \qquad (D.16)$$

$$^jS_i = M_k \cdot \frac{\partial T_k}{\partial (^j\theta_i)} \qquad (D.17)$$

where $i = 1,2,3 \; ; \quad j = 1,2$

5. B_n

B_n is a scalar factor as follows.

$$B_n = \frac{\ell}{2} \left[\, ^a\hat{\theta}_2^2 \cdot \frac{d}{dn_1} \left(\frac{1}{^a h_1}\right) + \, ^s\hat{\theta}_2^2 \cdot \frac{d}{dn_1} \left(\frac{1}{^s h_1}\right) \right. \qquad (D.18)$$

$$+ \, ^a\hat{\theta}_1^2 \cdot \frac{d}{dn_2} \left(\frac{1}{^a h_2}\right) + \, ^s\hat{\theta}_1^2 \cdot \frac{d}{dn_2} \left(\frac{1}{^s h_2}\right) \left. \right]$$

$$+ \, \delta - \frac{\ell \cdot \hat{N}}{EA}$$

APPENDIX E

APPROXIMATIONS OF RELATION BETWEEN TOTAL AND RELATIVE ROTATIONS
OF A FRAME MEMBER

It is necessary that Eqs. (3.31) and (3.32) are approximated to form the tangent stiffness matrix for frame-type elements because Eqs. (3.31) and (3.32) have high order terms and are too complicated to formulate. To keep simplicity of the formulations and get the original purpose, the following approximations from Eqs. (3.24), (3.27), and (3.28) need to be considered at most on Eqs. (3.31) and (3.32).

$$\tan \frac{^1\hat{\theta}_1}{2} = - (h \cdot {}^1A + \ell \cdot {}^1B + m \cdot {}^1C) \qquad (E.1)$$

$$\tan \frac{^1\hat{\theta}_2}{2} = - (h \cdot {}^1D + \ell \cdot {}^1E + m \cdot {}^1F) \qquad (E.2)$$

$$\tan \frac{^1\hat{\theta}_3}{2} = - (h \cdot r + \ell \cdot s + m \cdot t) \qquad (E.3)$$

$$\tan \frac{^2\hat{\theta}_1}{2} = \tan \frac{^1\hat{\theta}_1}{2} + \left(\tan \frac{^2\theta_1}{2} - \tan \frac{^1\theta_1}{2}\right) \cdot {}^1A + \left(\tan \frac{^2\theta_2}{2} - \tan \frac{^1\theta_2}{2}\right) \cdot {}^1B$$

92

$$+ \left(\tan \frac{^2\theta_3}{2} - \tan \frac{^1\theta_3}{2} \right) \cdot ^1C \qquad \qquad \text{(E.4)}$$

$$\tan \frac{^2\hat{\theta}_2}{2} = \tan \frac{^1\hat{\theta}_2}{2} + \left(\tan \frac{^2\theta_1}{2} - \tan \frac{^1\theta_1}{2} \right) \cdot ^1D + \left(\tan \frac{^2\theta_2}{2} - \tan \frac{^1\theta_2}{2} \right) \cdot ^1E$$

$$+ \left(\tan \frac{^1\theta_3}{2} - \tan \frac{^2\theta_3}{2} \right) \cdot ^1F \qquad \qquad \text{(E.5)}$$

$$\tan \frac{^2\hat{\theta}_3}{2} = \tan \frac{^1\hat{\theta}_3}{2} + \left(\tan \frac{^2\theta_1}{2} - \tan \frac{^1\theta_1}{2} \right) \cdot r + \left(\tan \frac{^2\theta_2}{2} - \tan \frac{^1\theta_2}{2} \right) \cdot s$$

$$+ \left(\tan \frac{^1\theta_3}{2} - \tan \frac{^2\theta_3}{2} \right) \cdot t \qquad \qquad \text{(E.6)}$$

Substituting Eqs. (3.14), (3.15), and (3.24) into Eqs. (E.1) to (E.3), one obtains the following equations as:

$$\tan \frac{^1\hat{\theta}_1}{2} = \frac{1}{1 + e} \left[2r \cdot \left(\tan \frac{^1\theta_1}{2} \tan \frac{^1\theta_2}{2} - \tan \frac{^1\theta_3}{2} \right) \right. \qquad \text{(E.7)}$$

$$+ s \cdot \left(1 - \tan^2 \frac{^1\theta_1}{2} + \tan^2 \frac{^1\theta_2}{2} - \tan^2 \frac{^1\theta_3}{2} \right) + 2t \cdot \left(\tan \frac{^1\theta_2}{2} \tan \frac{^1\theta_3}{2} + \tan \frac{^1\theta_1}{2} \right) \left. \right\}$$

$$\tan \frac{{}^1\hat{\theta}_2}{2} = \frac{-1}{1+e} \{r \cdot (1 + \tan^2 \frac{{}^1\theta_1}{2} - \tan^2 \frac{{}^1\theta_2}{2} - \tan^2 \frac{{}^1\theta_3}{2}) \qquad (E.8)$$

$$+ 2s \cdot (\tan \frac{{}^1\theta_1}{2} \cdot \tan \frac{{}^1\theta_2}{2} + \tan\frac{{}^1\theta_3}{2})$$

$$+ 2t \cdot (\tan \frac{{}^1\theta_1}{2} \cdot \tan \frac{{}^1\theta_3}{2} - \tan\frac{{}^1\theta_2}{2}) \}$$

$$\tan \frac{{}^1\hat{\theta}_3}{2} = 0 \qquad (E.9)$$

where $e = {}^1G \cdot r + {}^1H \cdot s + {}^1I \cdot t$

Equations (E.4) to (E.9) are the approximated relations between the relative and total (rigid plus relative) rotations for forming the tangent stiffness matrix of the element.

94

APPENDIX F

TABLES

Table 1 Cross-sectional areas of the members
of Thompson's strut structure

Member's Number	Case 1, 2	Case 3	Case 4
1-13, 17-21	$54.84(\text{cm})^2$	54.84	54.84
15	54.84	51.61	54.84
14, 16	54.84	54.84	51.61
22 - 35	51.61	51.61	51.61

All members have solid circular cross sections.

Young's modulus is 7.03×10^5 (kg/cm^2).

In Case 1, the local buckling of individual is not considered.

Table 2(a)   Nodal coordinates of the arch-truss structure

Nodal Number	z Coordinate	x Coordinate
1, 19	∓ 3429.0	0.00
·2, 18	∓ 3048.0	50.65
3, 17	∓ 2667.0	34.75
4, 16	∓ 2286.0	83.82
5, 15	∓ 1905.0	65.30
6, 14	∓ 1524.0	110.85
7, 13	∓ 1143.0	87.99
8, 12	∓ 762.0	128.50
9, 11	∓ 381.0	100.05
10	0.0	134.6

In the second column, (−) and (+) respectively indicate the z-coordinates of the first and second members identified in the first column.

Table 2(b) Cross-sectional areas of the members
of the arch-truss structure

Member's Number	Case 1, 2	Case 3
1 - 10, 35	51.61(cm^2)	51.61
11, 12	64.52	64.52
13 - 16	83.87	83.87
17, 18	96.77	96.77
19 - 22	103.23	103.23
23, 24	161.29	161.29
25, 26	193.55	193.55
27, 28	258.06	193.55
29 - 32	290.32	290.32
33, 34	309.68	309.68

All members have solid circular cross sections.

Young's modulus is $7.03 \times 10^5 (kg/cm^2)$.

In Case 1, the local buckling of individual members is not considered.

Table 3 Thompson's strut structure with global imperfections

All members have solid circular cross sections, with areas as follows:

No. 1 – No. 21 ---------- 54.84(cm^2)

No. 22 – No. 35 ---------- 51.61(cm^2)

Young's modulus is 7.03 x 10^5(kg/cm^2).

	Member's Buckling	System Imperfection*
Case 1	No	No
Case 2	Yes	No
Case 3	Yes	Yes Maximum value of the imperfection is 1.32(cm)
Case 4	Yes	Yes Maximum value of the imperfection is 2.64(cm)

* Imperfection mode is of a half sine wave shape, from node no. 1 to node no. 19; and the initial x positions of the nodes are located along the half sine wave.

Table 4. Coordinates of the Nodes of Example 1

node	(1) Perfect Geometry x_1	x_2	x_3	(2) Imperfect Geometry x_3
1	0.0	0.0	0.0	0.0
2	25.0	0.0	2.0	1.8
3	12.5	-21.65	2.0	2.0
4	-12.5	-21.65	2.0	2.0
5	-25.0	0.0	2.0	1.8
6	-12.5	21.65	2.0	2.0
7	12.5	21.65	2.0	2.0
8	43.30	-25.0	8.216	8.216
9	0.0	-50.0	8.216	8.216
10	-43.30	-25.0	8.216	8.216
11	-43.30	25.0	8.216	8.216
12	0.0	50.0	8.216	8.216
13	43.30	25.0	8.216	8.216

Table D.1. Matrix of $\underset{\approx}{A}_{dd}$

	$^1u_1$ $^2u_1$	$^1u_2$ $^2u_2$	$^1u_3$ $^2u_3$	$^1\theta_1$	$^2\theta_1$	$^1\theta_2$	$^2\theta_2$	$^1\theta_3$	$^2\theta_3$
$^1u_1$ $^2u_1$	$F_{11}\cdot\underset{\approx}{E}$	$F_{12}\cdot\underset{\approx}{E}$	$F_{13}\cdot\underset{\approx}{E}$	$^1G_{11}\cdot\underline{I}$	$^2G_{11}\cdot\underline{I}$	$^1G_{12}\cdot\underline{I}$	$^2G_{12}\cdot\underline{I}$	$^1G_{13}\cdot\underline{I}$	$^2G_{13}\cdot\underline{I}$
$^1u_2$ $^2u_2$		$F_{22}\cdot\underset{\approx}{E}$	$F_{23}\cdot\underset{\approx}{E}$	$^1G_{21}\cdot\underline{I}$	$^2G_{21}\cdot\underline{I}$	$^1G_{22}\cdot\underline{I}$	$^2G_{22}\cdot\underline{I}$	$^1G_{23}\cdot\underline{I}$	$^2G_{23}\cdot\underline{I}$
$^1u_3$ $^2u_3$			$F_{33}\cdot\underset{\approx}{E}$	$^1G_{31}\cdot\underline{I}$	$^2G_{31}\cdot\underline{I}$	$^1G_{32}\cdot\underline{I}$	$^2G_{32}\cdot\underline{I}$	$^1G_{33}\cdot\underline{I}$	$^2G_{33}\cdot\underline{I}$
$^1\theta_1$				$^{11}H_{11}$	$^{12}H_{11}$	$^{11}H_{12}$	$^{12}H_{12}$	$^{11}H_{13}$	$^{12}H_{13}$
$^2\theta_1$		Symmetry			$^{22}H_{11}$	$^{21}H_{12}$	$^{22}H_{12}$	$^{21}H_{13}$	$^{22}H_{13}$
$^1\theta_2$						$^{11}H_{22}$	$^{12}H_{22}$	$^{11}H_{23}$	$^{12}H_{23}$
$^2\theta_2$							$^{22}H_{22}$	$^{21}H_{23}$	$^{22}H_{23}$
$^1\theta_3$								$^{11}H_{33}$	$^{12}H_{33}$
$^2\theta_3$									$^{22}H_{33}$

Table D.2. Vector of $\underset{\sim}{A}_{nd}$ Table D.3. Vector of $\underset{\sim}{B}_{d}$

$$
\left\{
\begin{array}{c}
L_1 \cdot \underline{\underline{I}} \\
L_2 \cdot \underline{\underline{I}} \\
L_3 \cdot \underline{\underline{I}} \\
{}^{1}N_1 \\
{}^{2}N_1 \\
{}^{1}N_2 \\
{}^{2}N_2 \\
{}^{1}N_3 \\
{}^{2}N_3
\end{array}
\right\}
\qquad\qquad
\left\{
\begin{array}{c}
R_1 \cdot \underline{\underline{I}} \\
R_2 \cdot \underline{\underline{I}} \\
R_3 \cdot \underline{\underline{I}} \\
{}^{1}S_1 \\
{}^{2}S_1 \\
{}^{1}S_2 \\
{}^{2}S_2 \\
{}^{1}S_3 \\
{}^{2}S_3
\end{array}
\right\}
$$

APPENDIX G

ILLUSTRATIONS
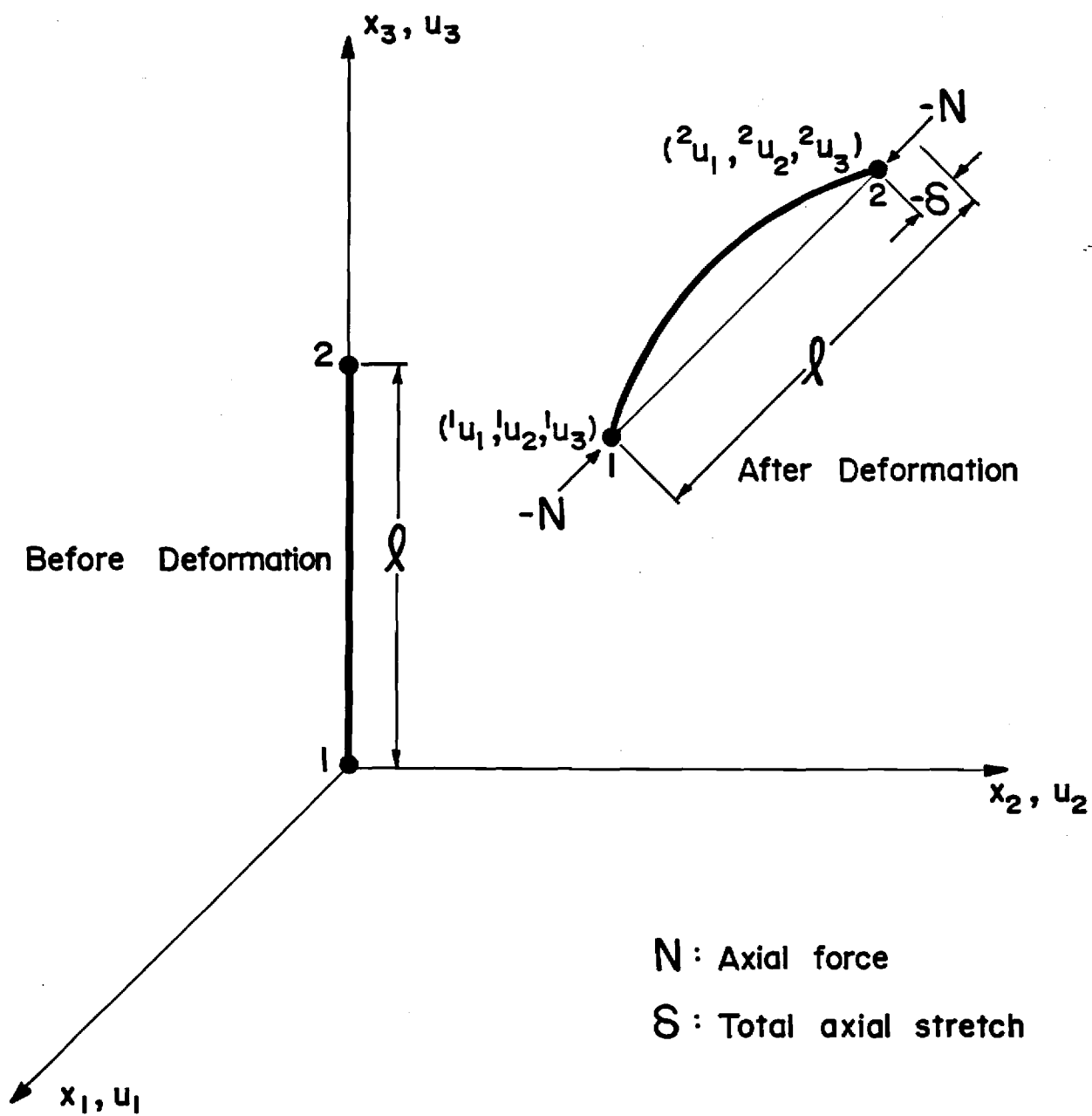
Fig. 1. Nomenclature for Kinematics of Deformation of a Space Truss Member.

N : Axial force

δ : Total axial stretch
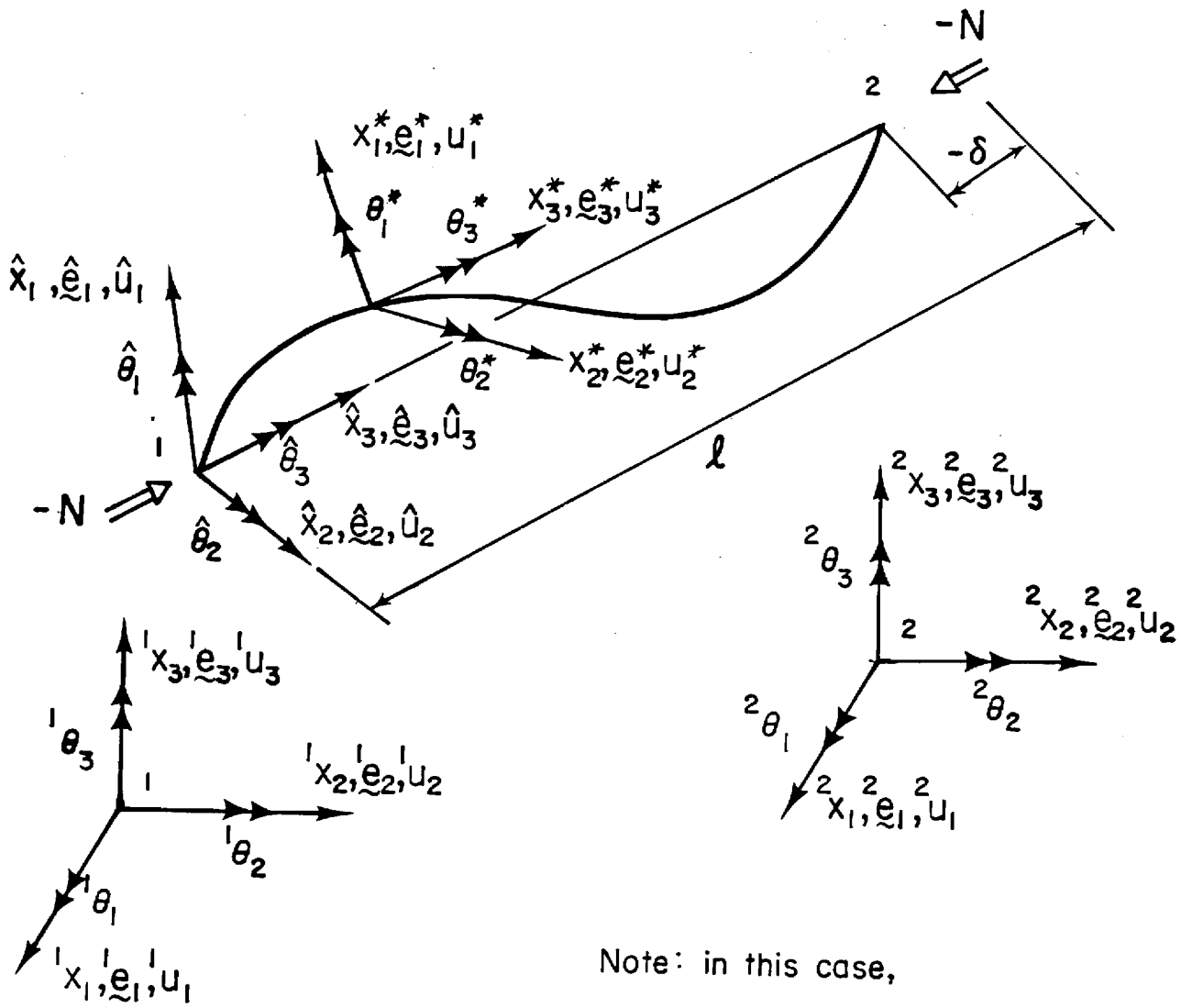
Fig. 2. Nomenclature for Kinematics of Deformation of a Space Framed Member
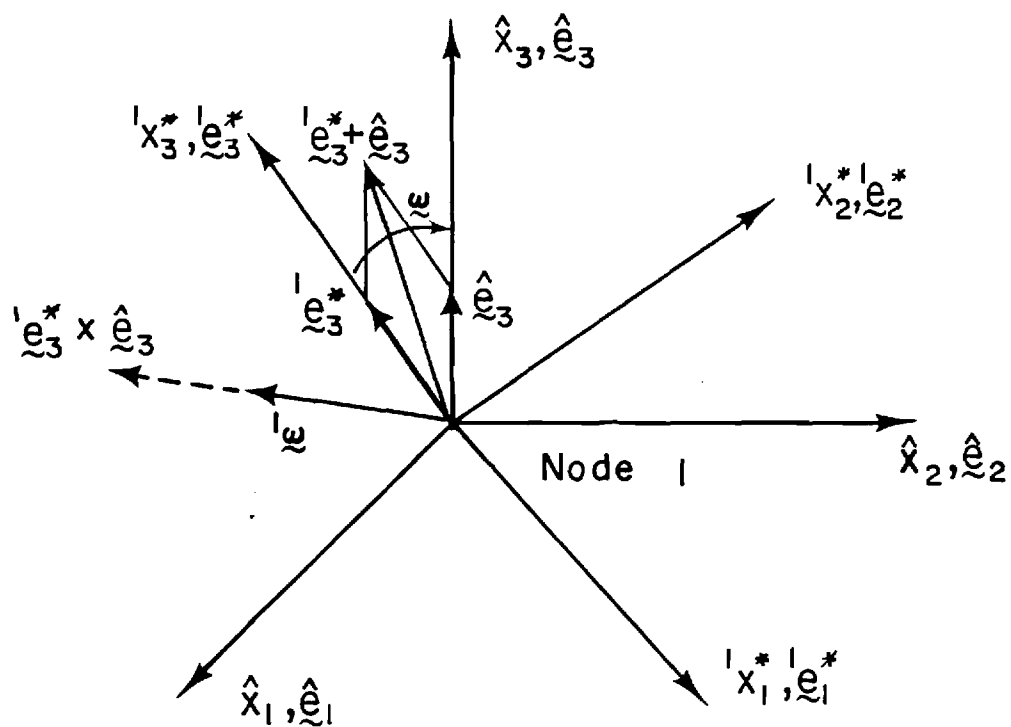
Fig. 3. Nomenclature for Transformation of Vectors by a Finite Rotation Vector $^1\underset{\sim}{w}$ at Node 1 of a Framed Member
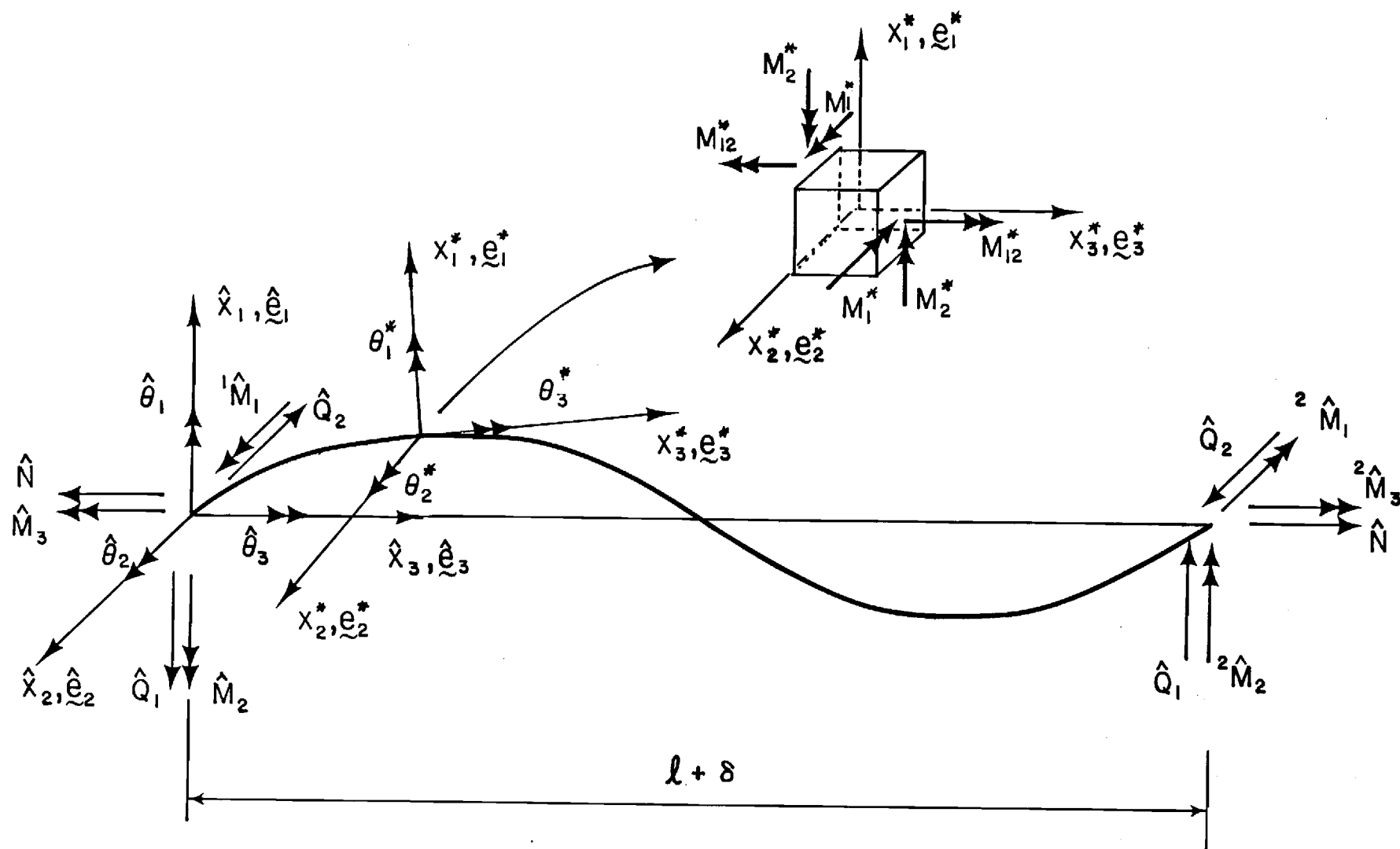
Fig. 4. Sign-Convention for System of Generalized Force on a Framed Member
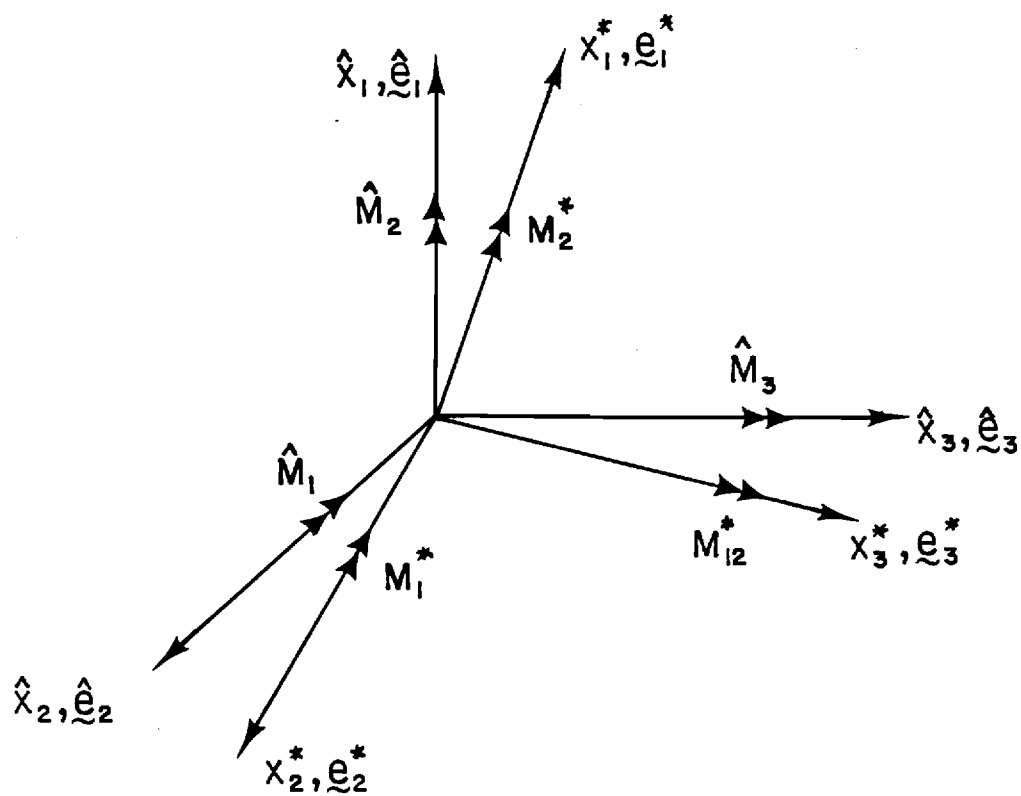
Fig. 5.   Representation of Moments M* and $\hat{M}$ of a
          Framed Member

108
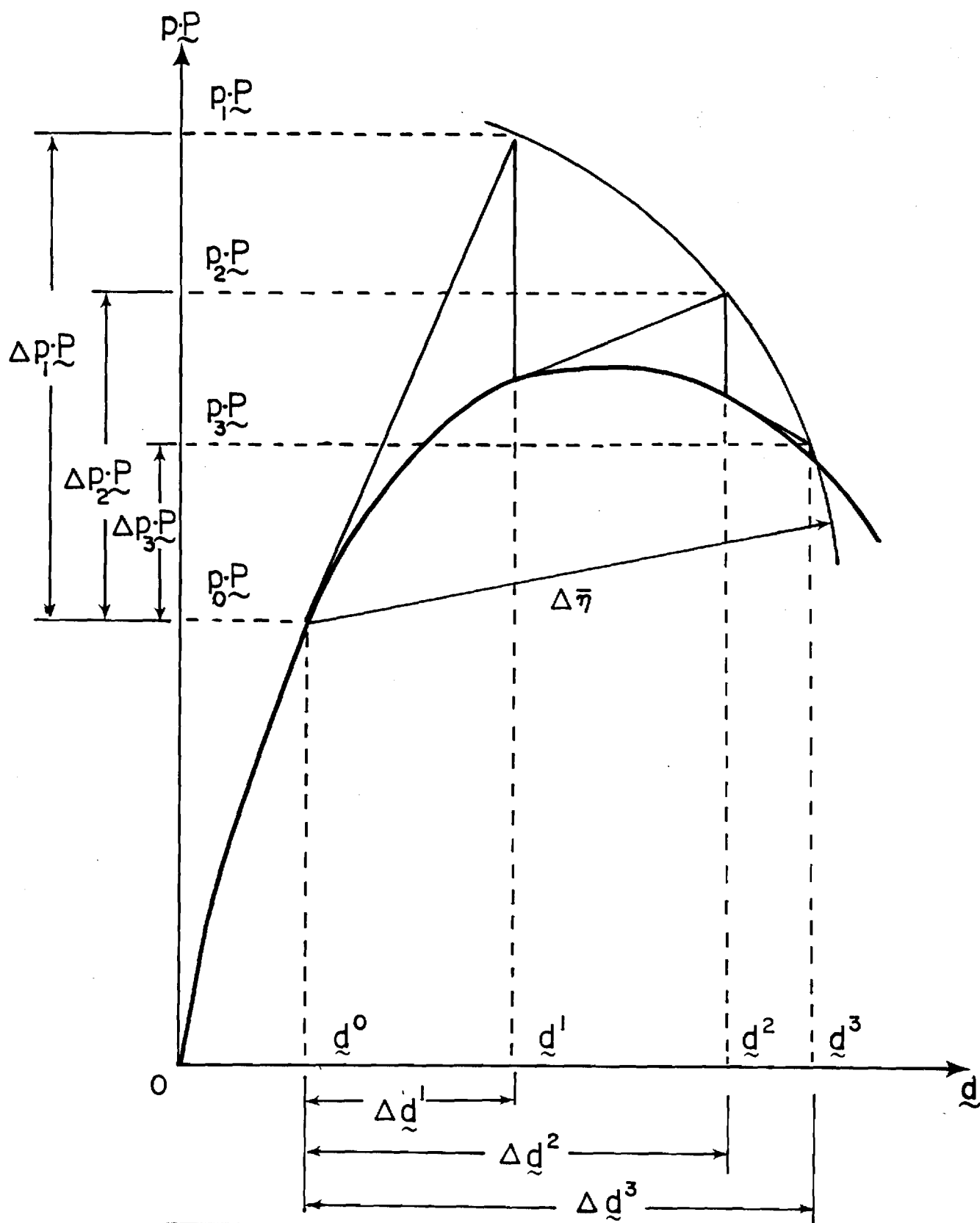
Fig. 6.   A Schematic Representation of the Arc-Length
Method for a One-Degree-of-Freedom System
($\gamma = 1$) with Newton-Raphson Procedure

109
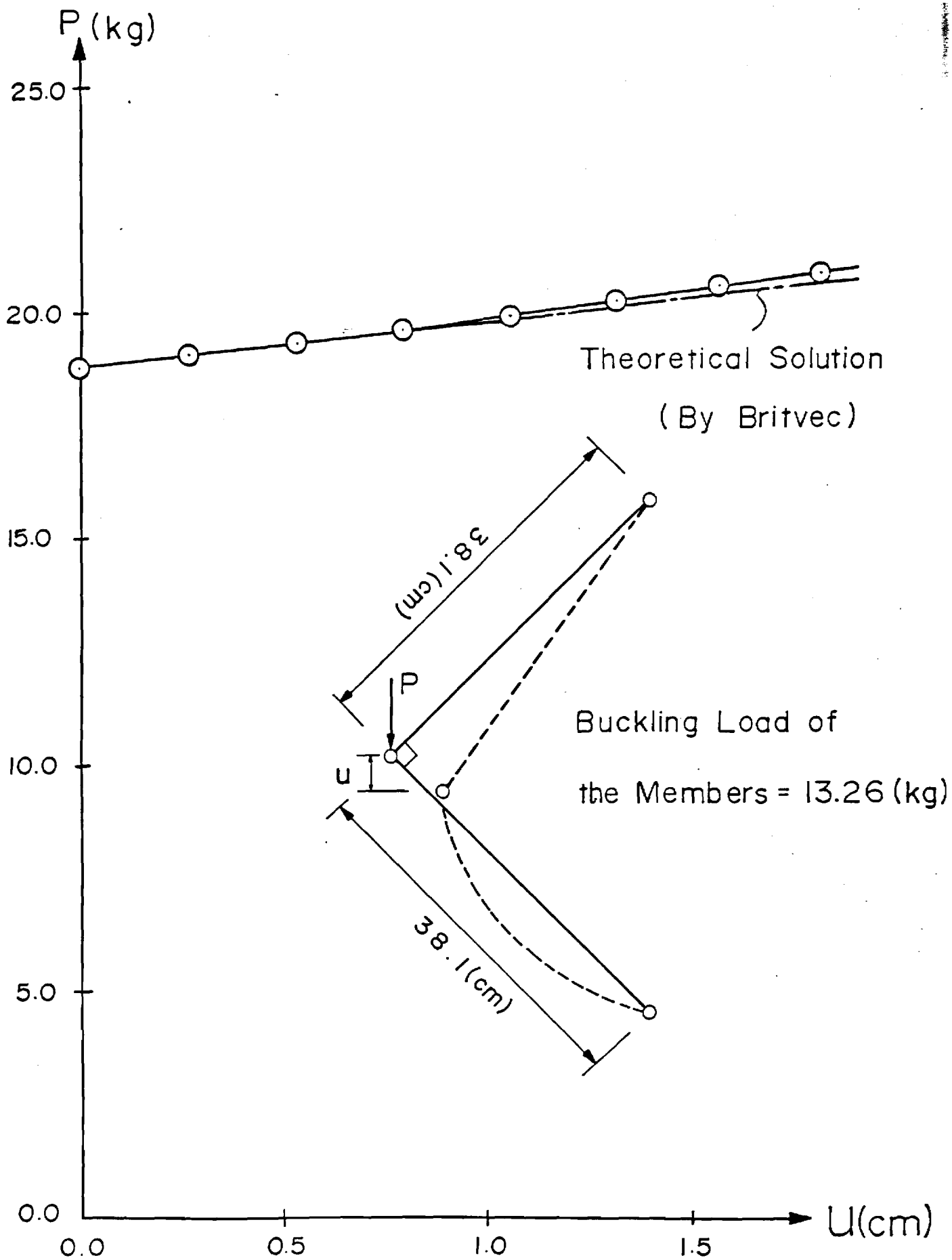
Fig. 7a. Britvec's Truss Structure (Example 1)
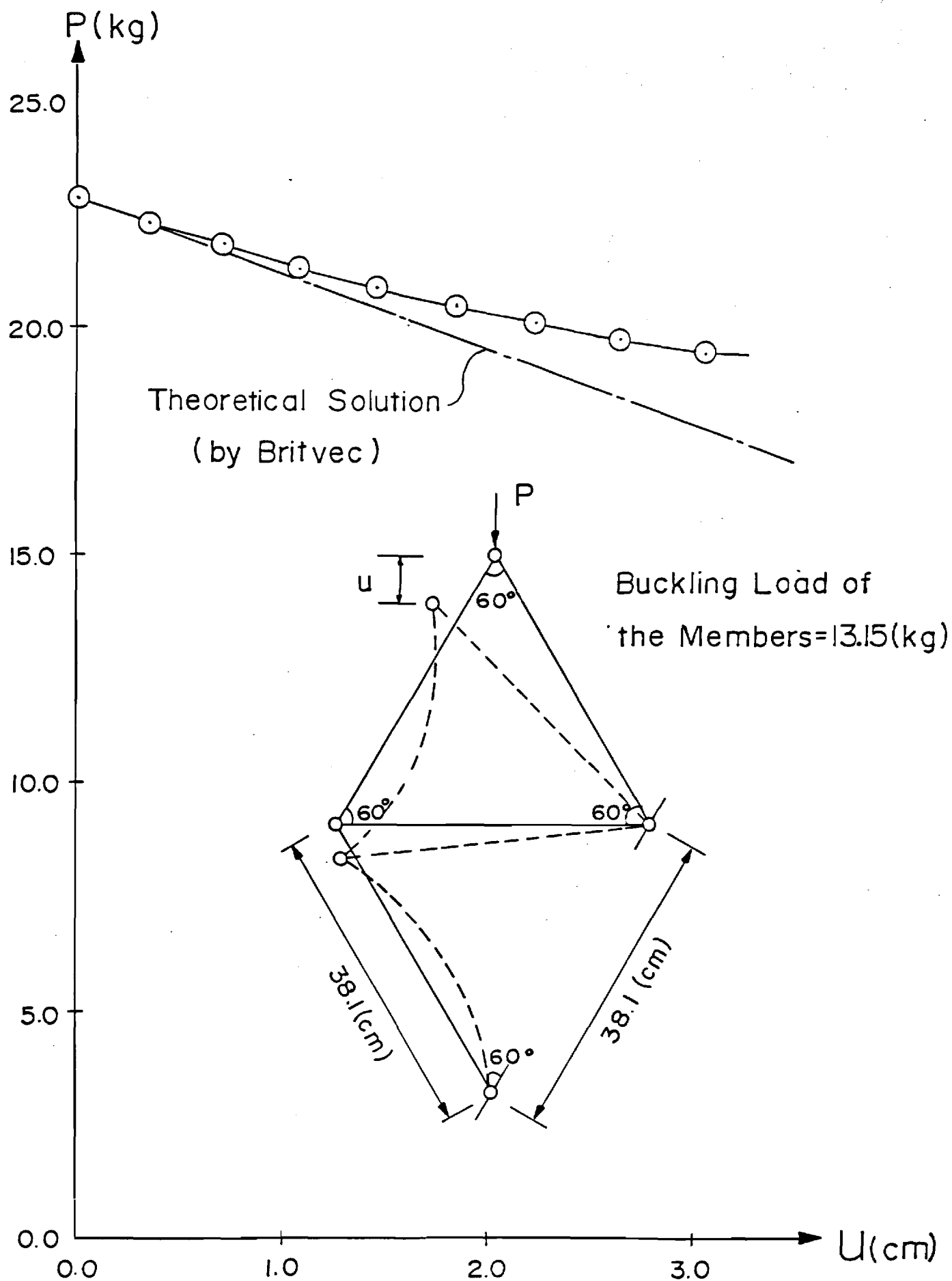
Fig. 7b. Britvec's Truss Structure (Example 2)

$$L = 38.1 \text{ (cm)}$$
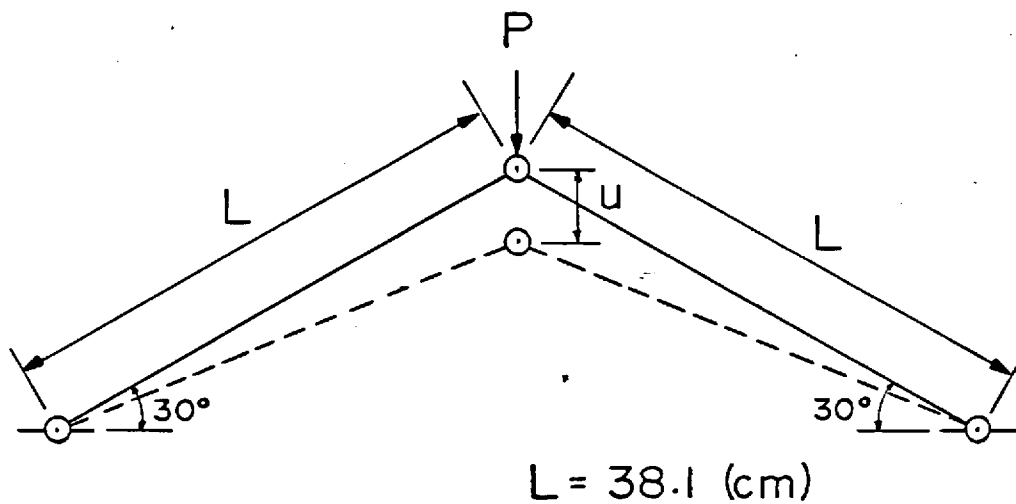
All members have solid circular sections, each of area 96.77(cm²).

Young's modulus is 7.03 X 10⁵ (kg/cm²).

Case 1 — Local buckling of each of the two members is ignored

Case 2 — Local buckling of only one of the two members is considered

Case 3 — Local buckling of both the members is considered

Fig. 8a. A Simple Truss Structure (Example 3)
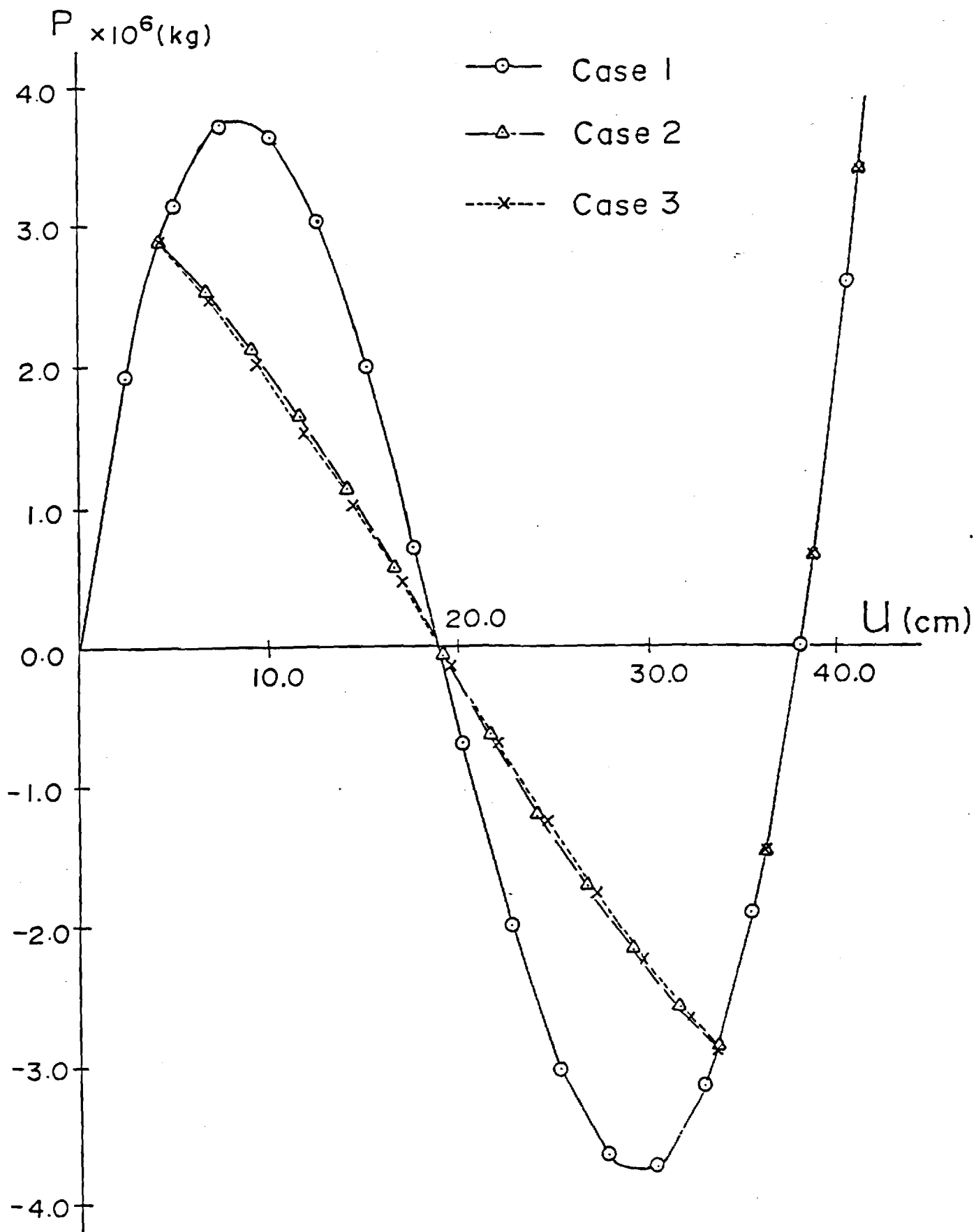
Fig. 8b. Load-Displacement Relation from the Simple
Truss Structure of Fig. 8a

L = 40.99 (cm)
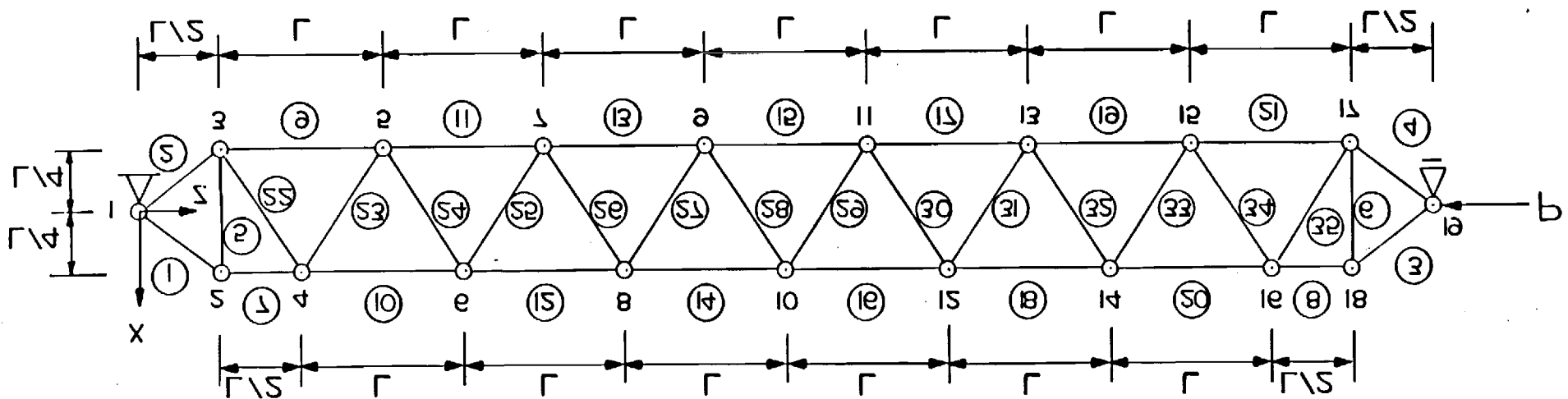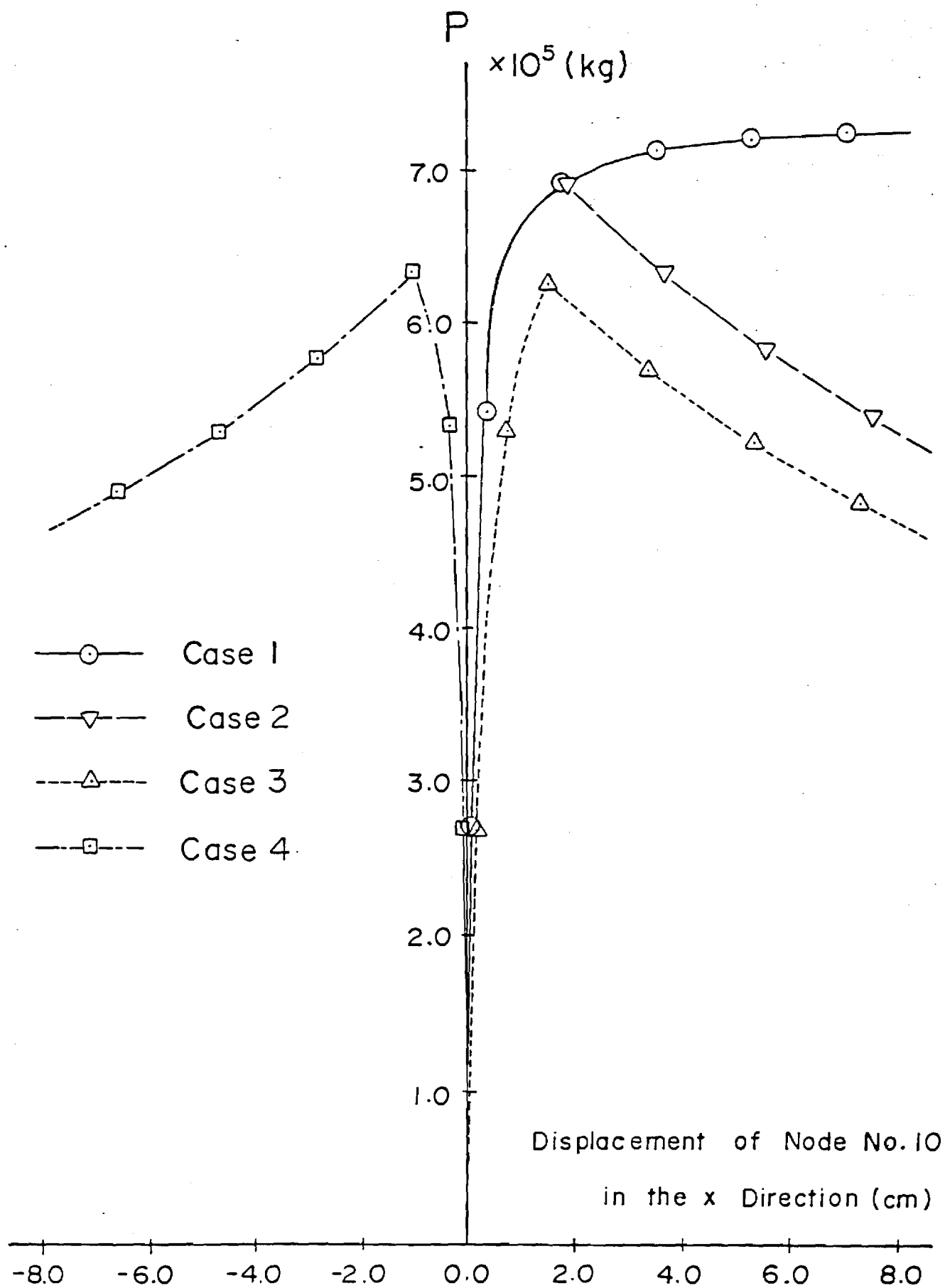
Fig. 9b. Load-Displacement Relation for Thompson's Strut
of Fig. 9a
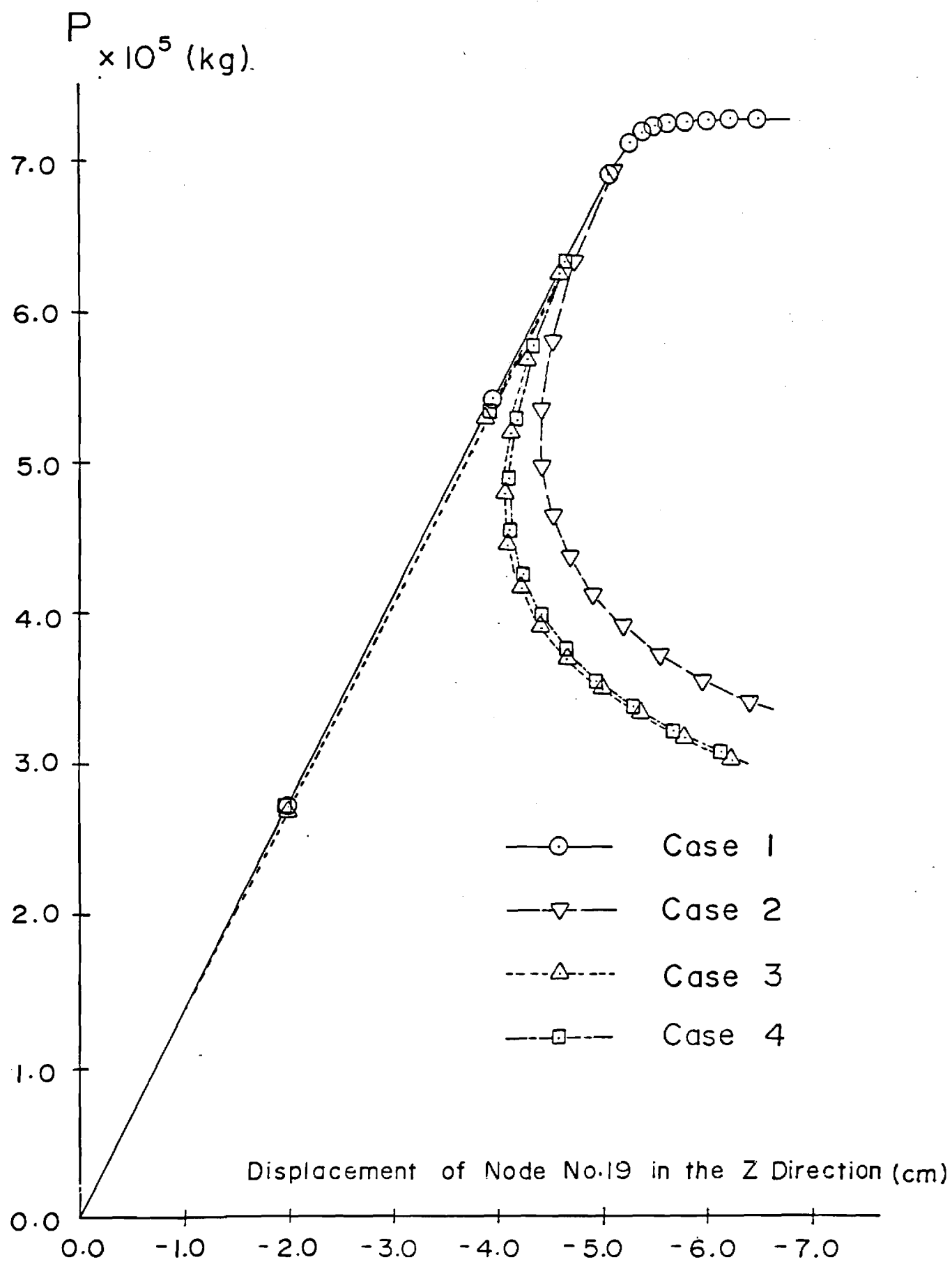
Fig. 9c. Load-Displacement Relation for Thompson's Strut
          of Fig. 9a

116
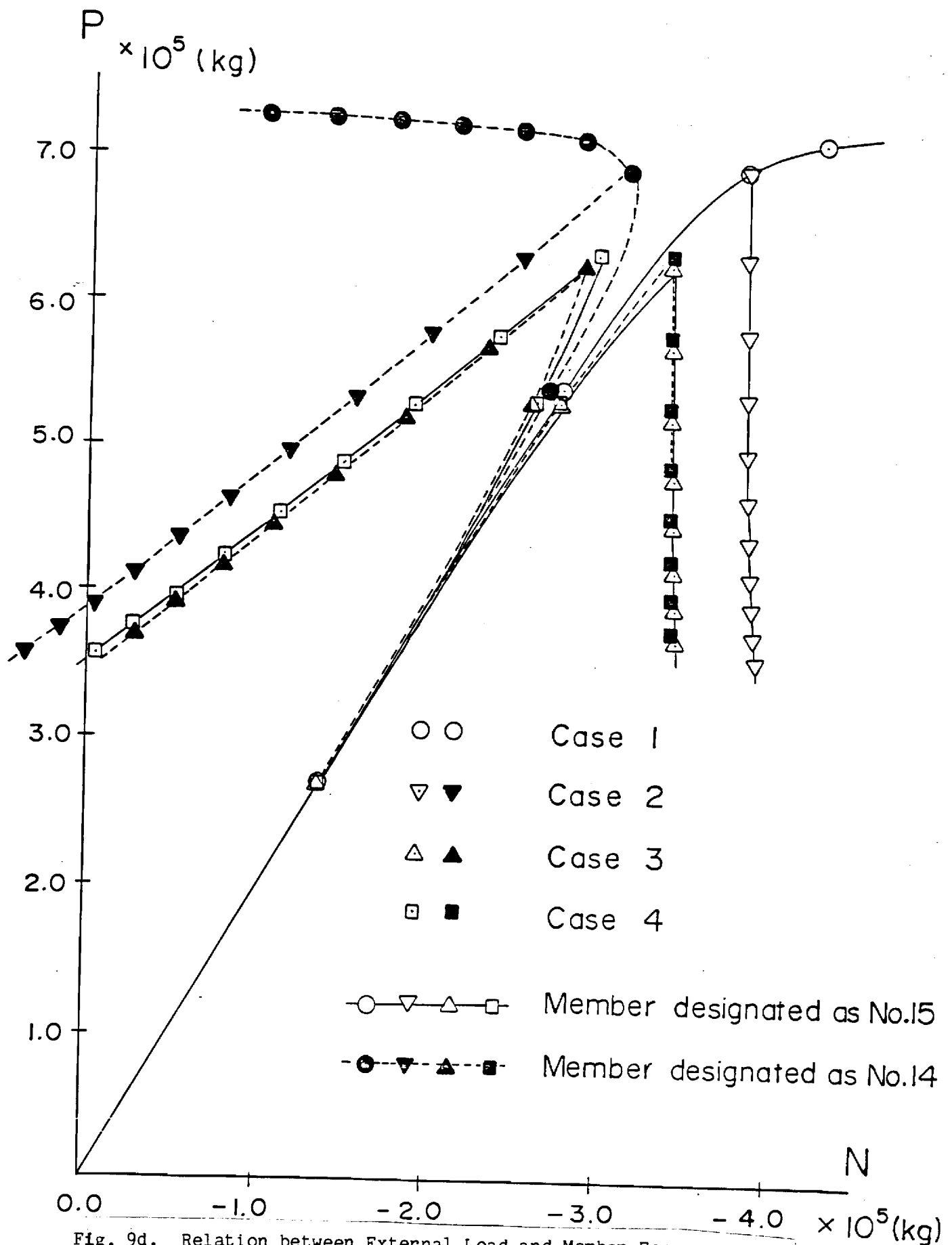
Fig. 9d. Relation between External Load and Member Forces for Thompson's Strut in the Pre- and Post-Buckled Ranges
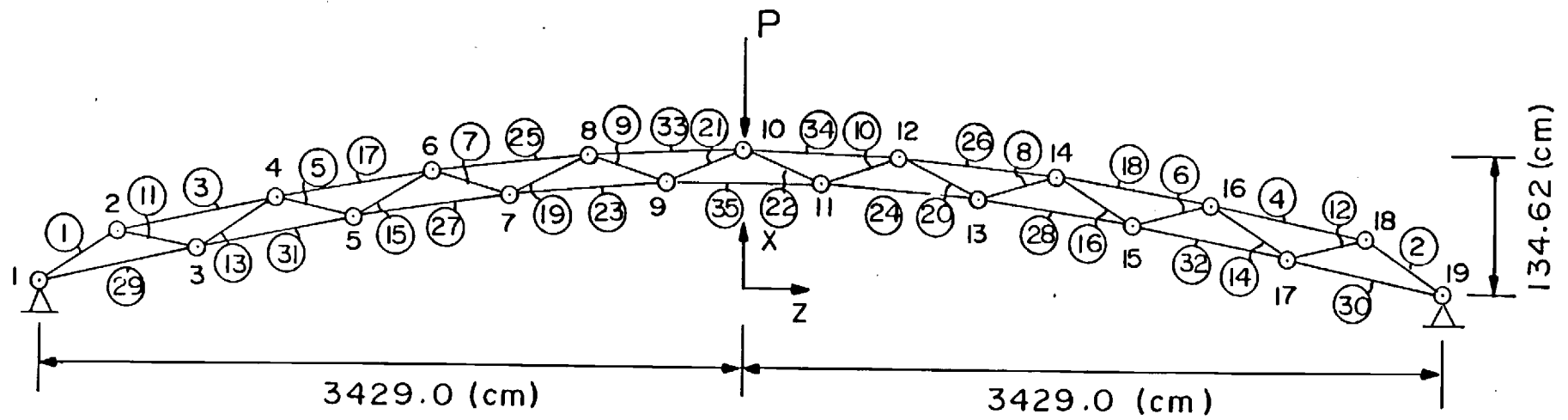
Fig. 10a. Arch-Truss Structure (Example 5)
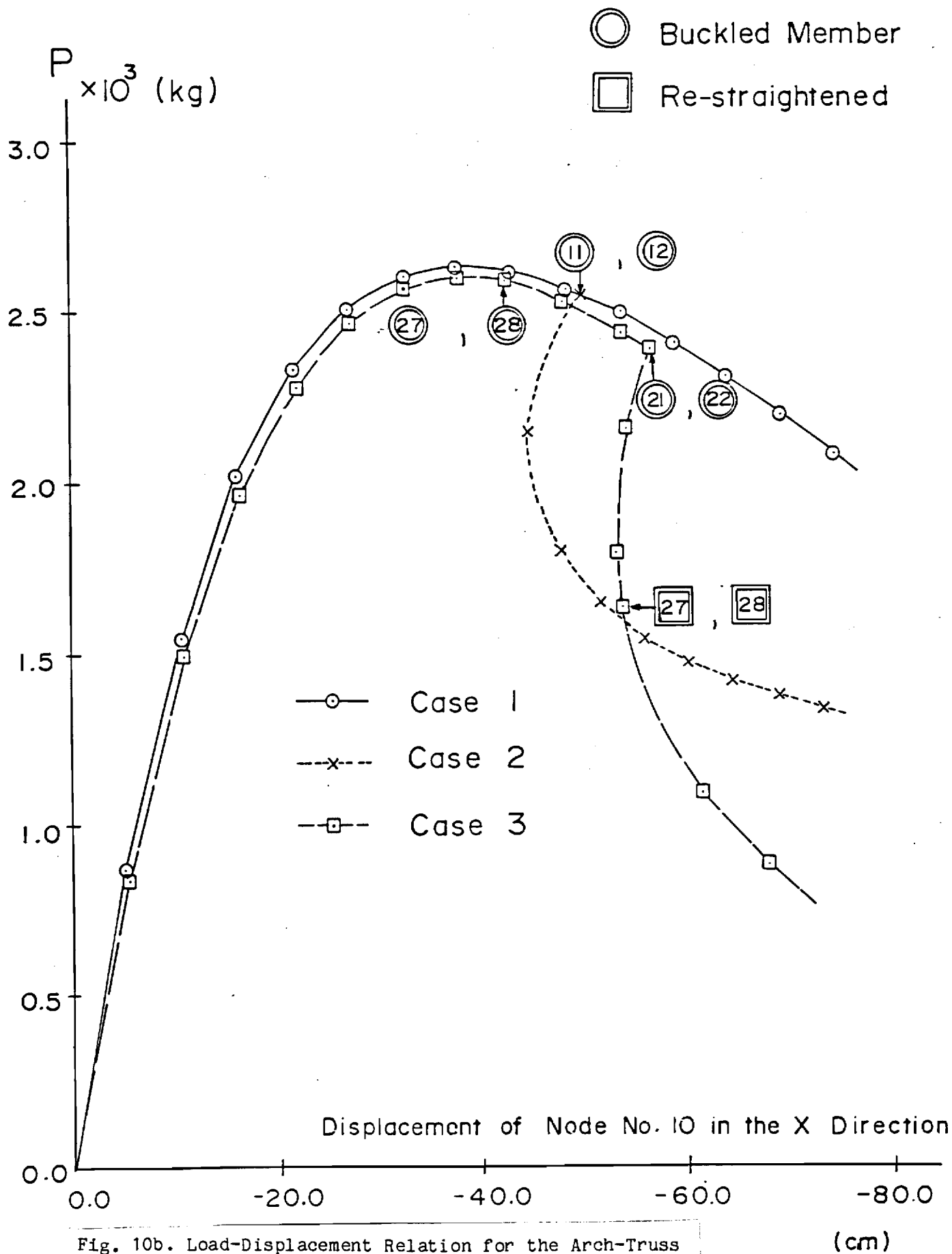
Fig. 10b. Load-Displacement Relation for the Arch-Truss
Structure of Fig. 10a
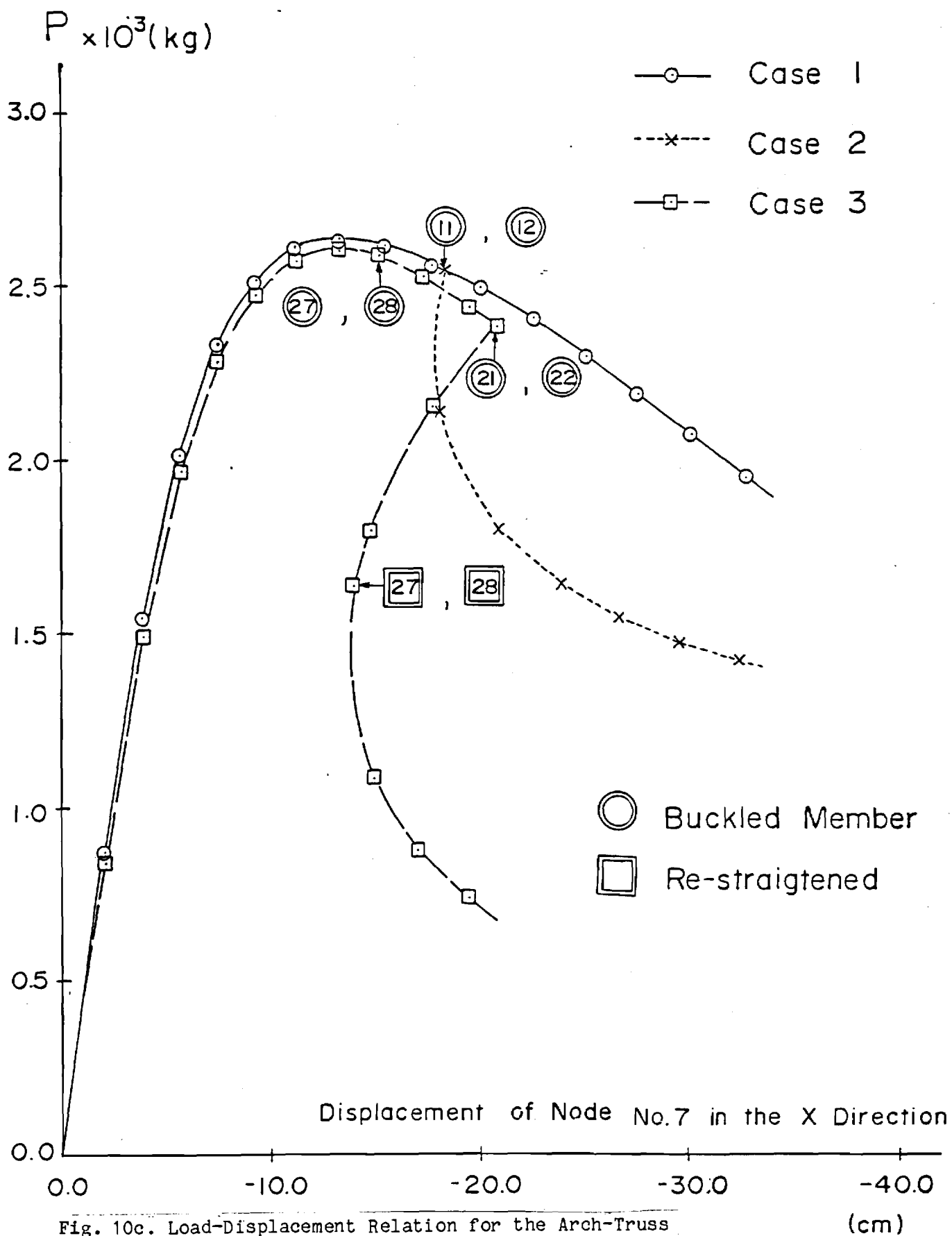
Fig. 10c. Load-Displacement Relation for the Arch-Truss
Structure of Fig. 10a
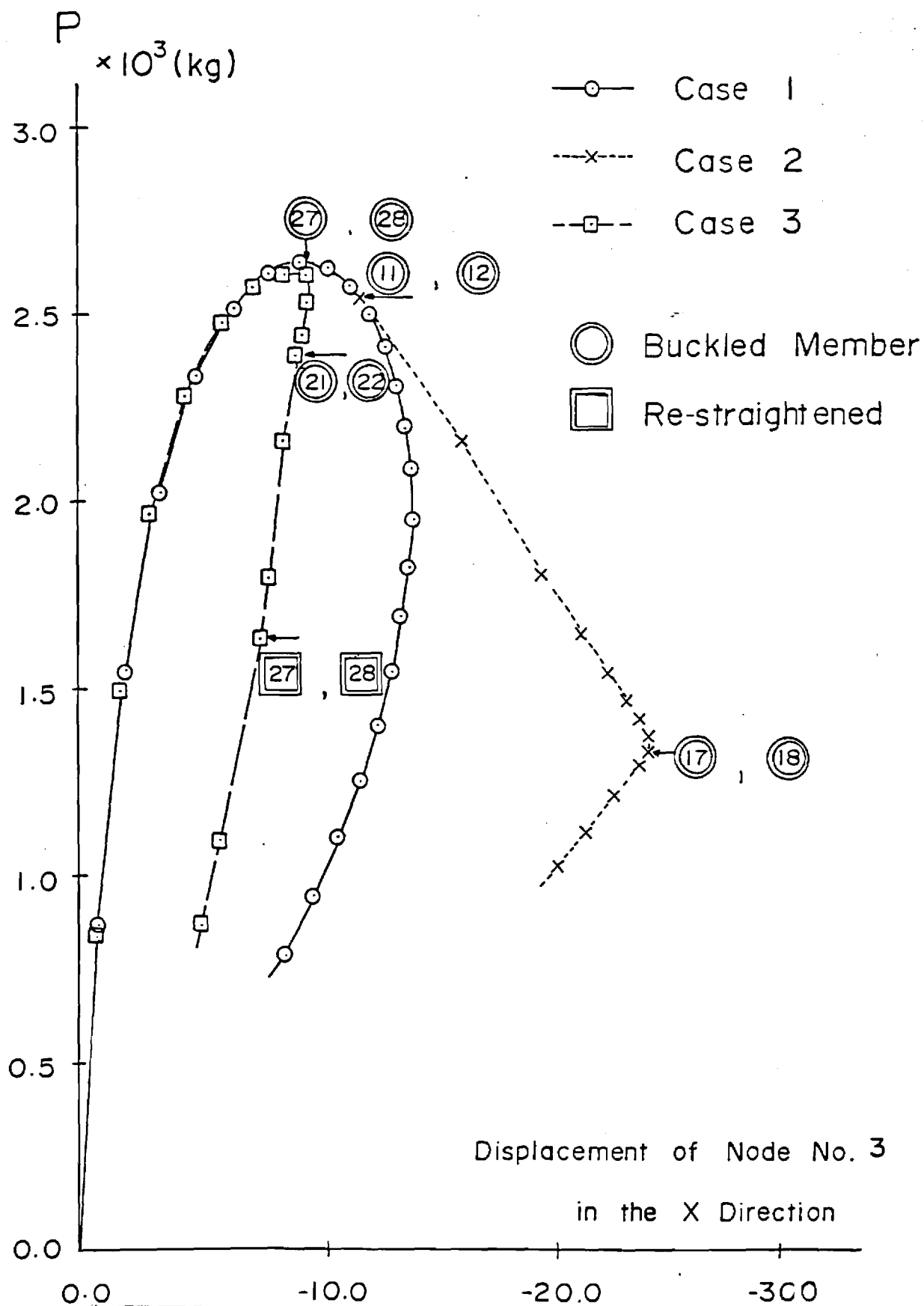
Fig. 10d. Load-Displacement Relation for the Arch-Truss Structure of Fig. 10a

(CM)
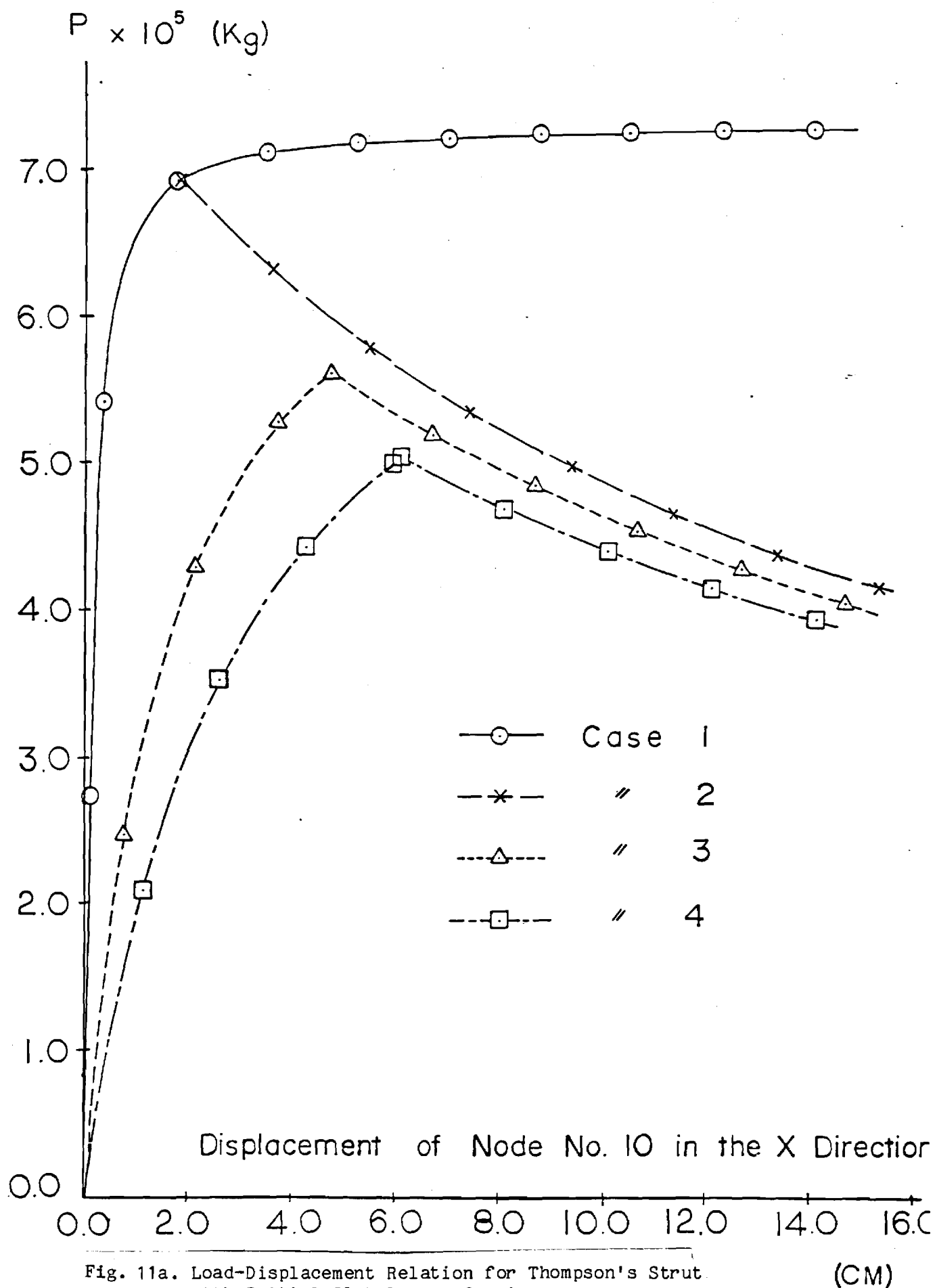
Fig. 11a. Load-Displacement Relation for Thompson's Strut
with Initial Global Imperfections

122
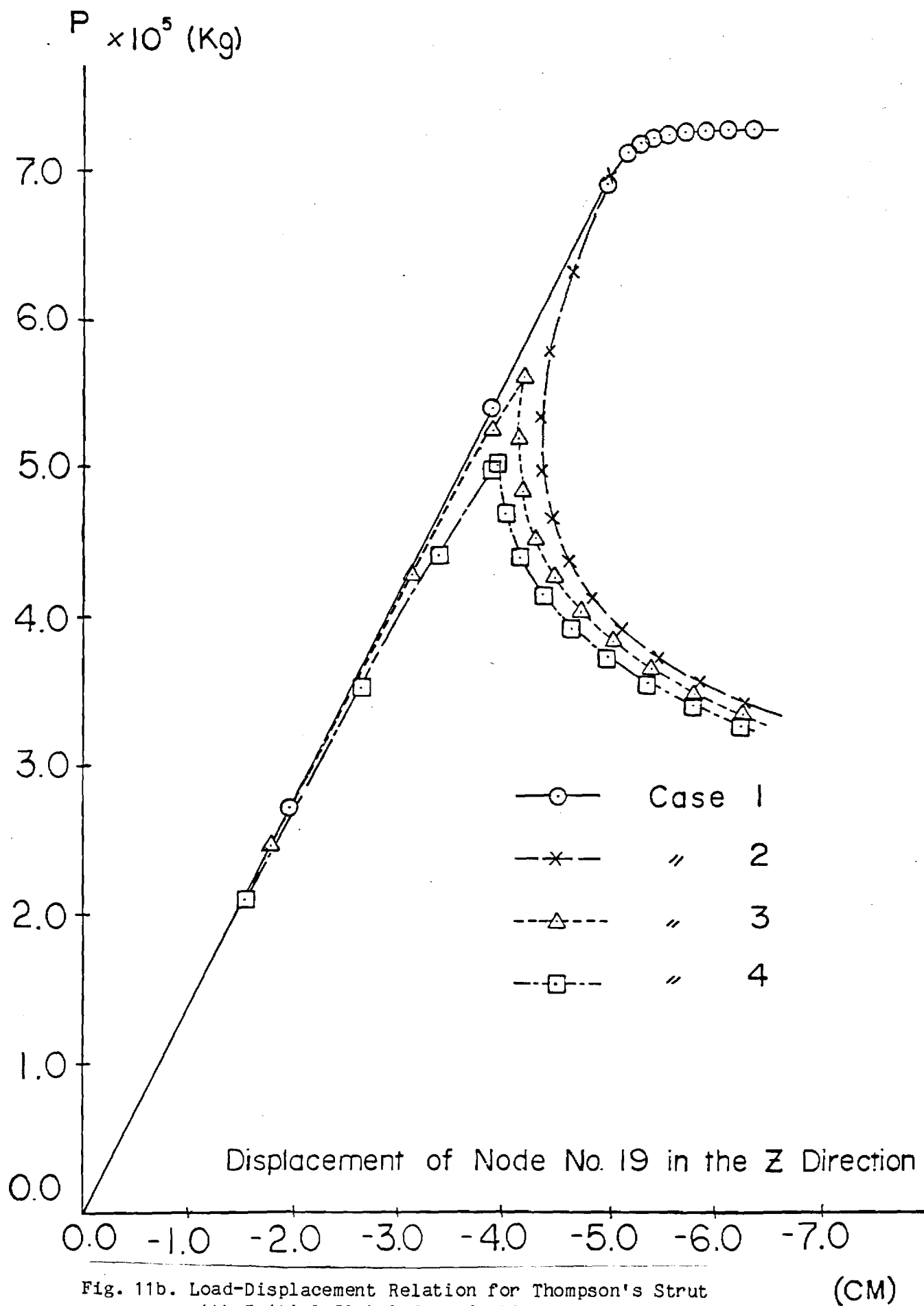
Fig. 11b. Load-Displacement Relation for Thompson's Strut
with Initial Global Imperfections

123
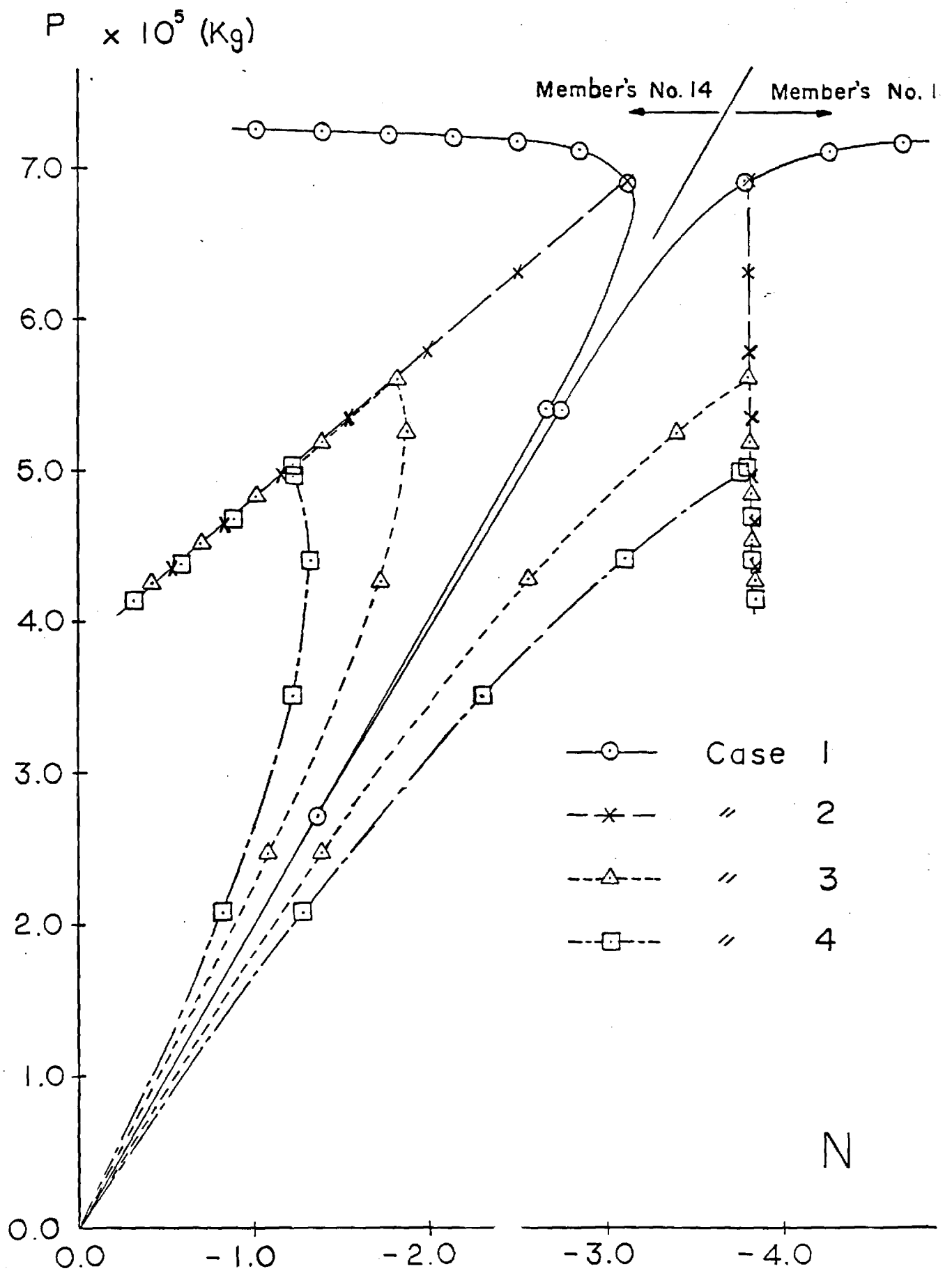
Fig. 11c. Relation between External Load and Member Forces for Thompson's Strut with Initial Global Imperfections
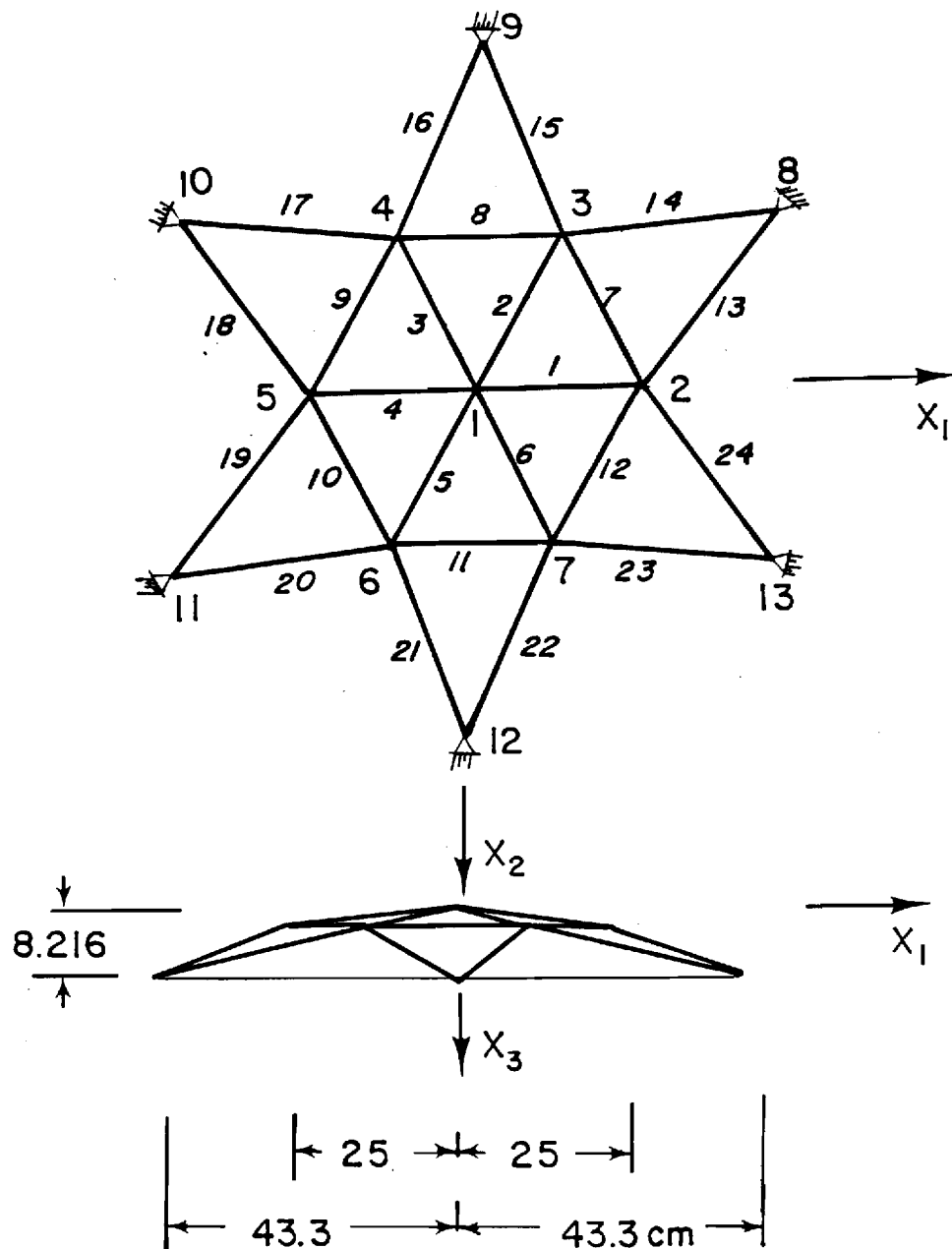
Fig. 12. Schematic of Shallow Geodesic Dome

125
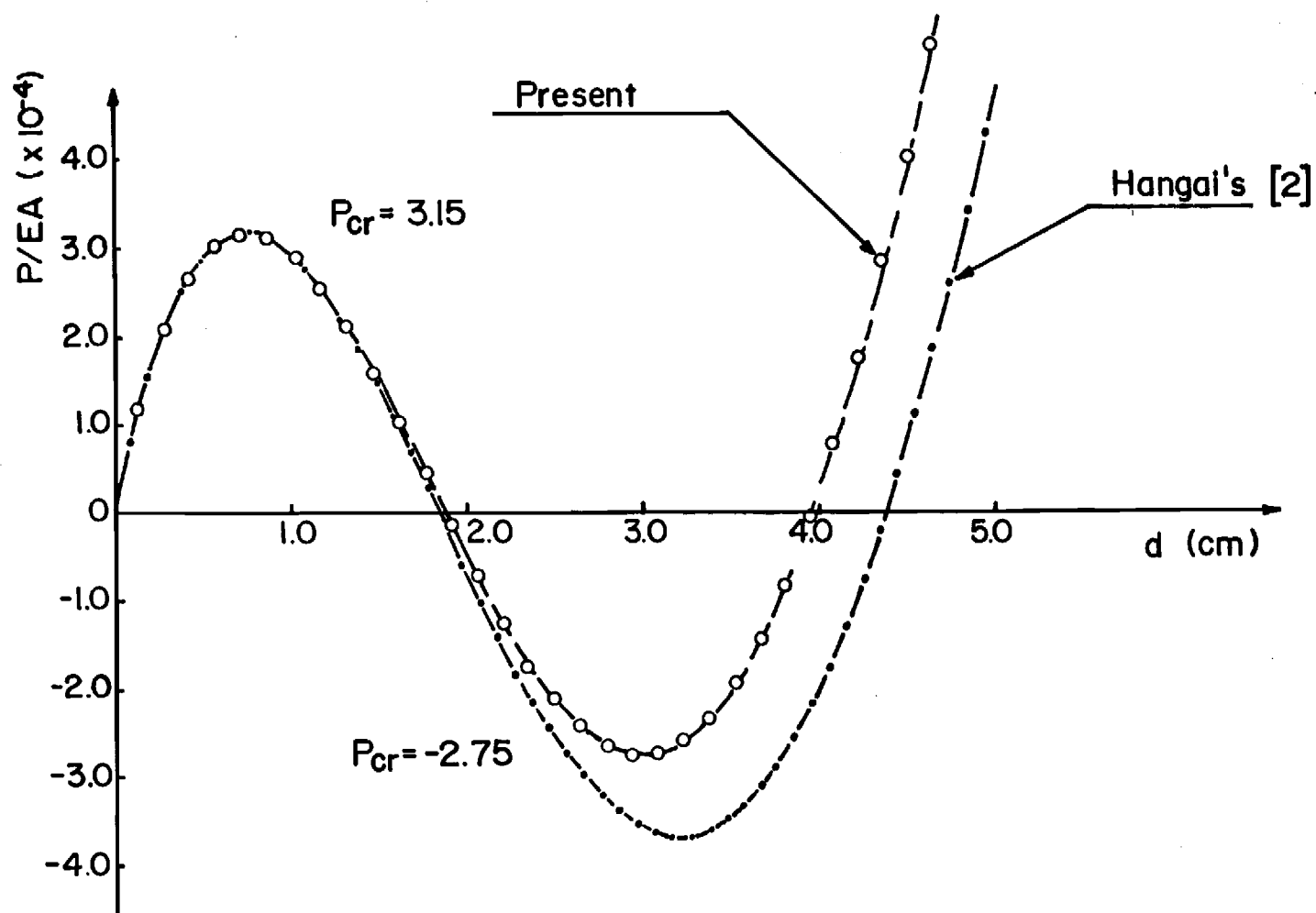
Fig. 13. Vertical Displacements of Central Node without the Influence of Local Buckling of Truss Members.
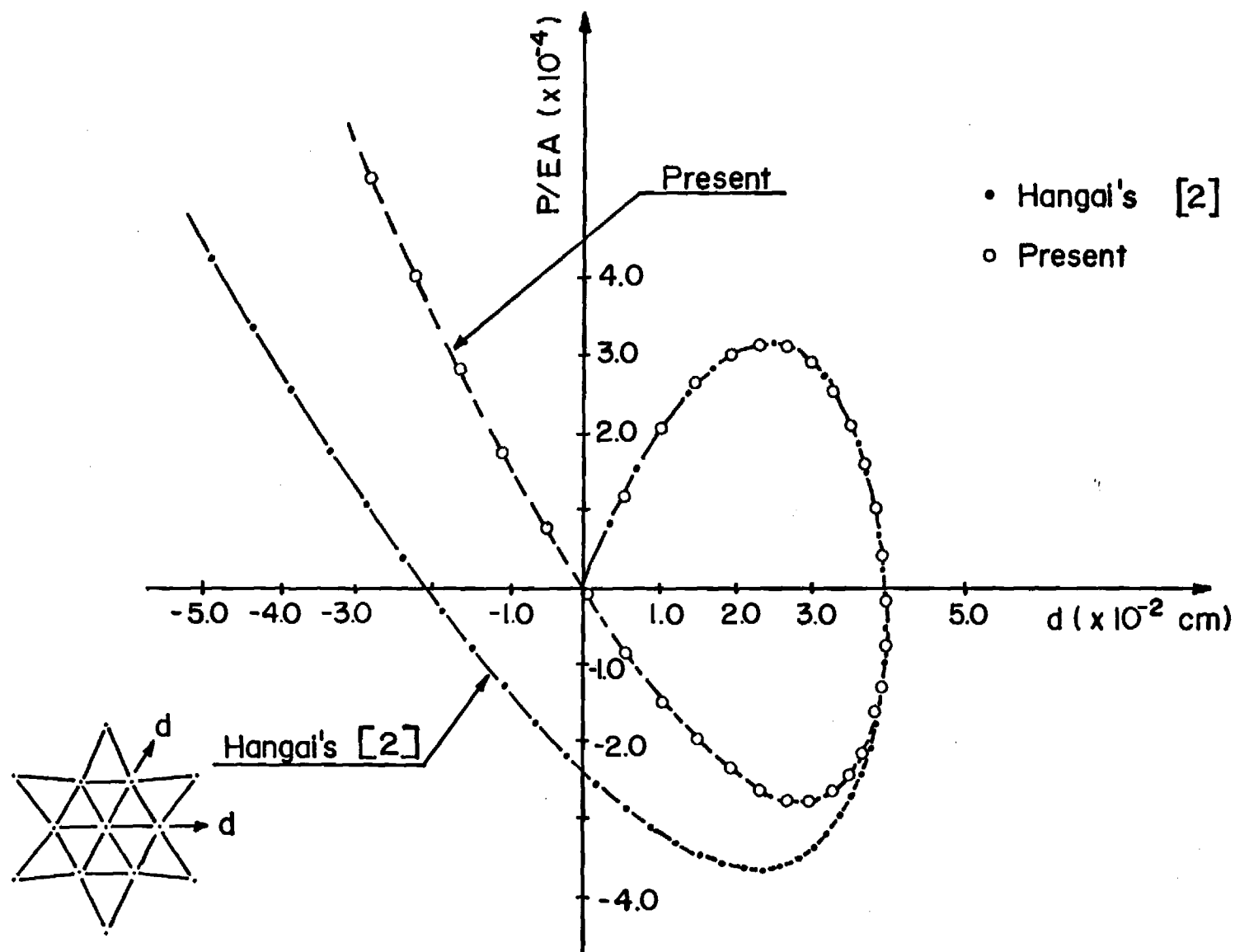
Fig. 14. Horizontal Radial Displacements of Non-Central Nodes without the Influence of Local Buckling of Truss Members.
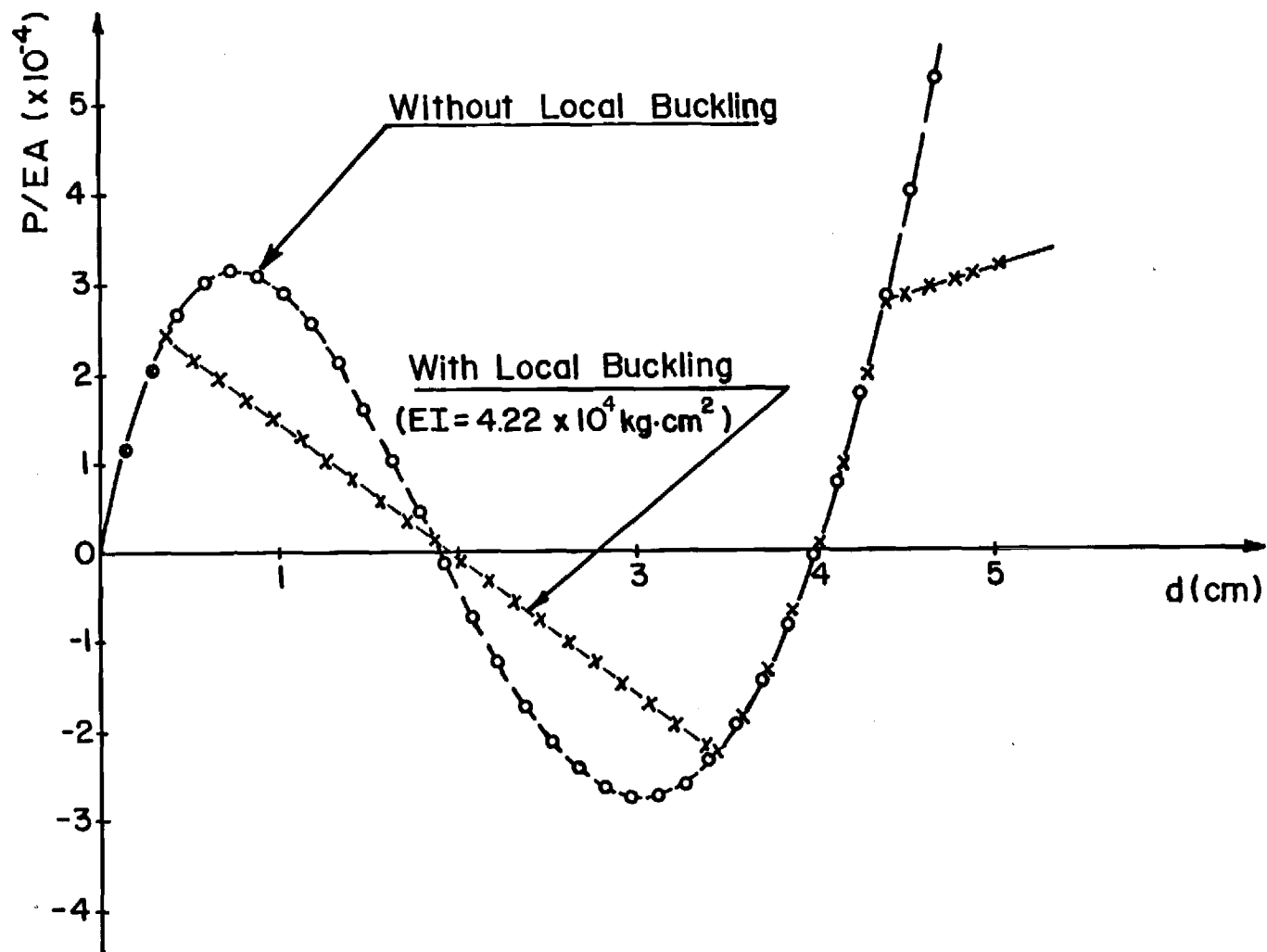
Fig. 15. Vertical Displacements of Central Node with and without the Influence of Local Buckling of Truss Members.
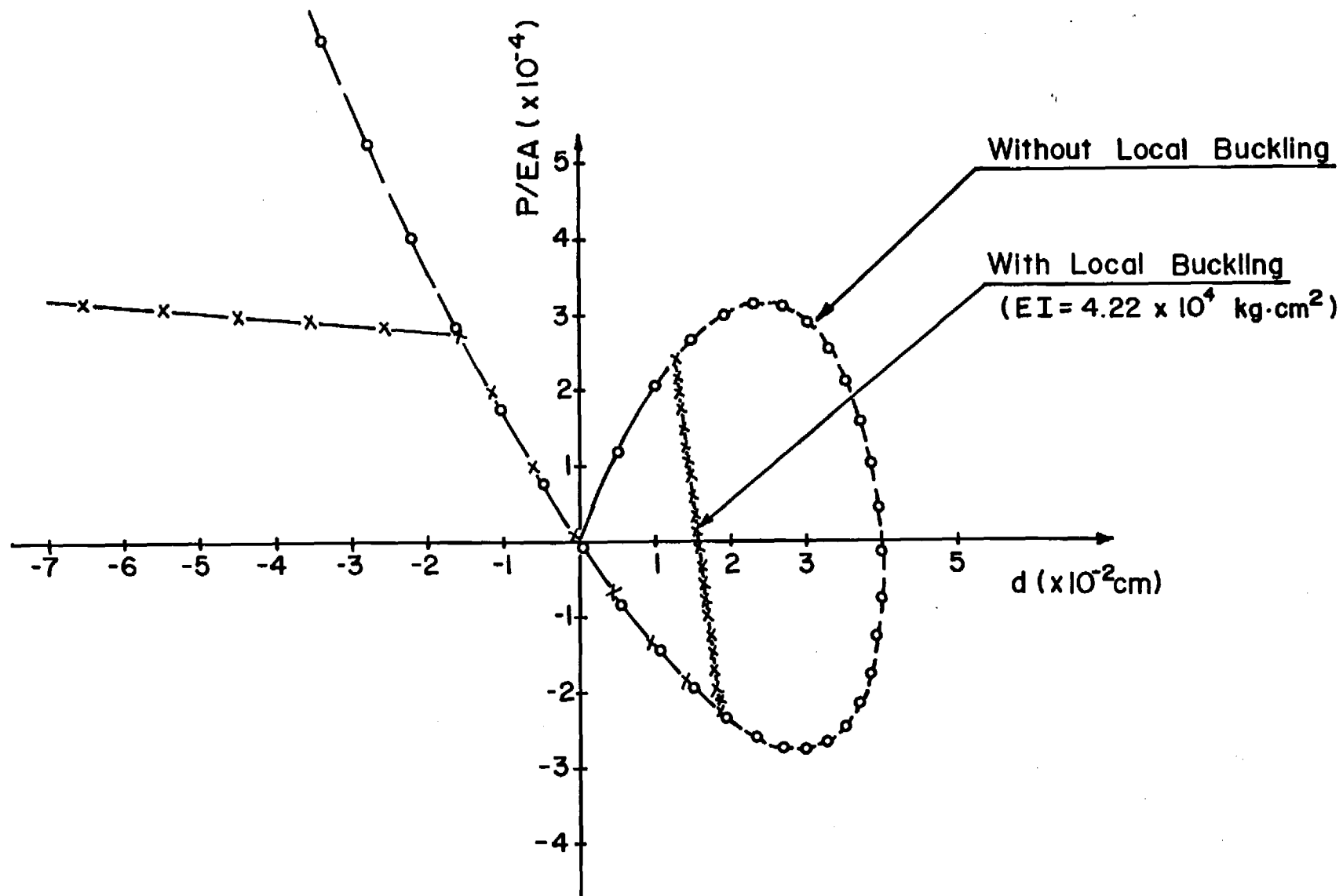
Fig. 16 . Horizontal Radial Displacements of Non-Central Nodes with and without the Influence of Local Buckling of Truss Members.
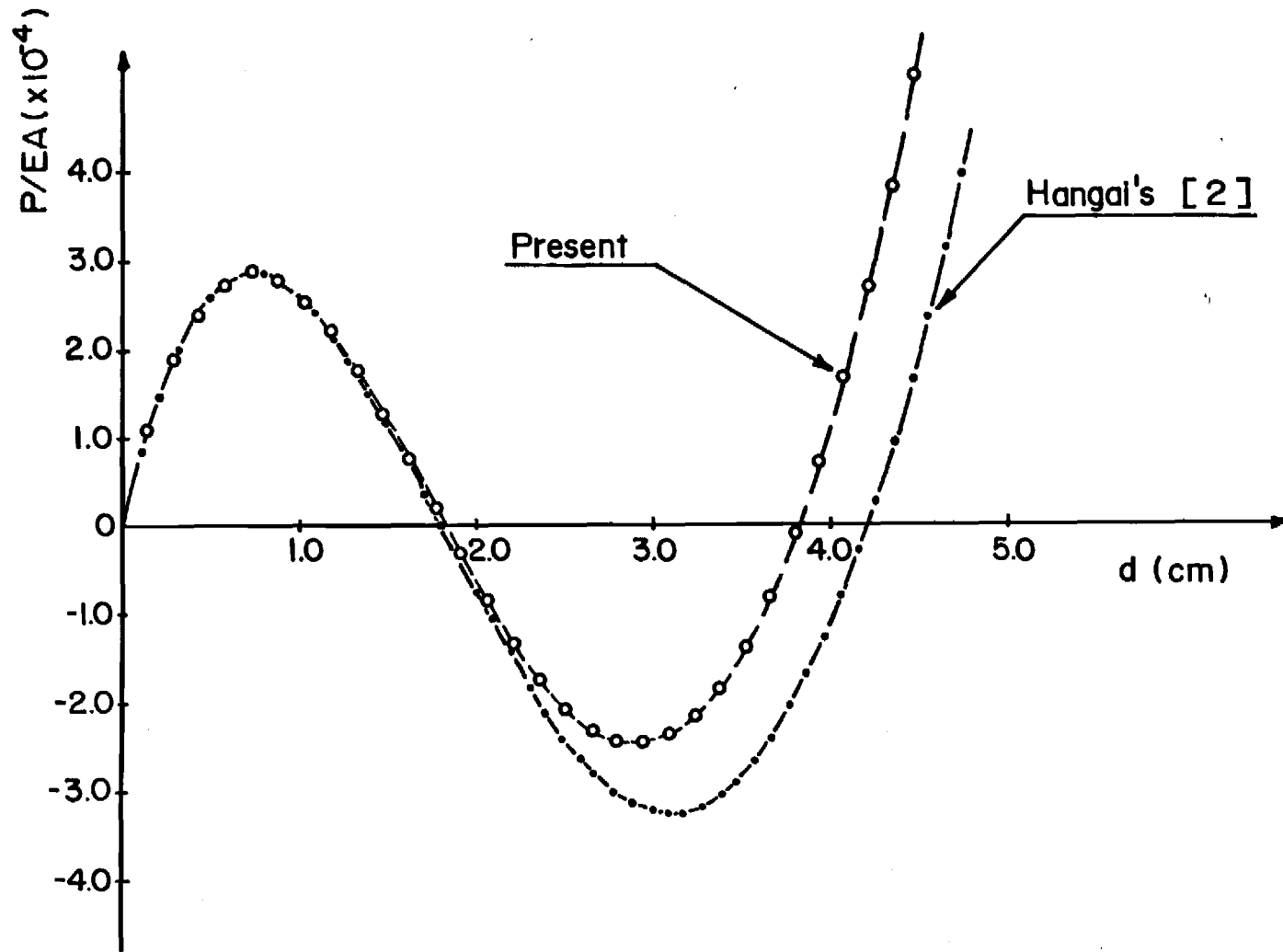
Fig. 17. Vertical Displacements of Central Node under Imperfect Geometry
without the Influence of Local Buckling of Truss Members

Node A : Imperfect Geometry Node
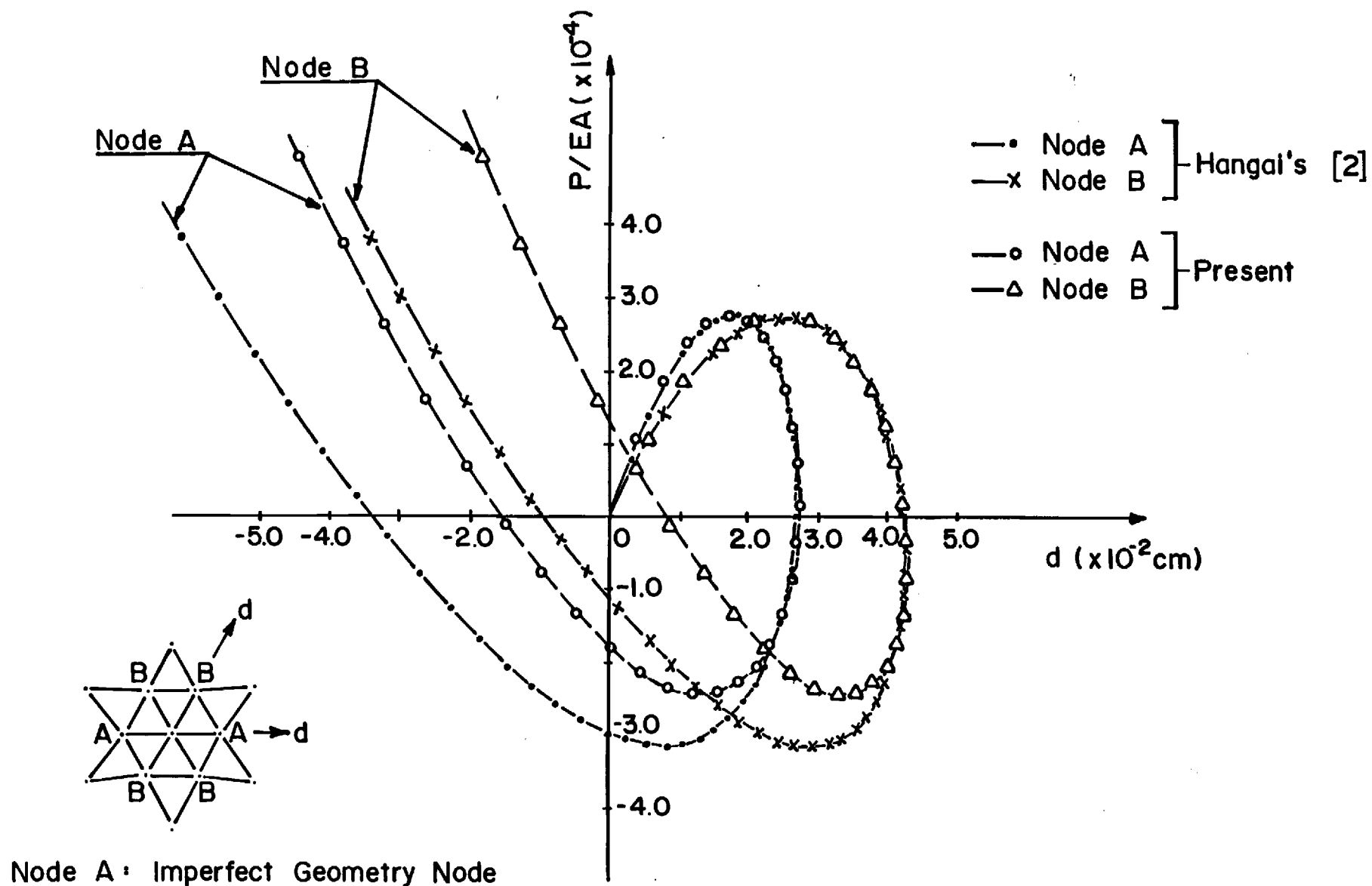
Fig. 18. Horizontal Radial Displacements of Non-Central Nodes under Imperfect Geometry without the Influence of Local Buckling of Truss Members.

$$\frac{P}{EA} = 2.41 \times 10^{-4}$$

$$\frac{P}{EA} = -2.27 \times 10^{-4}$$

$$\frac{P}{EA} = 2.67 \times 10^{-4}$$
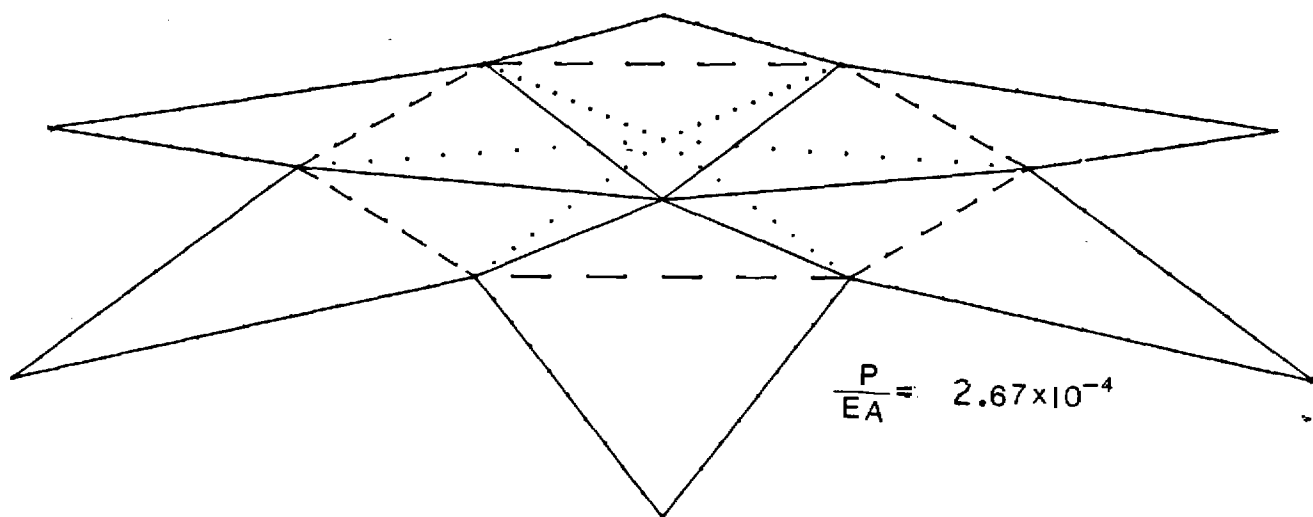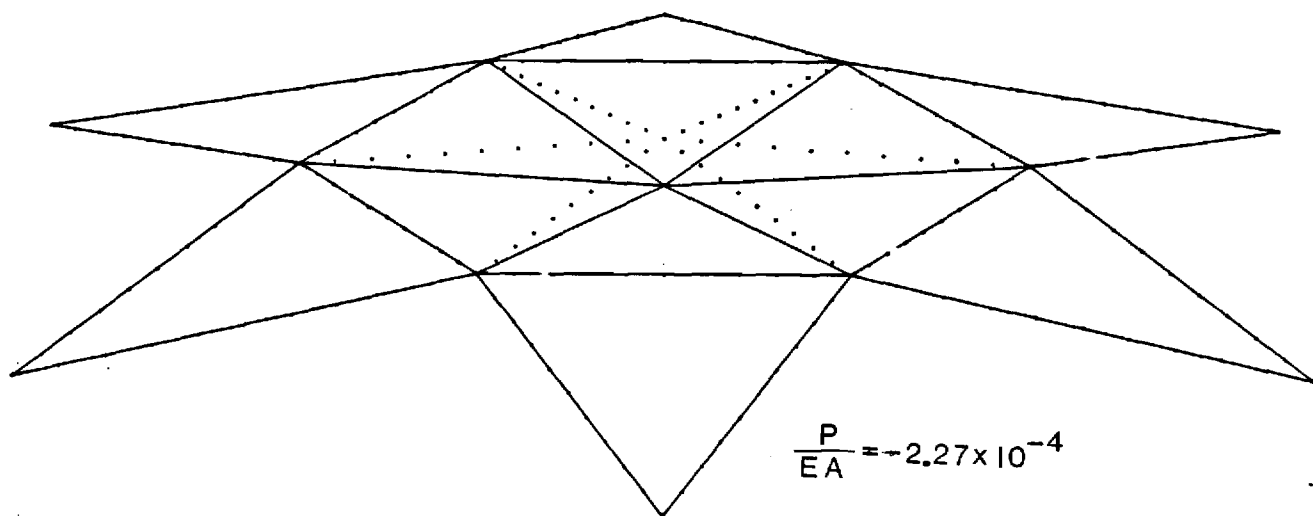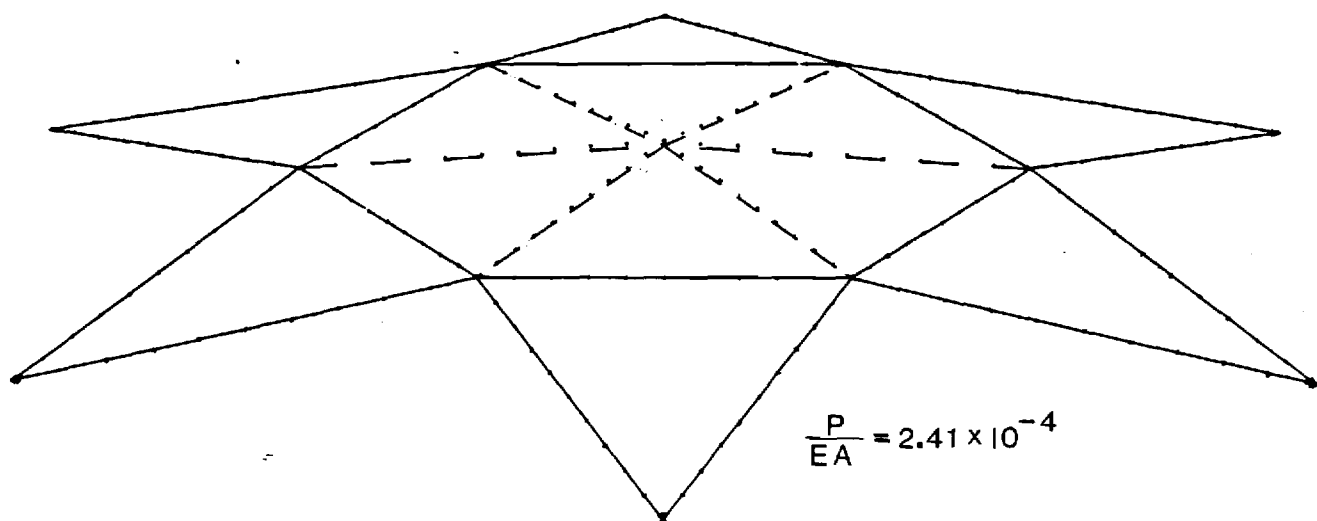
Fig. 19. Deformed Configurations of the Geodesic Dome
Shown in Fig. 12.

132

Equation of Surface

$$X_1^2 + X_2^2 + (X_3 + 7.2)^2 = 60.84$$

Loading System

P_1 : Concentrated Load in X_3
direction at all nodes

P_2 : Concentrated Load in X_3
direction at nodes having $X_1 \geq 0$, $X_2 \geq 0$

$a = 6.0\,m$
$f = 0.60\,m$
$L = 0.75\,m$

Fig. 20. Schematic of Shallow Geodesic Dome

133

Legend:
—————— Noor's Full System [32]
o Present

$p_1 = -5.132 \times 10^{-5}$

$p_1 = -7.184 \times 10^{-5}$

$p_1 = -10.263 \times 10^{-5}$

$p_1 = -15.395 \times 10^{-5}$

W/D
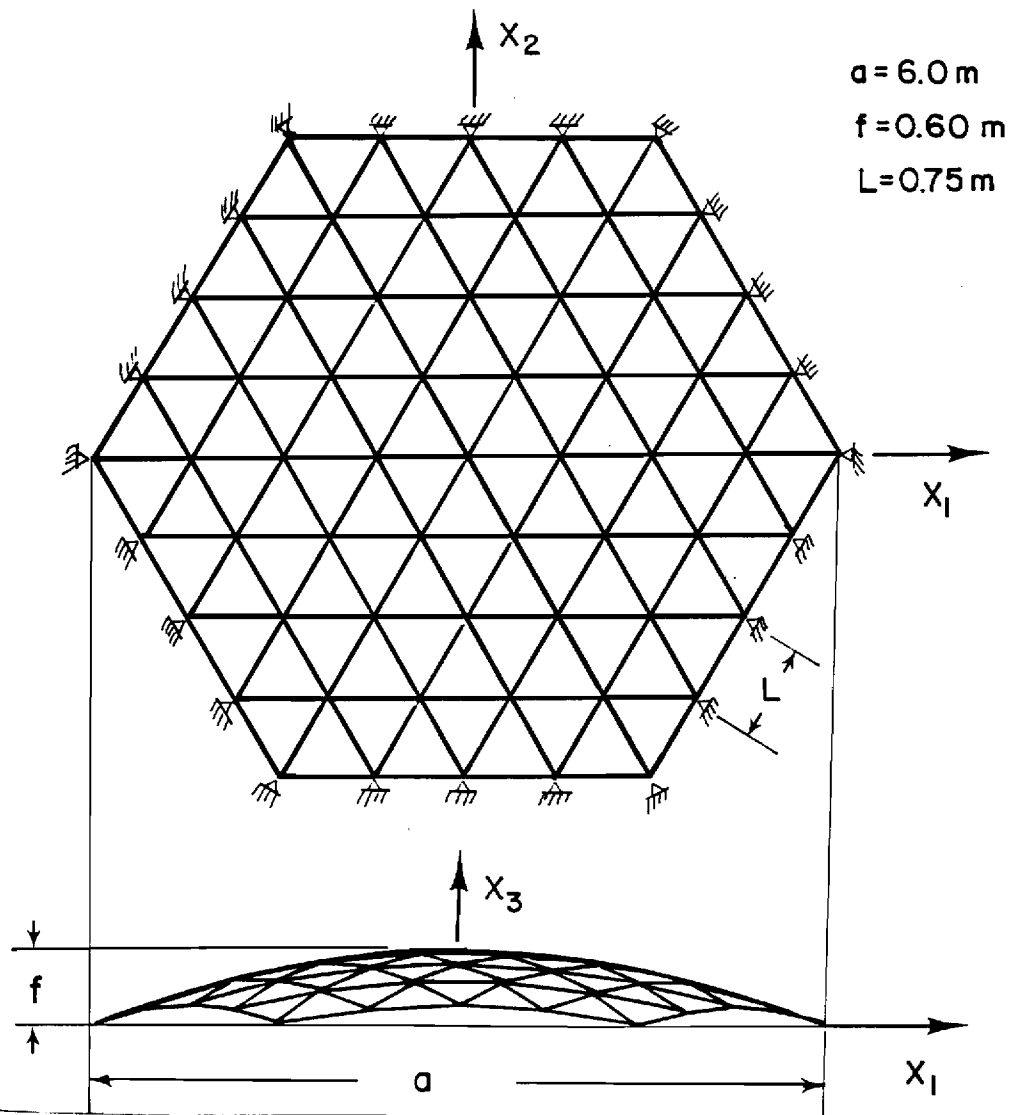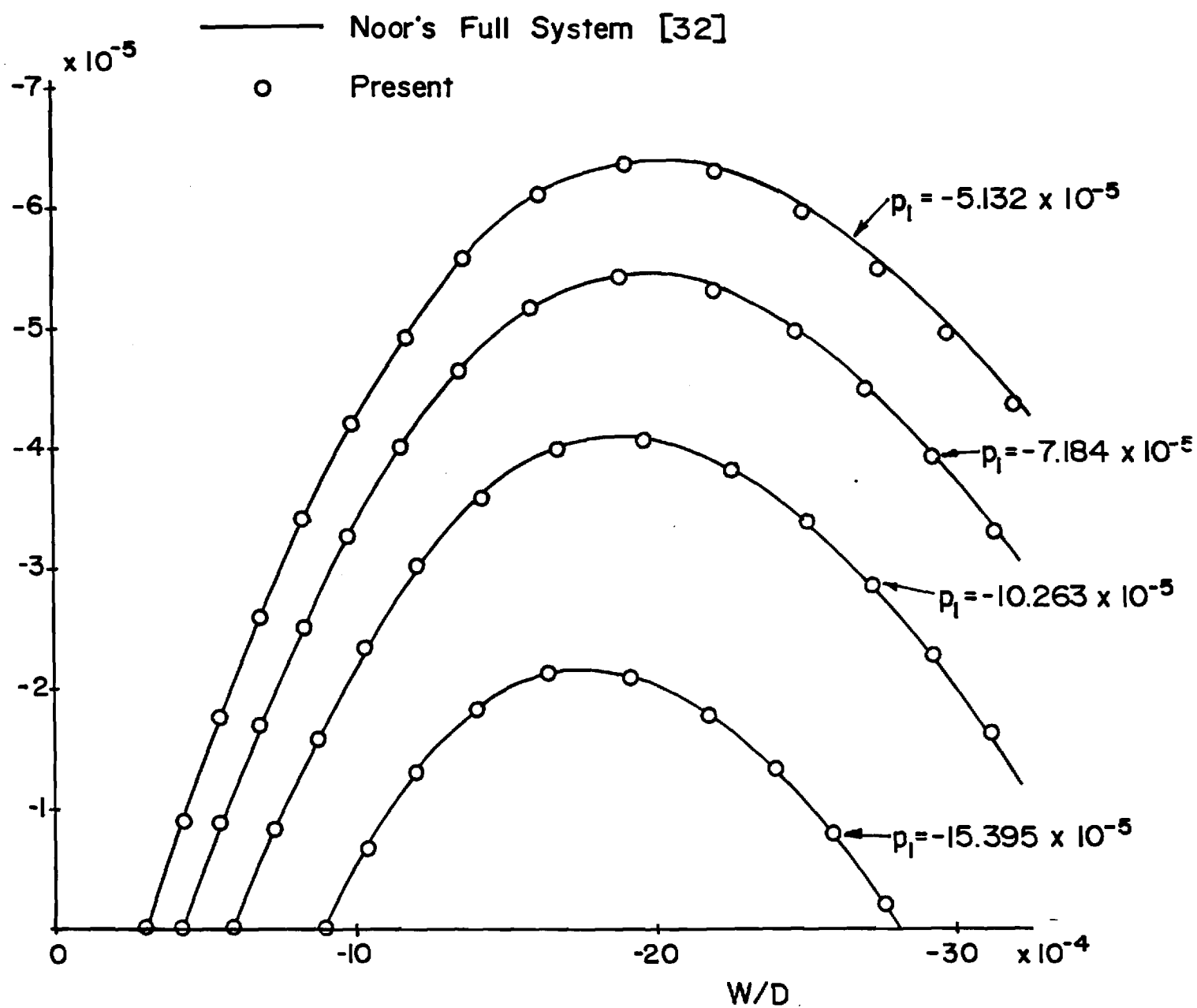
21. Vertical Displacements of Central Node under Various Combinations of Loads, P_1 & P_2, without the Influence of Local Buckling of Truss Members.
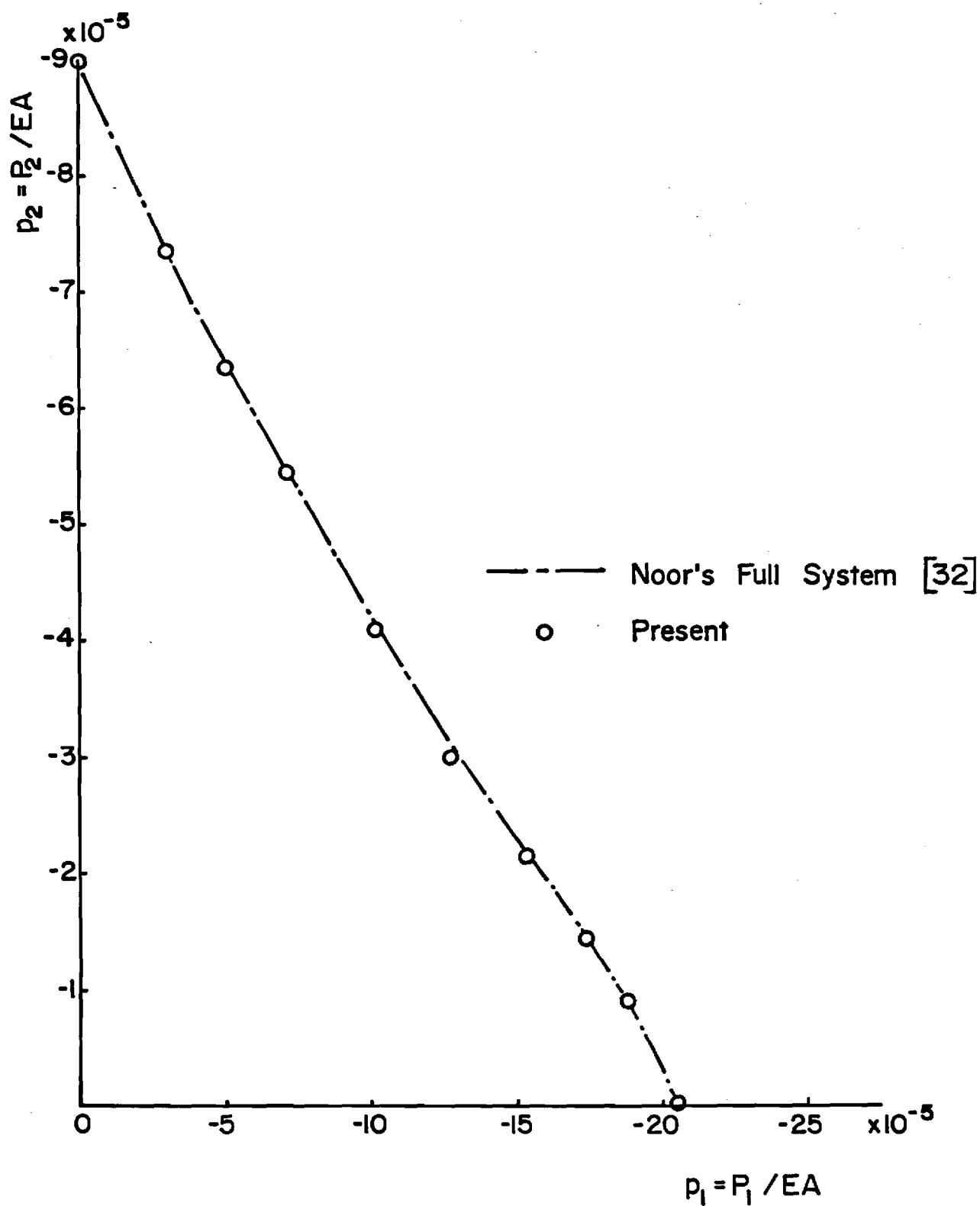
Fig. 22. Stability Boudary under Various Combinations of Loads, P_1 & P_2, without the Influence of Local Buckling of Truss Members.

135
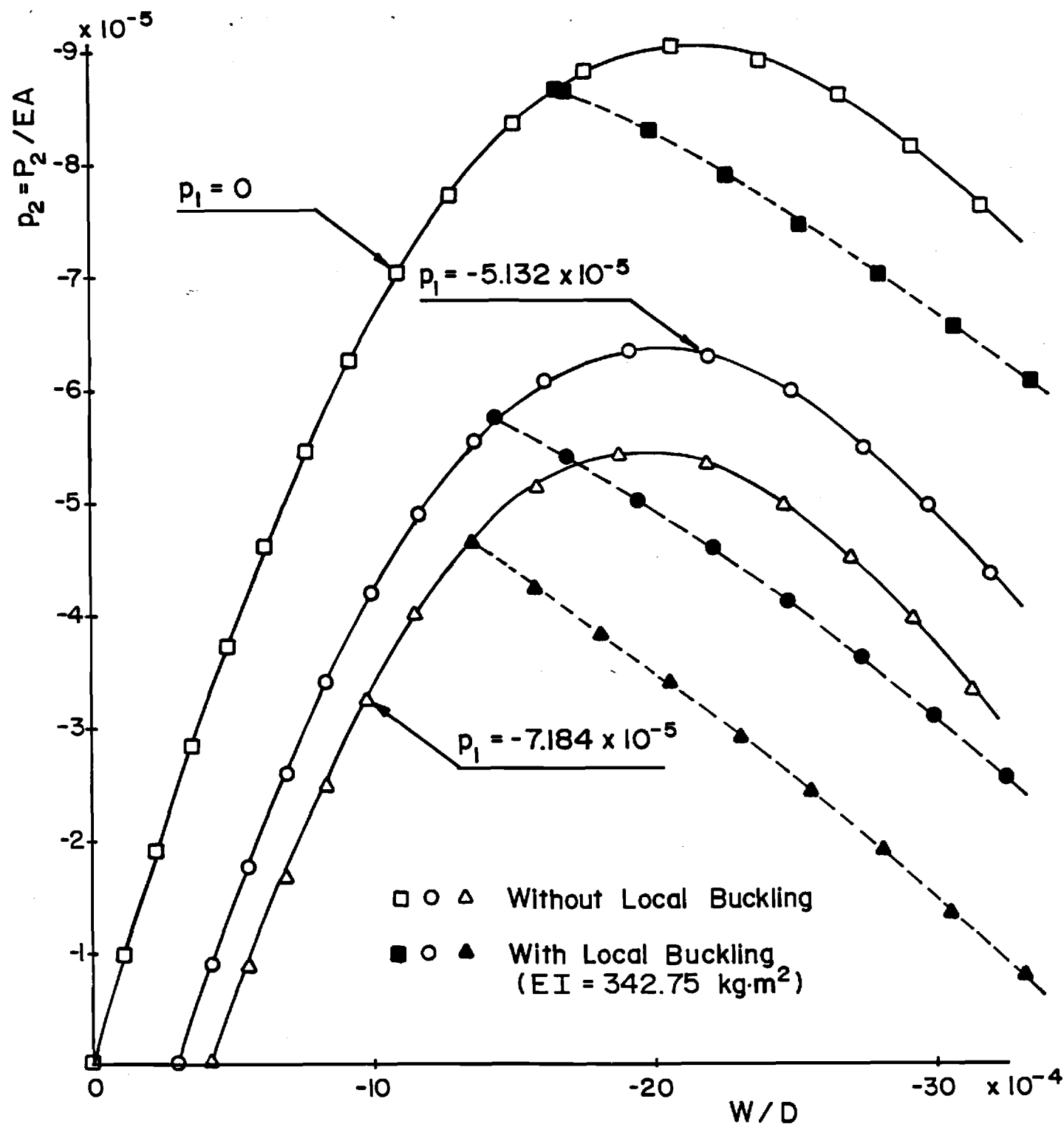
23. Vertical Displacements of Central Node under Various Combinations of Loads, P_1 & P_2, with and without the Influence of Local Buckling of Truss Members.
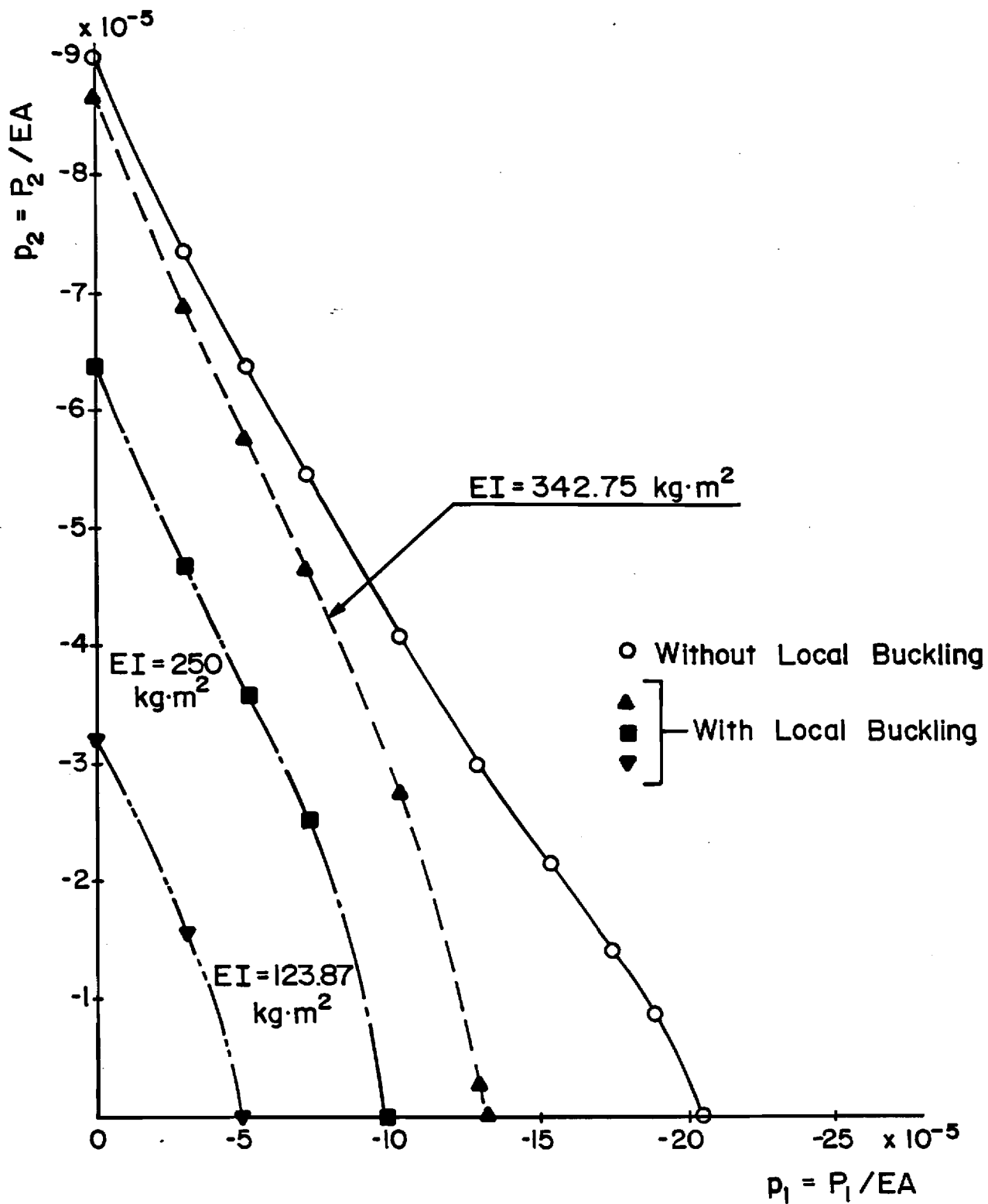
24. Stability Boundaries under Various Combinations of Loads, P_1 & P_2, with and without the Influence of Local Buckling of Truss Members
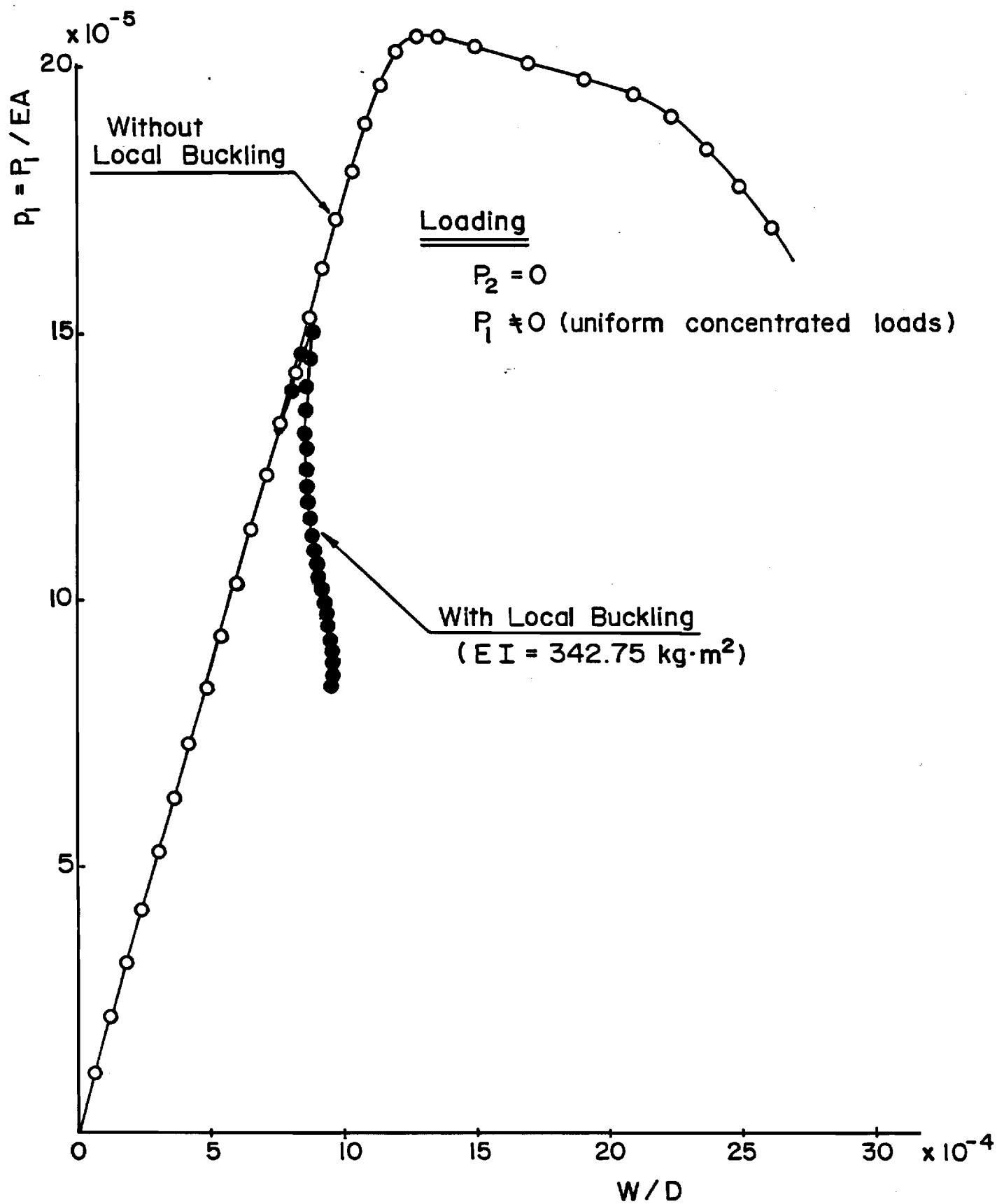
Fig. 25. Vertical Displacements of Central Node under Load P_1 with and without the Influence of Local Buckling of Truss Members

$p_1 = 13.19$

$p_1 = 15.16$

$p_1 = 12.85$
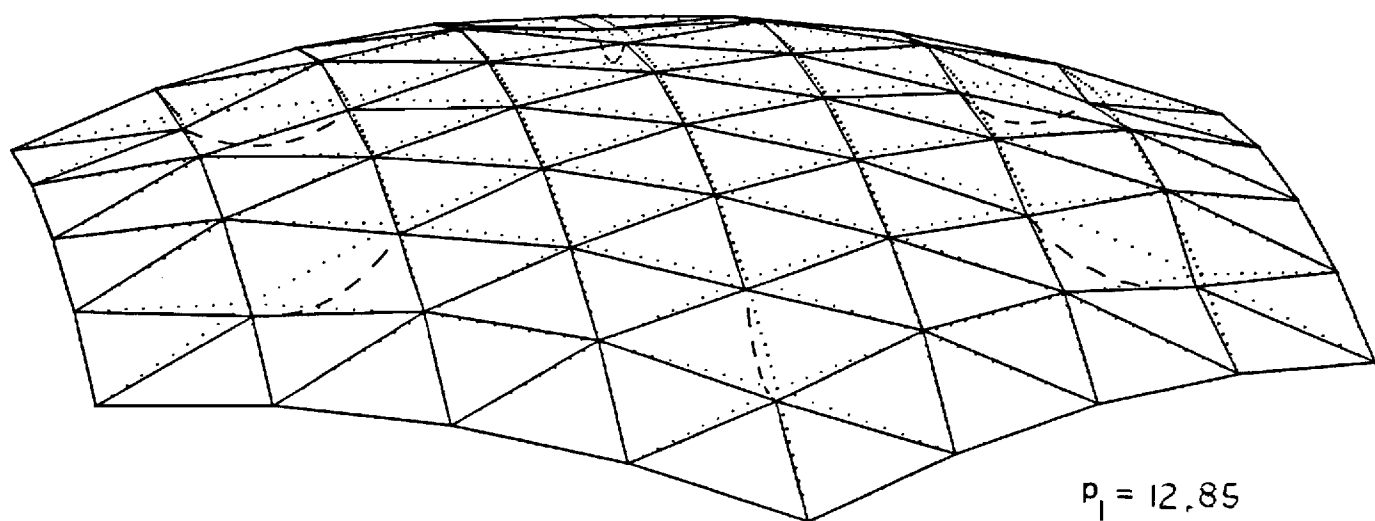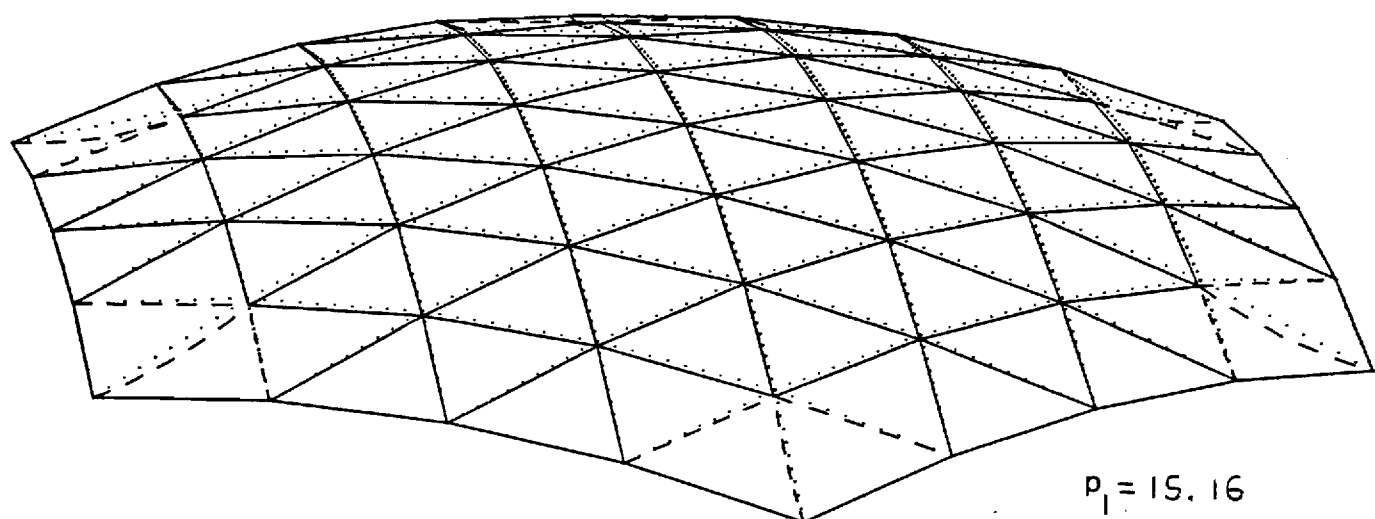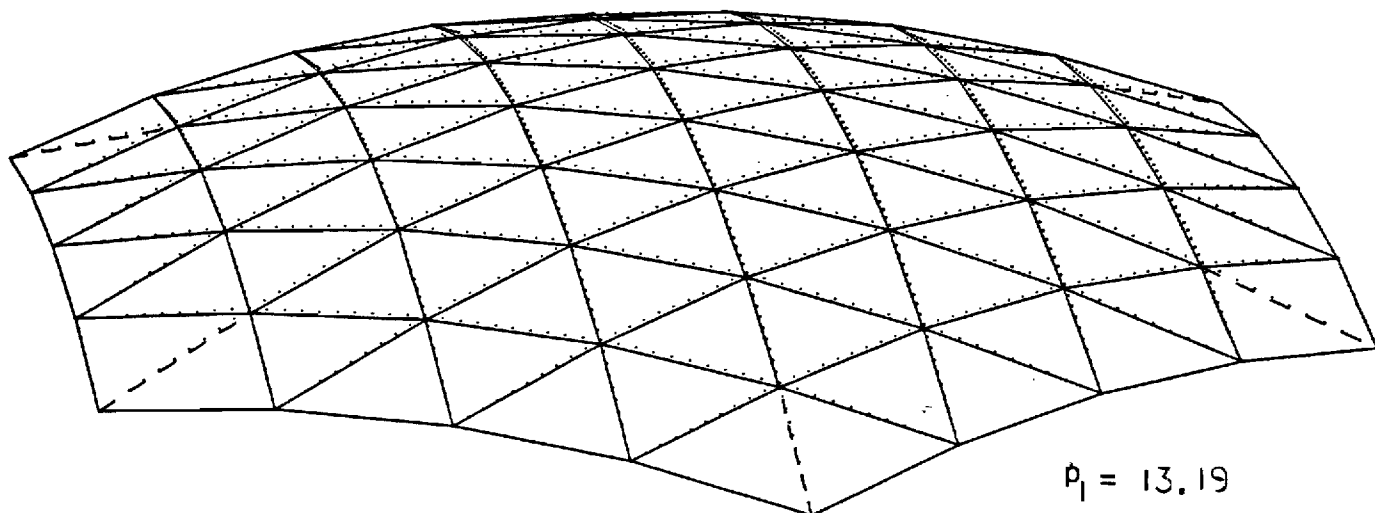
Fig. 26. Deformed Configurations of the Geodesic Dome
Shown in Fig. 20

139

MATERIAL PROPERTY

MEMBER	EA LB	EI LB IN^2
LONGERONS	7.08×10^6	2.16×10^6
DIAGONAL, BATTENS	2.70×10^5	6.43×10^4
SHORT LONGERONS	1.65×10^8	2.20×10^8
HORISONTAL DIAGONAL	1.37×10^8	1.52×10^8
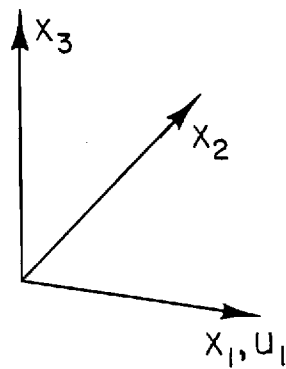
Fig. 27. Schematic of a Twelve-Bay Space Truss under Axial Loads

140
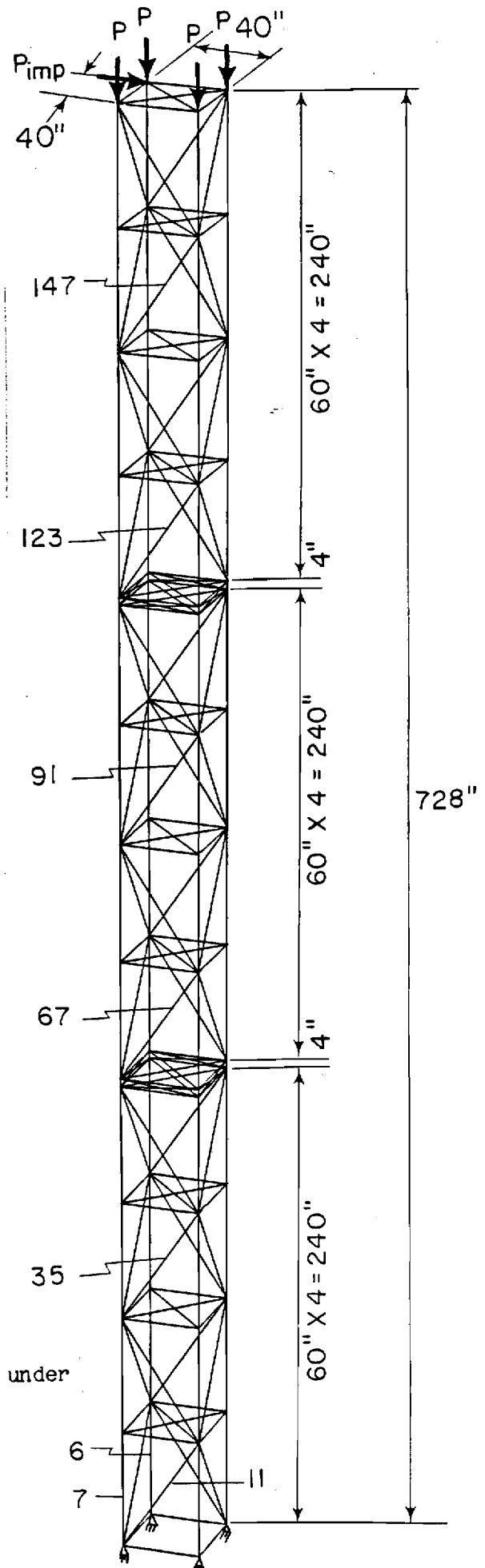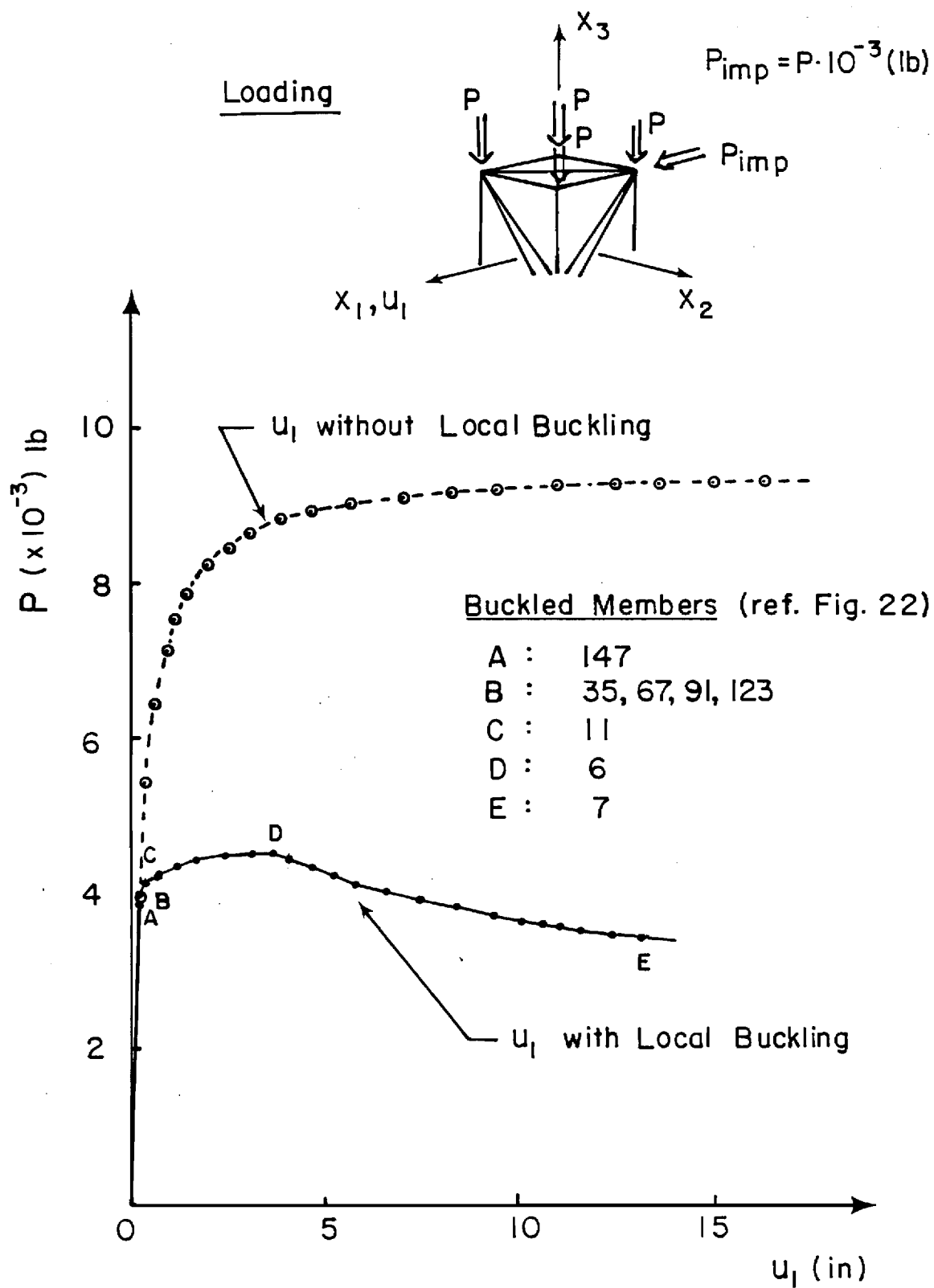
Fig. 28. Deflections at Free end under Axial Loads with and without the Influence of Local Buckling of Truss Members

141

MATERIAL PROPERTY

MEMBER	EA LB	EI LB IN²
LONGERONS	7.08×10^6	2.16×10^6
DIAGONAL, BATTENS	2.70×10^5	6.43×10^4
SHORT LONGERONS	1.65×10^8	2.20×10^8
HORISONTAL DIAGONAL	1.37×10^8	1.52×10^8
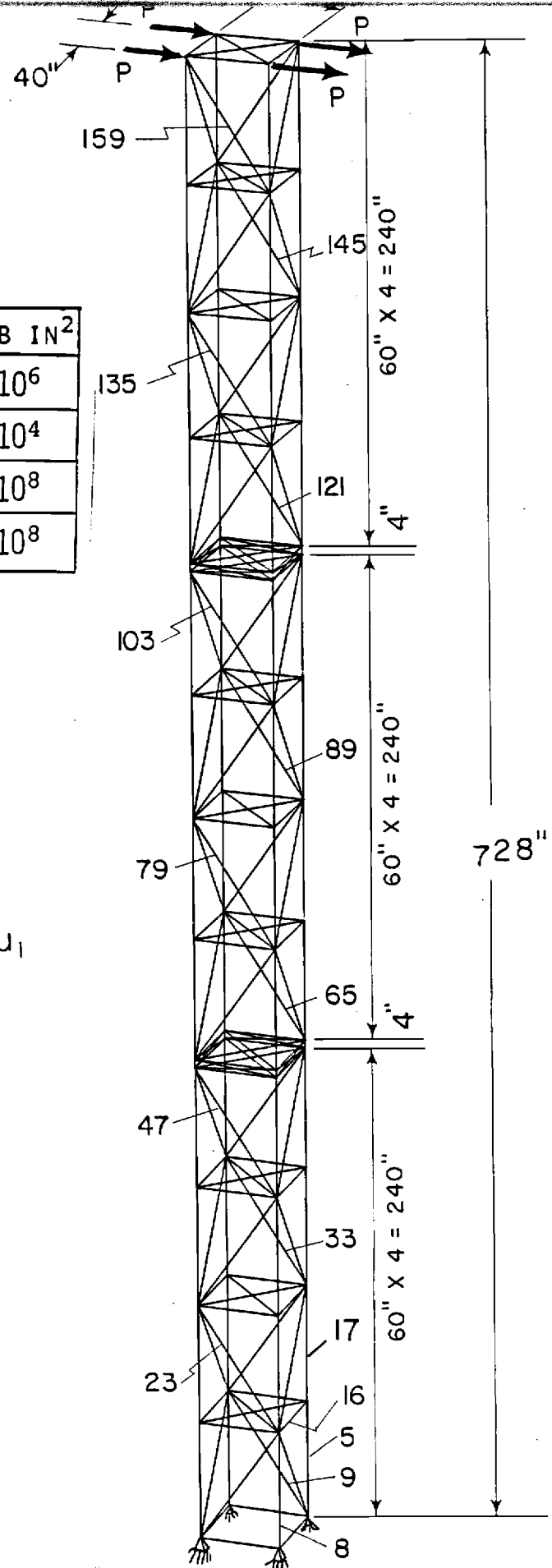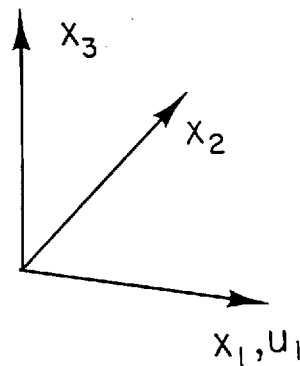
Fig. 29. Schematic of a Twelve-Bay Space Truss under Bending Loads

142
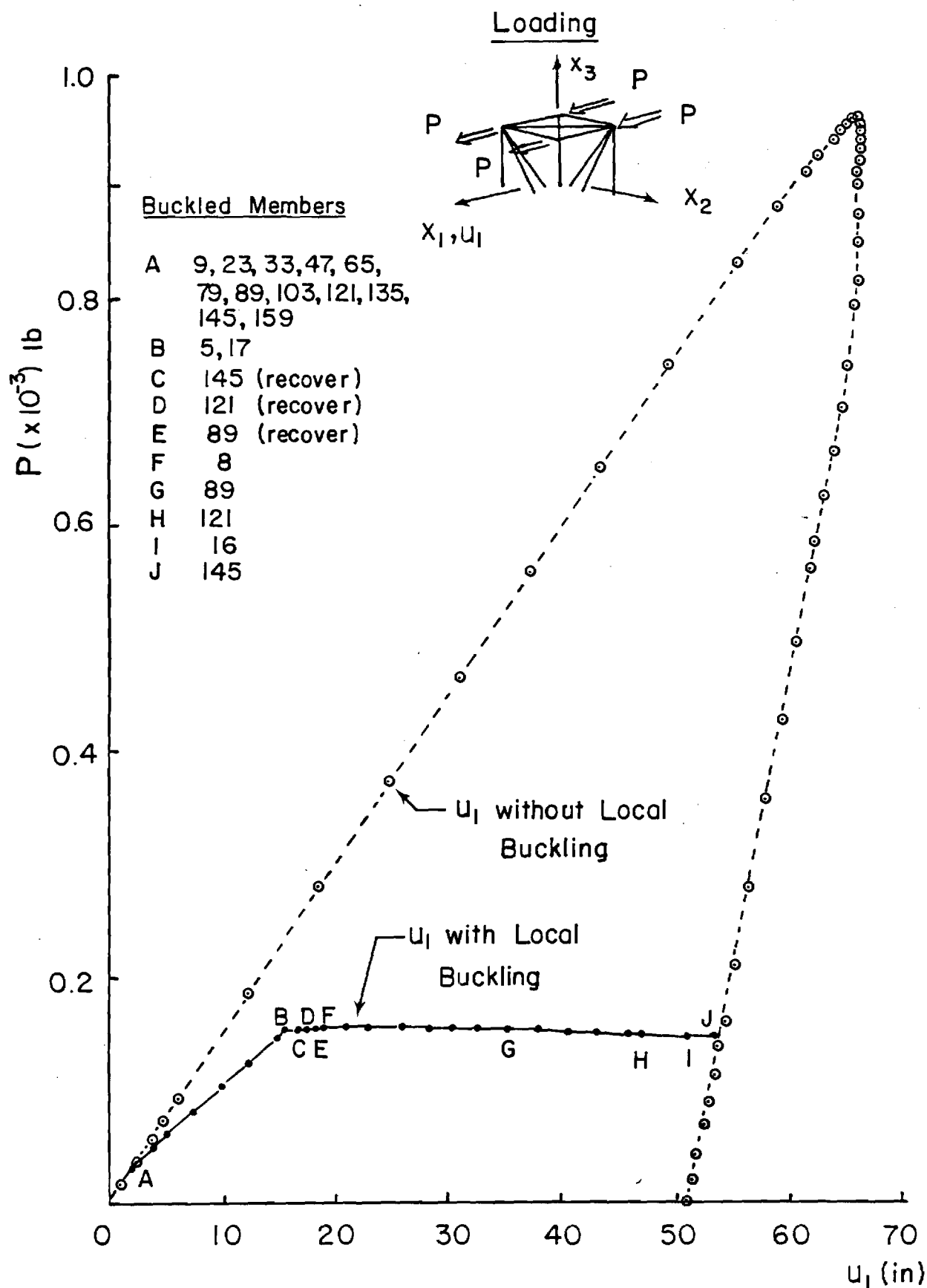
Fig. **30.** Deflections at Free End under Bending Loads with and without the Influence of Local Buckling of Truss Members

143

At State E

P = 155.69 lb

u_1 = 18.52 in
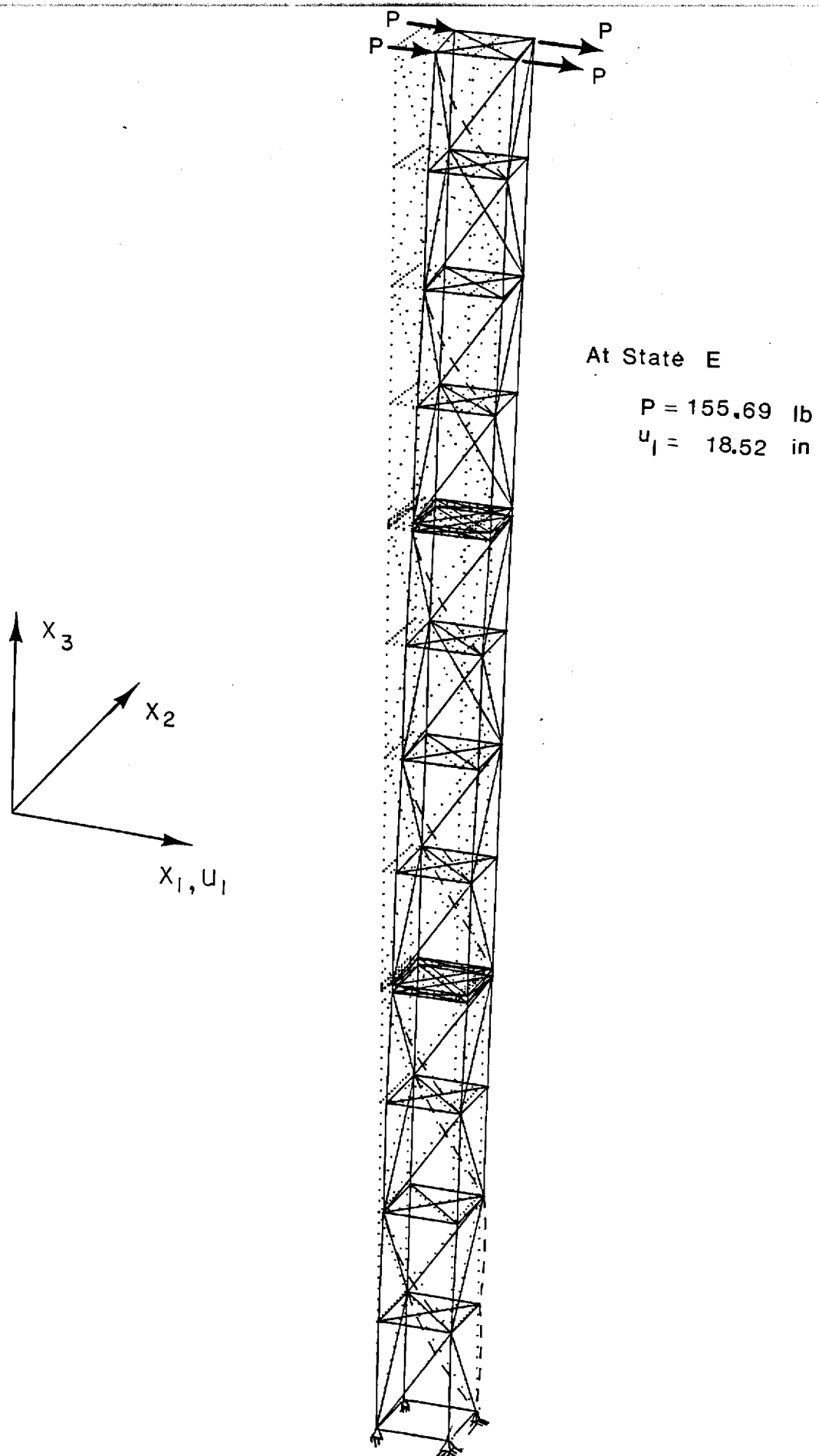
Fig. 31. Deformed Configurations of a Twelve-Bay Space
Truss Shown in Fig. 27

144

$A = 1.0 \ (in^2)$

$I = 0.8333 \ (in^4)$

$l = 100.0 \ (in)$

$E = 10^7 \ (psi)$

$e/l = 0.001$

N

e

δ_V

δ_H

l

e

N
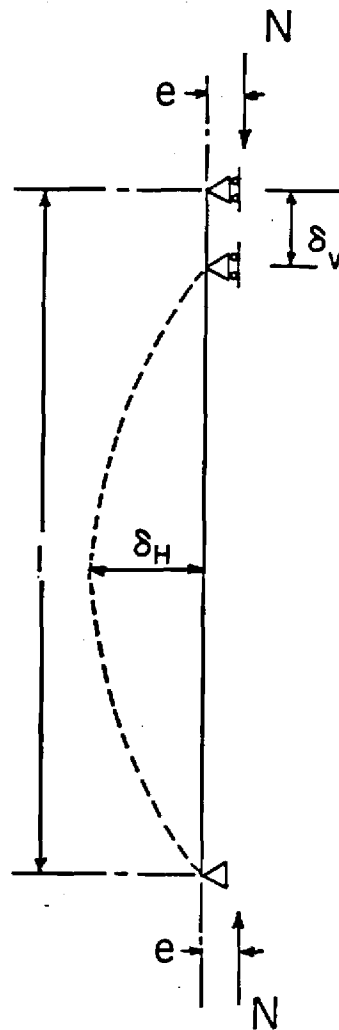
Fig. 32a. Problem Definition for an Eccentrically Loaded Column
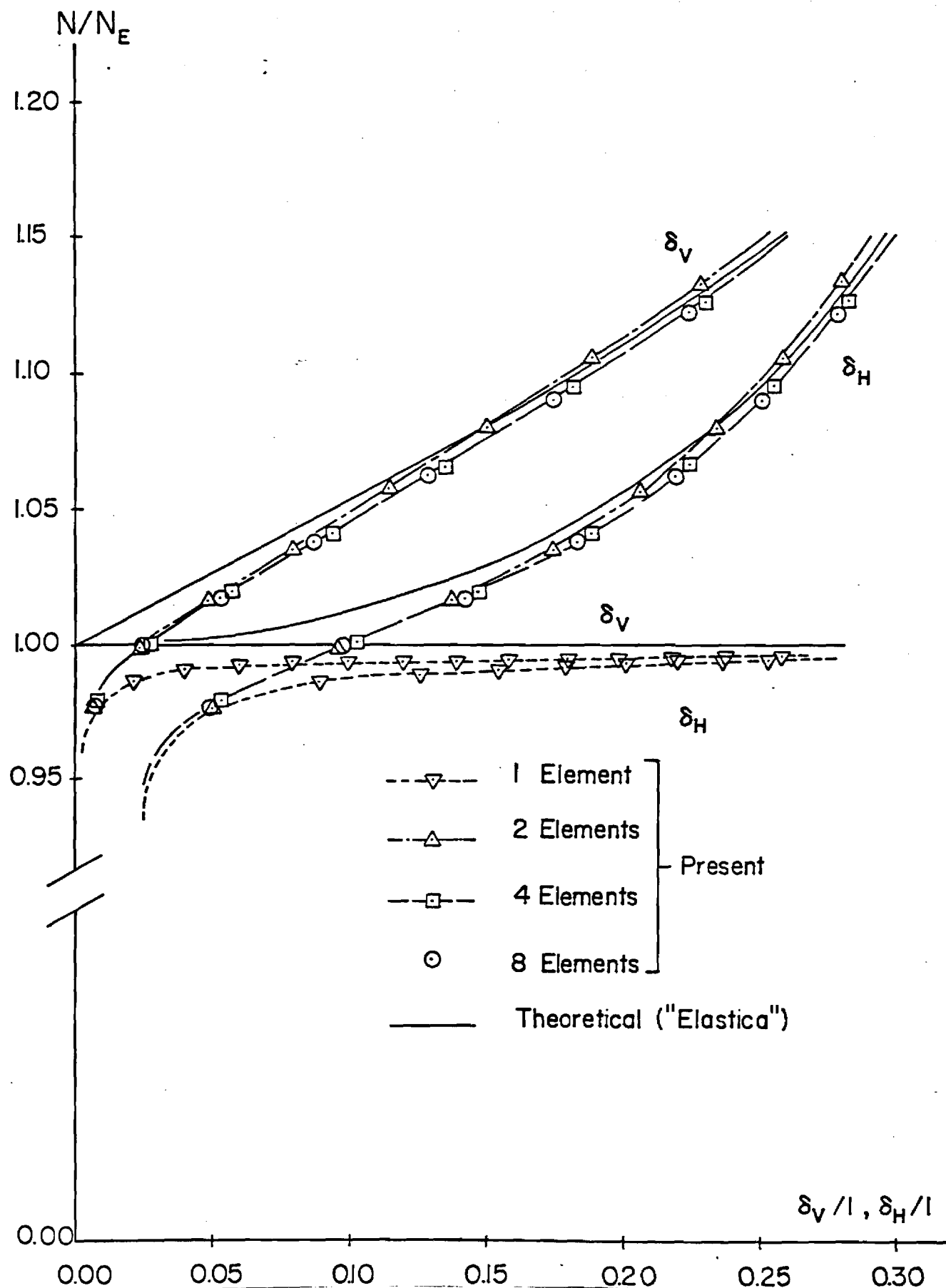
Fig. 32b. Dependence of Axial and Transverse Displacements
on Axial Load for a Buckled Column Under Axial
Eccentric Load: Convergence of Solution
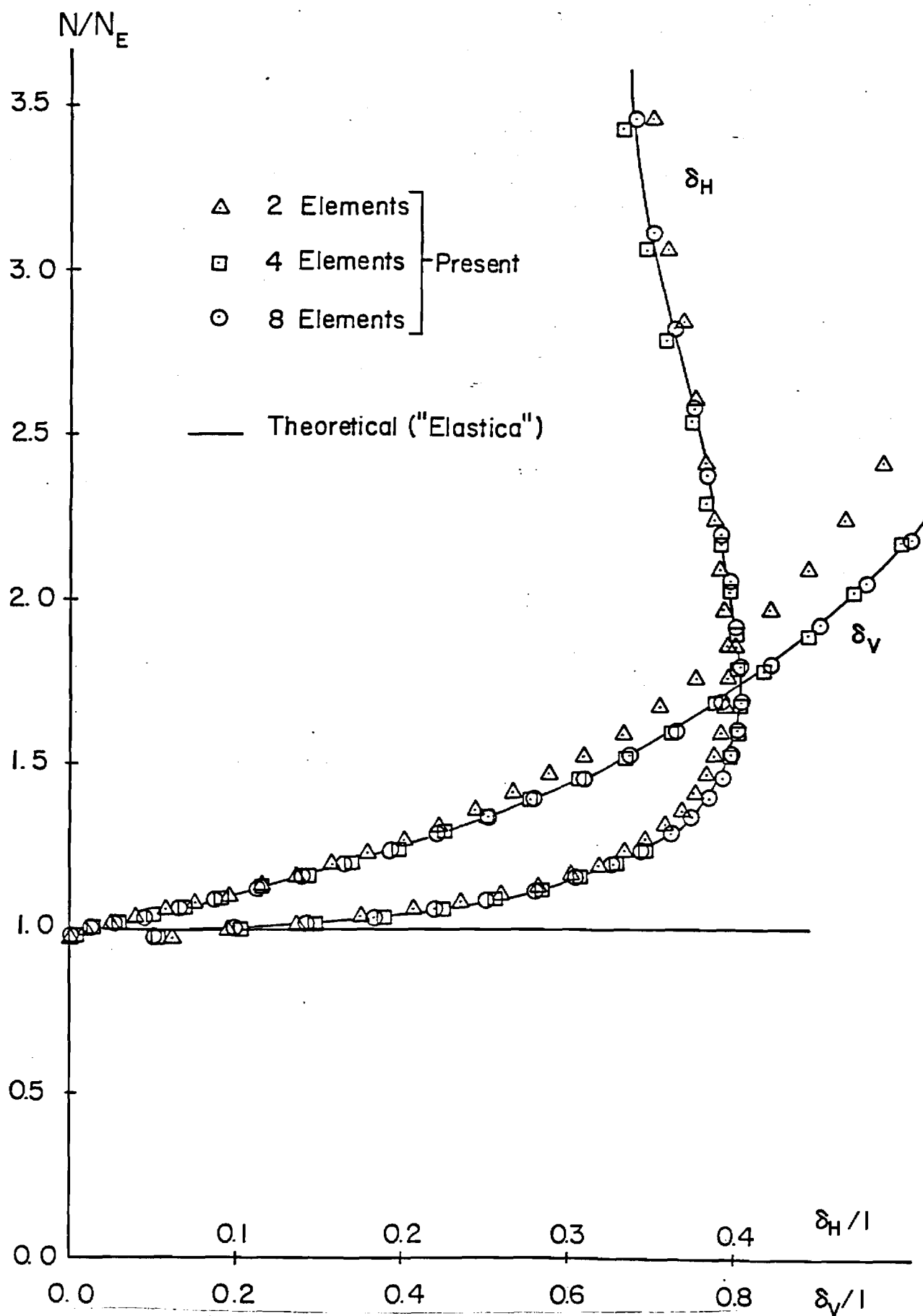
Fig. 32c. Results Similar to Those in Fig. 32b, Except for a
Wider Range of Deformations
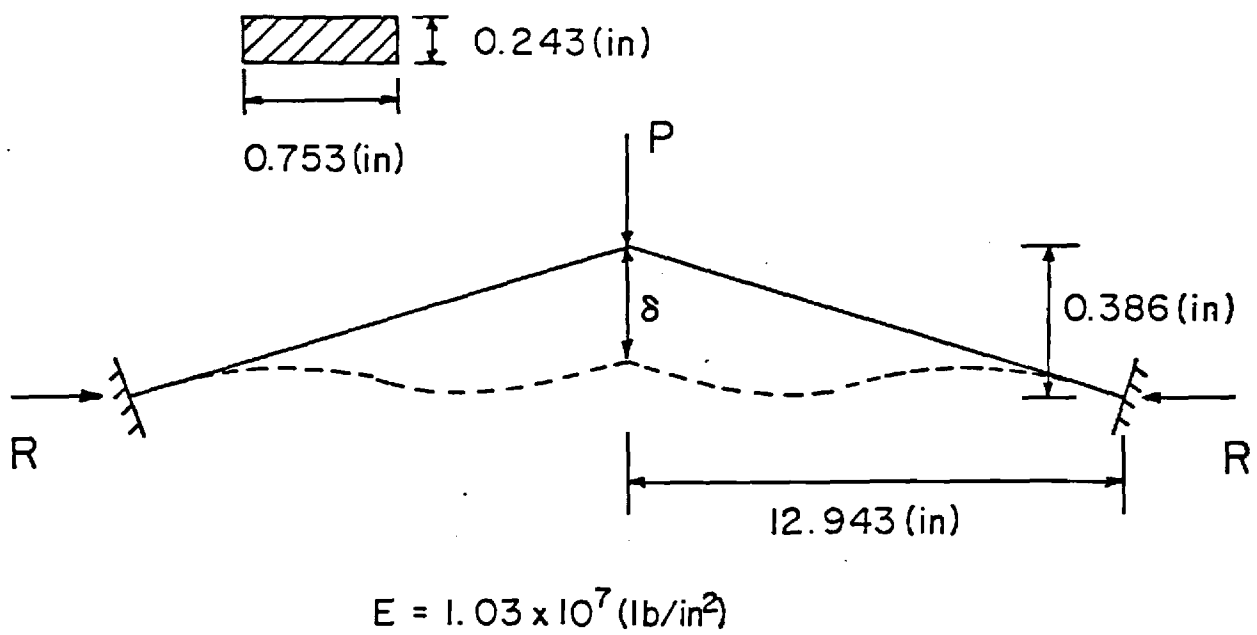
Fig. 33a. Schematic of Williams' Toggle

148
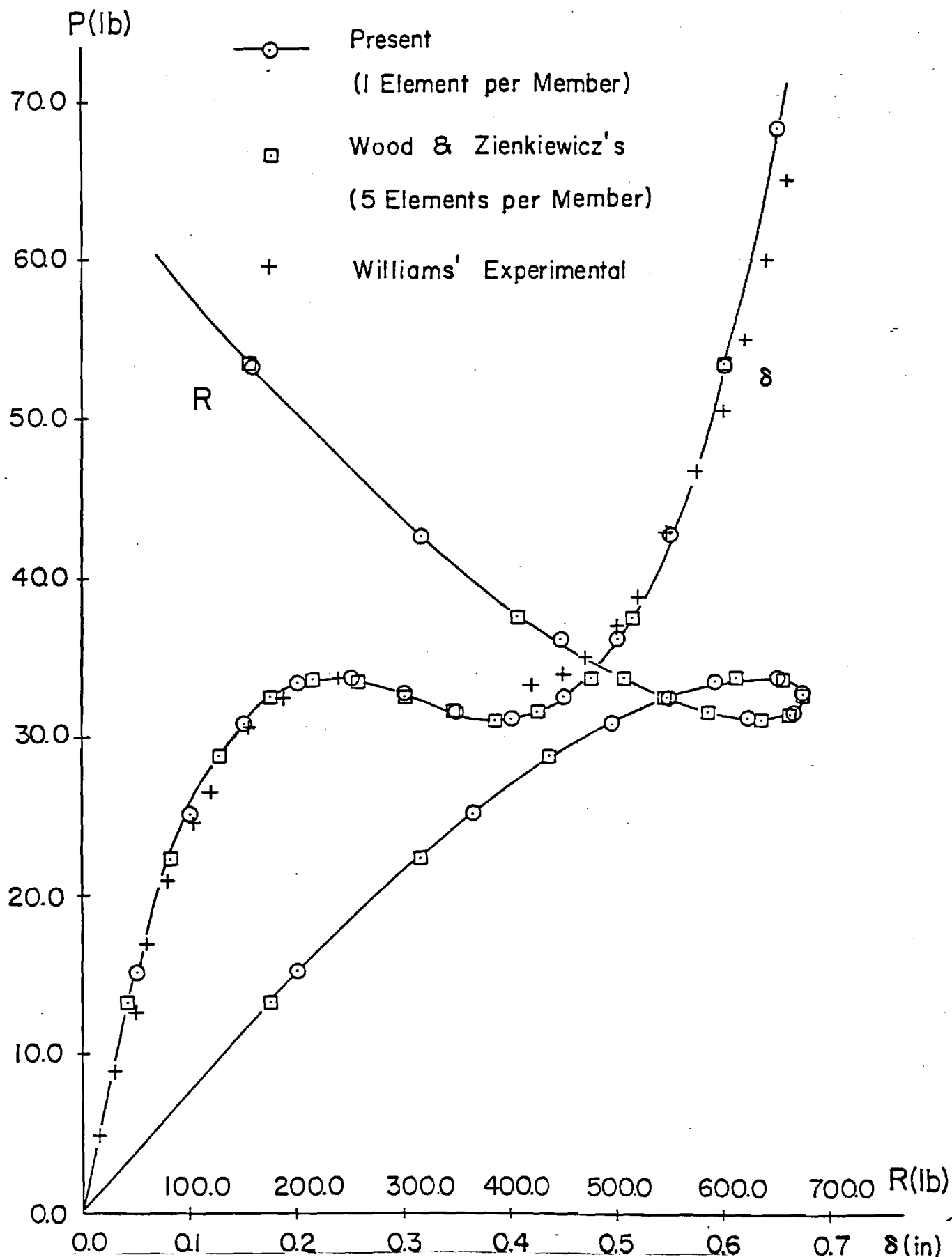
Fig. 33b. Variations of Load-Point Displacement and Support
Reaction with Load, for Williams' Toggle in the
Post-Buckling Range
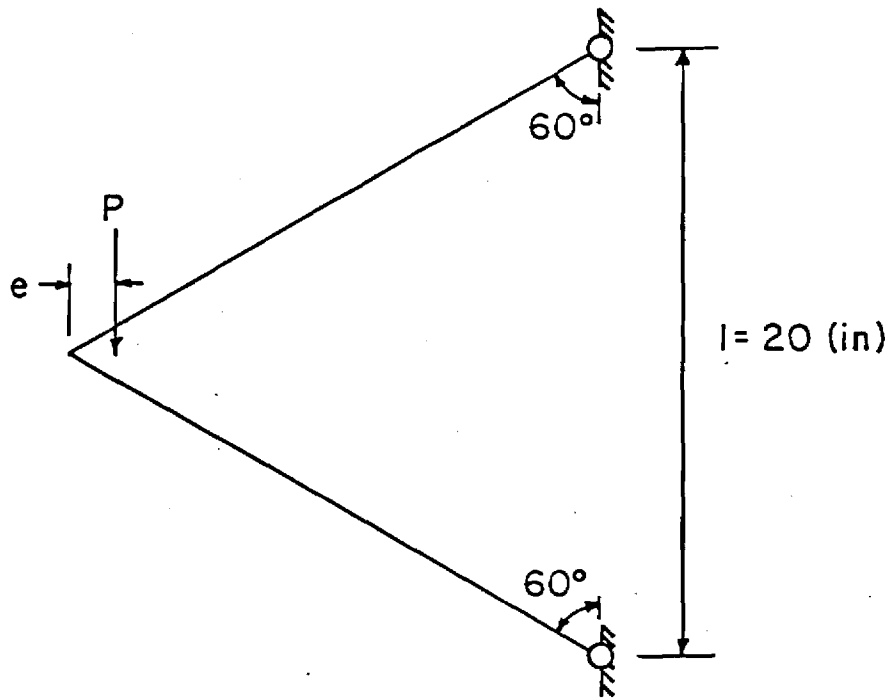
149

Cross-sectional Area of Members = 0.0625 (in^2)

Euler Buckling Load of Each Member (Treated as a Pinned-Pinned Beam) = 8.1 (lb)

Case 1 e/l = -0.001 (Mode (a))

Case 2 e/l = 0.001 (Mode (β))

Fig. 34a. Schematic of Britvec and Chilver's Two-Bar Frame

150
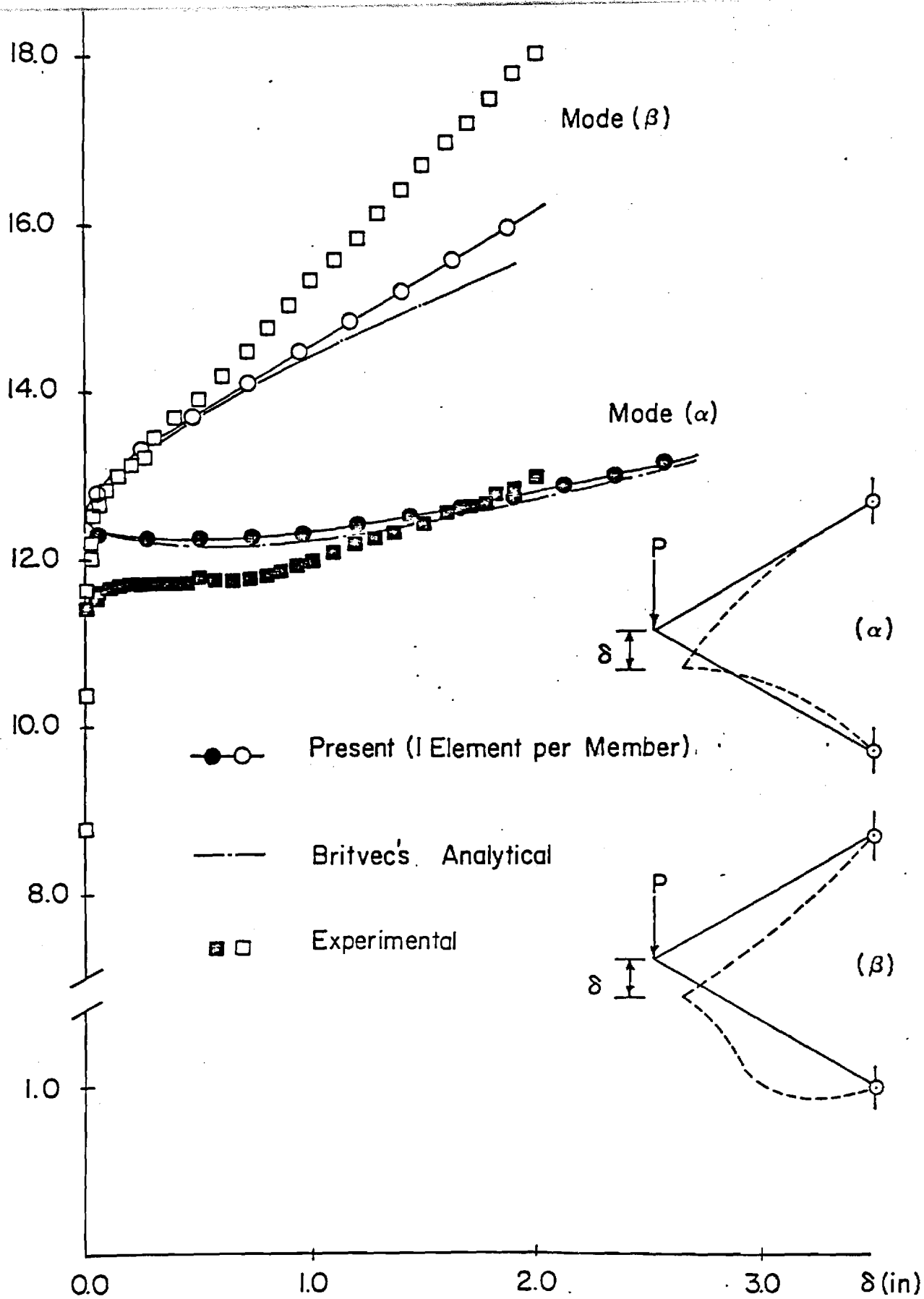
Fig. 34b. Two Modes of Post-Buckling Deformation for
Problem of Fig. 34a
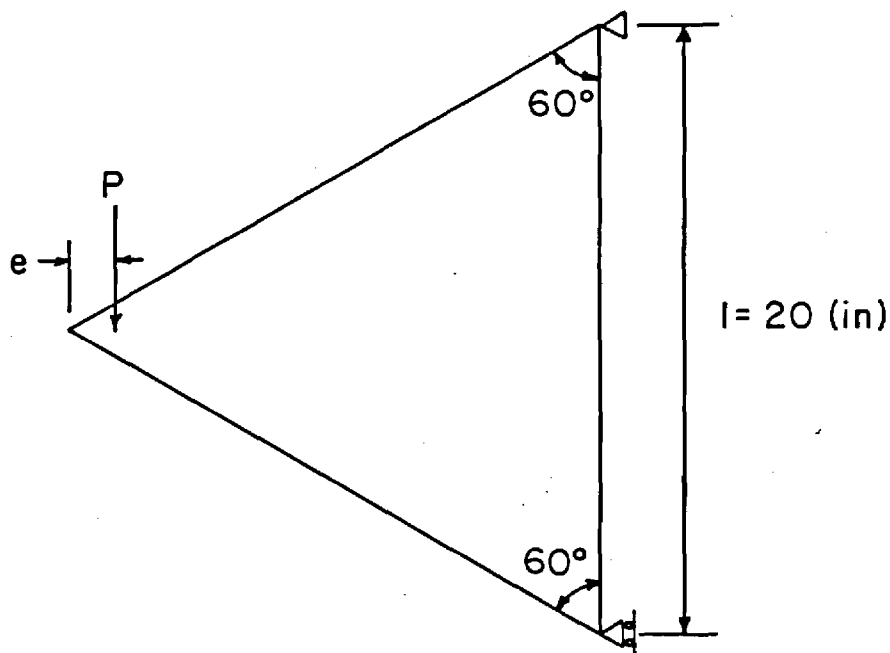
Cross-sectional Area of Members = 0.0625 (in^2)

Euler Buckling Load of Each Member (Treated as a Pinned-Pinned Beam) = 8.1 (lb)

Case 1 e/l = -0.001 (Mode (α))

Case 2 e/l = 0.001 (Mode (β))

Fig. 35a. Schematic of Britvec and Chilver's Three-Bar Frame
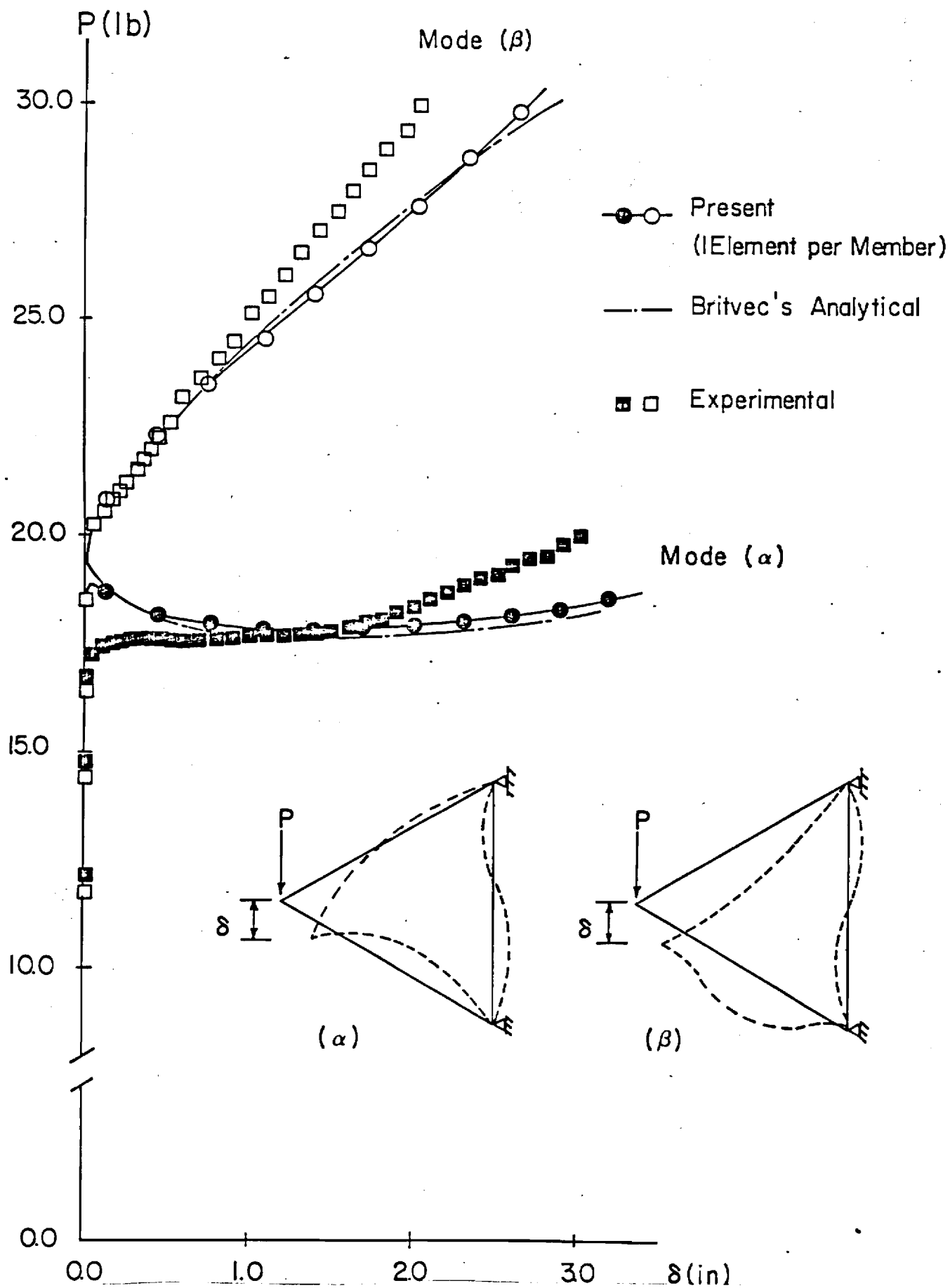
Fig. 35b. Two Modes of Deformation of the Three-Bar Frame

153
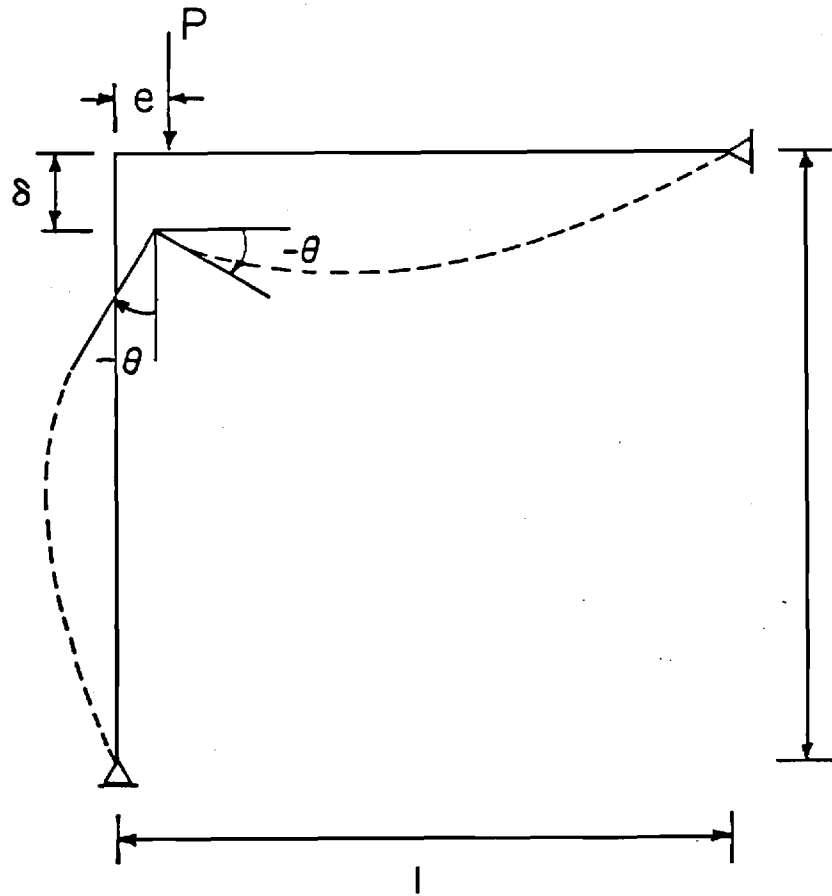
$$A = 600.0 \ (in^2) \ , \quad I = 60000.0 \ (in^4)$$

$$l = 1000.0 \ (in) \ , \quad E = 10000.0 \ (psi)$$

$$P_E = 13.885 \ EI/l^2 \quad (e = 0)$$

Fig. 36a. Eccentrically Loaded Right-Angled Frame

154
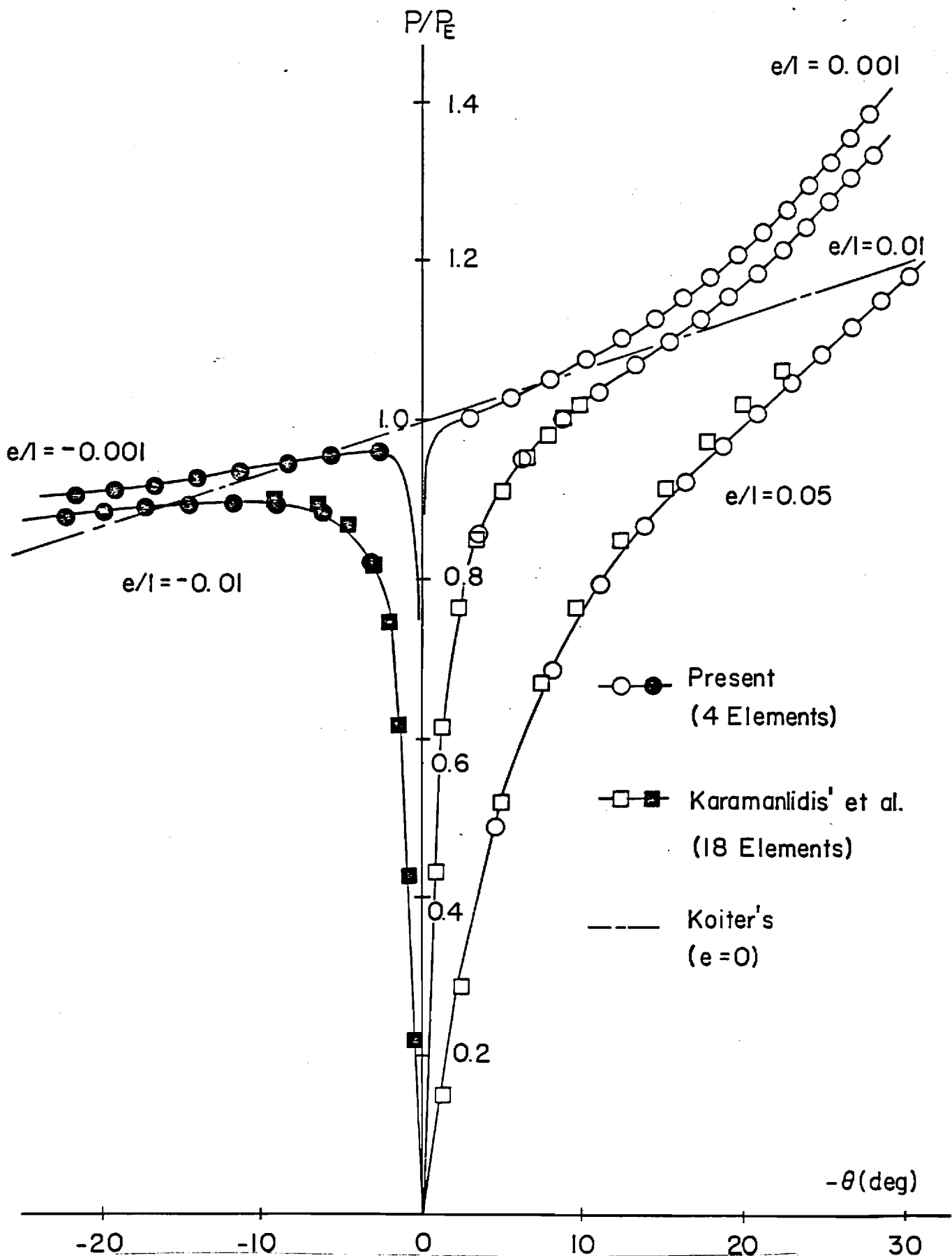
Fig. 36b. Variation of Corner-Rotation of a Right-Angled Frame
for Various Values of Load-Eccentricity (e/ℓ), in the
Post-Buckling Range

155
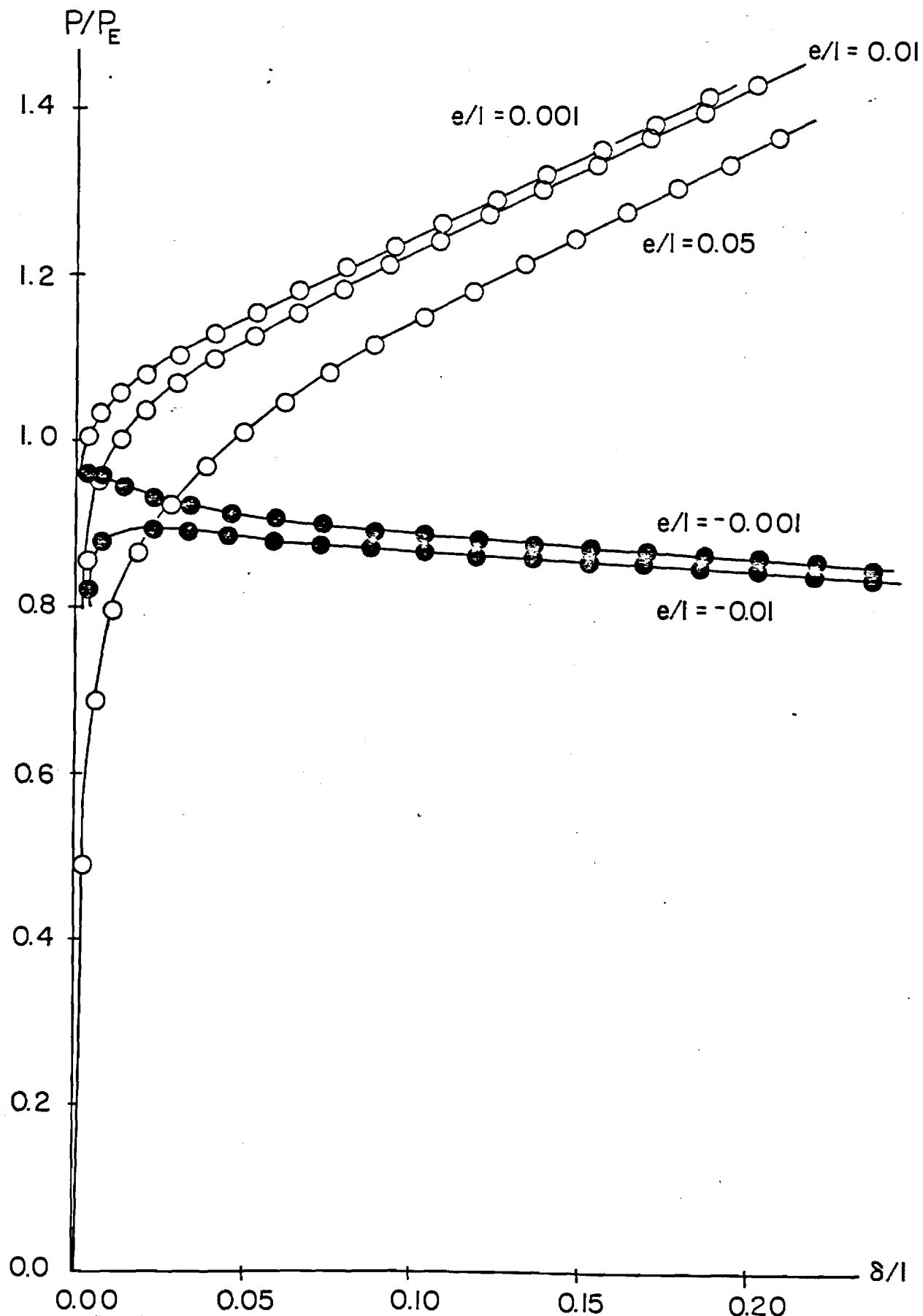
Fig. 36c. Variation of Vertical-Displacement (of the Corner)
with Load, for Various Values of Load Eccentricity
(e/ℓ), in the Post-Buckling Range
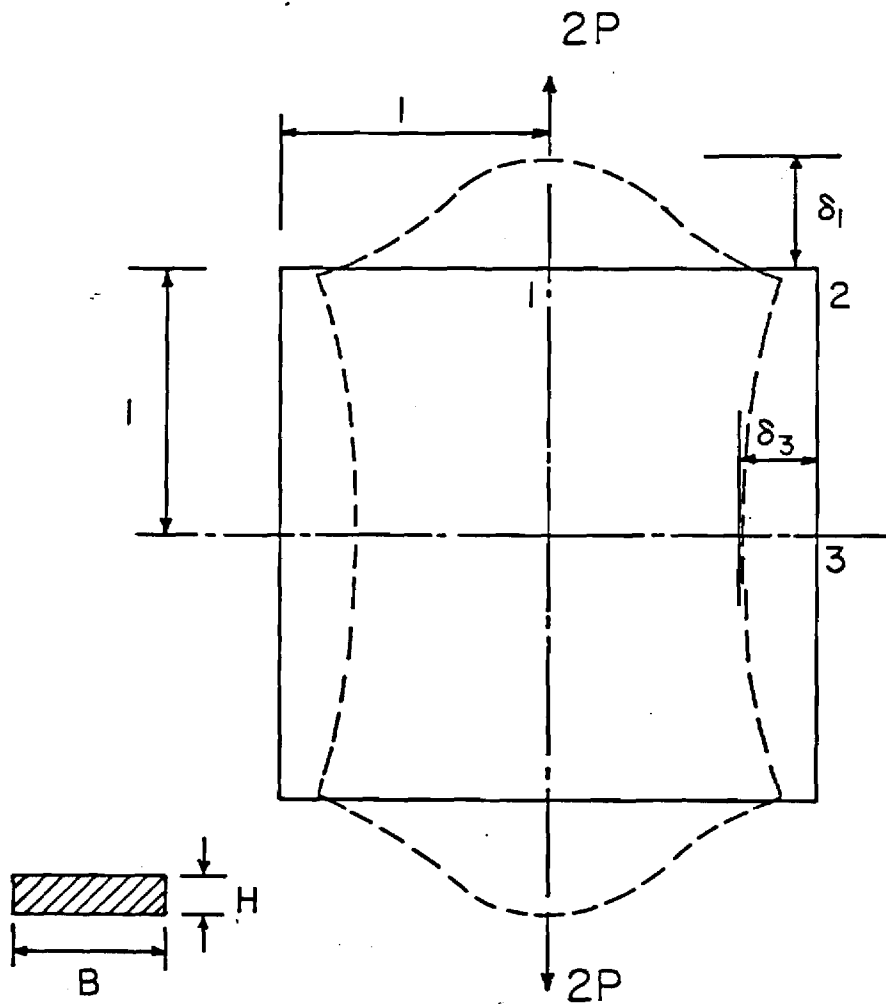
$$B = 1.0 \ (in) \quad , \quad H = 0.25 \ (in)$$

$$I = 8.5 (in) \quad , \quad E = 10^6 \ (psi)$$

Fig. 37a. Schematic of a Four-Member Square Frame
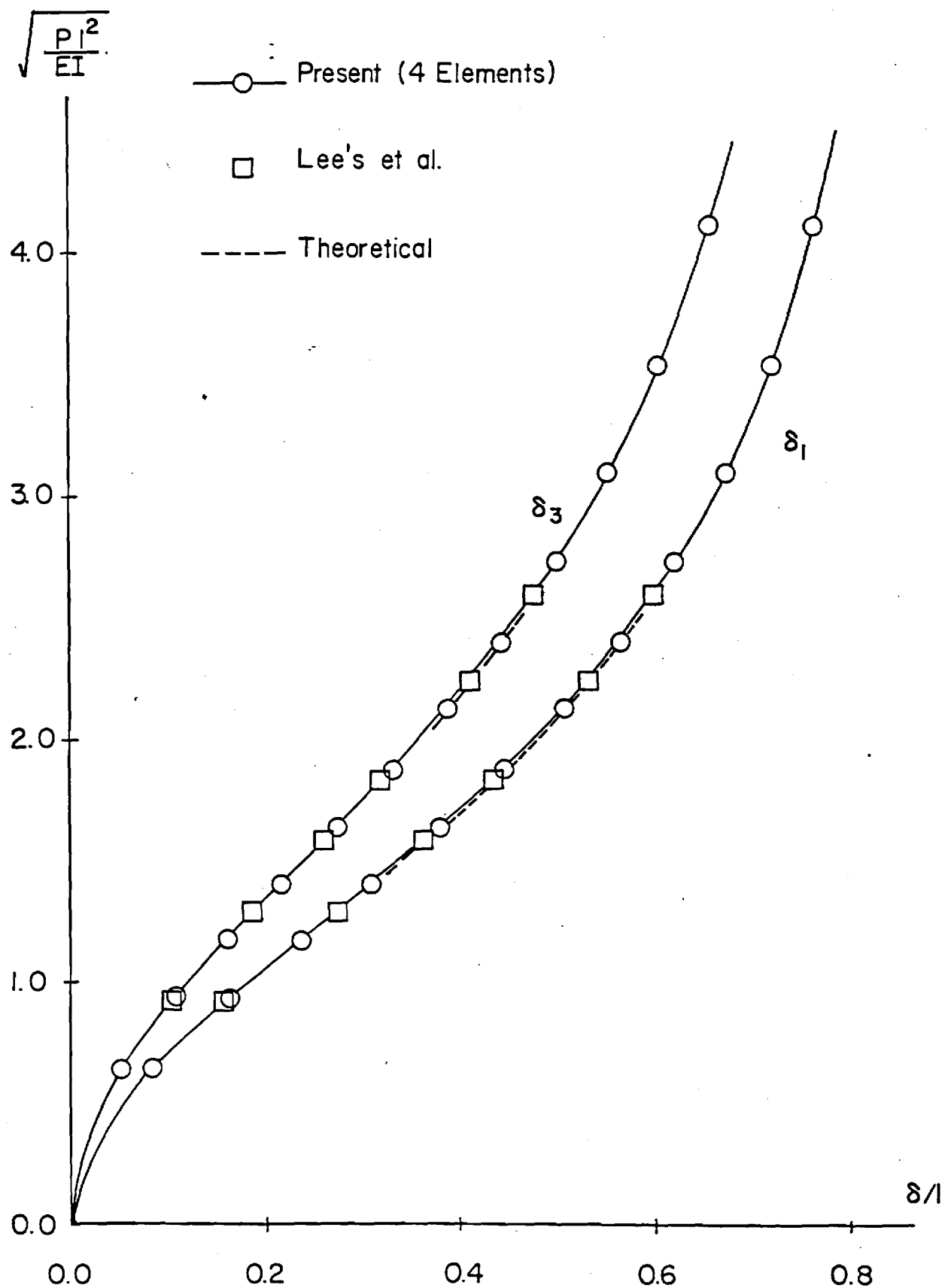
Fig. 37b. Variation of Displacements δ_1 and δ_3 (See Fig. 37a]
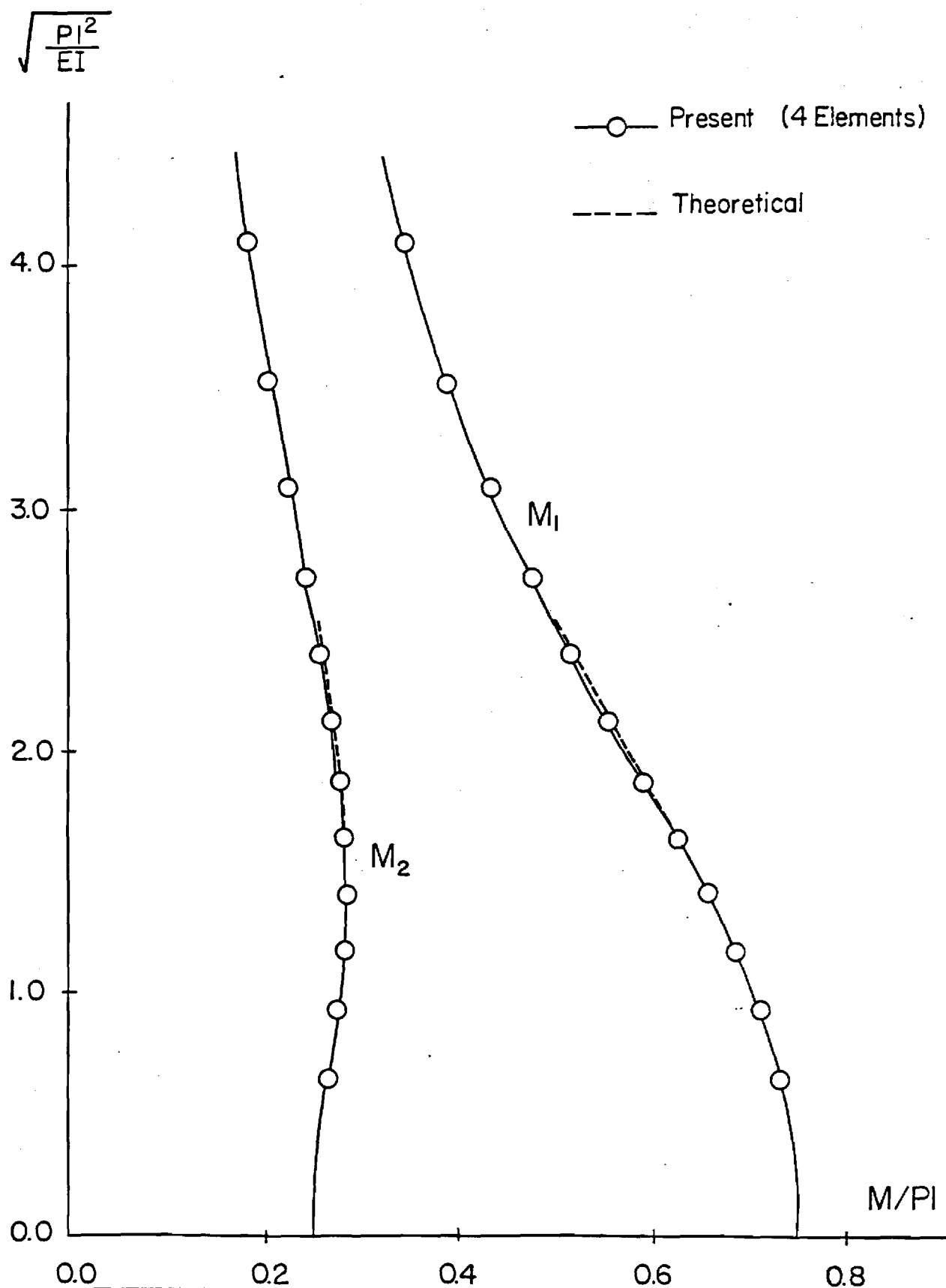with Load for a Square-Frame

Fig. 37c. Variation of Moments M_1 and M_2 (at Points 1, 2 in Fig. 37a) with Load, for a Square-Frame
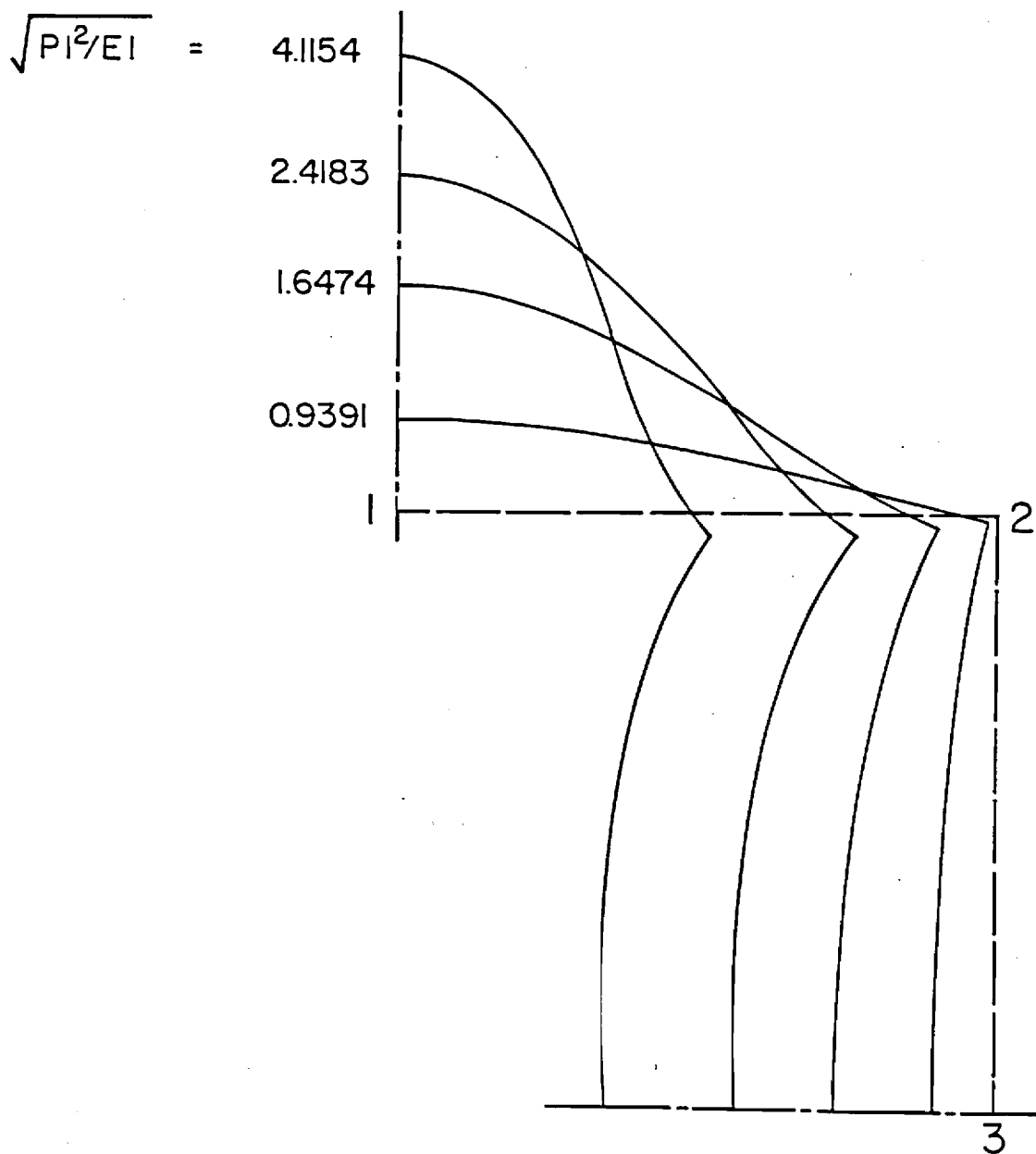
$$\sqrt{Pl^2/EI} \ = \quad 4.1154$$

2.4183

1.6474

0.9391

Fig. 37d. Deformation Profiles at Various Load Levels
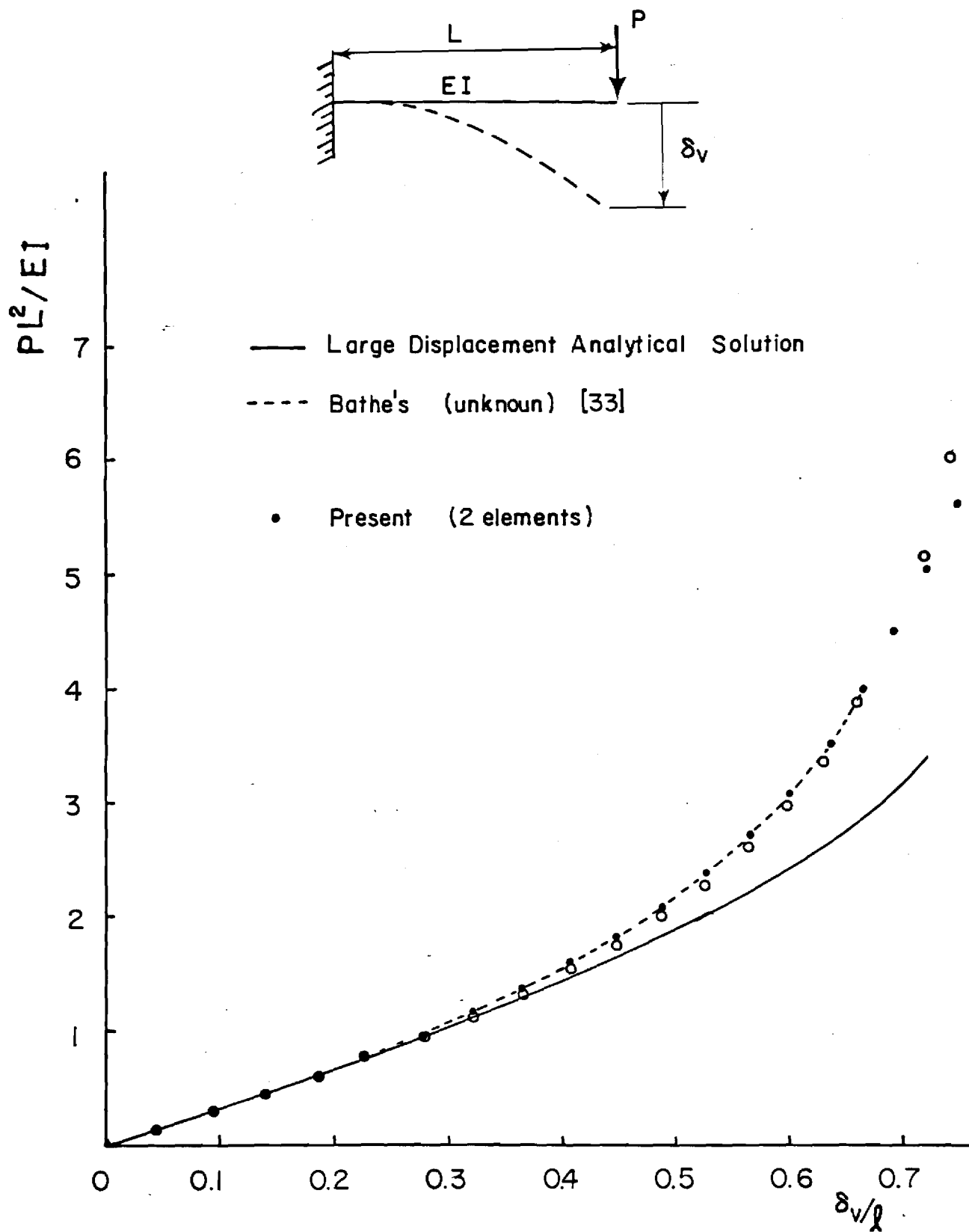for a Square-Frame

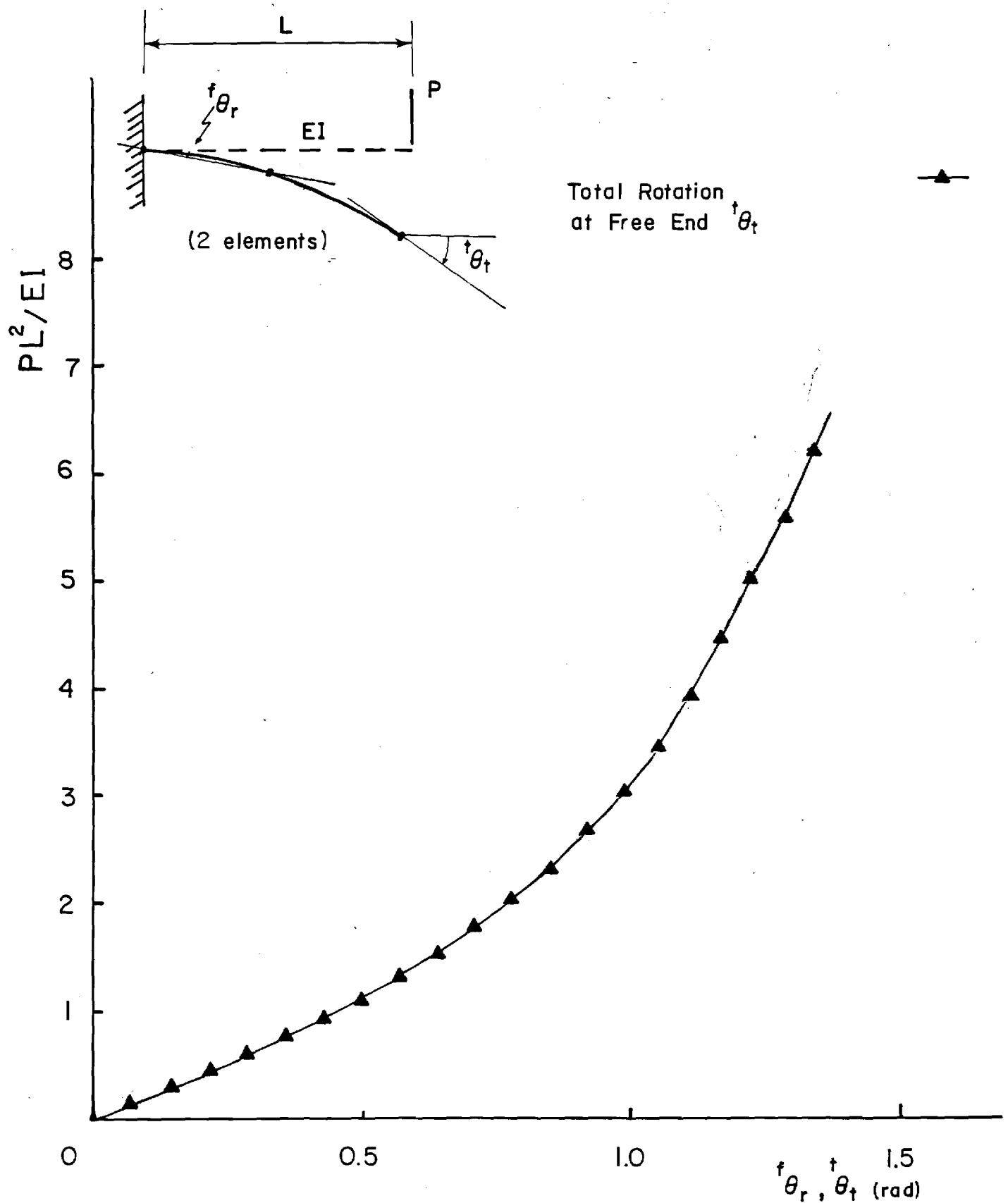Fig. 38. Deflections of a Cantilever under a Concentrated
Load

161

Fig. 39. Rotations of a Cantilever under a Concentrated Load

Material Property

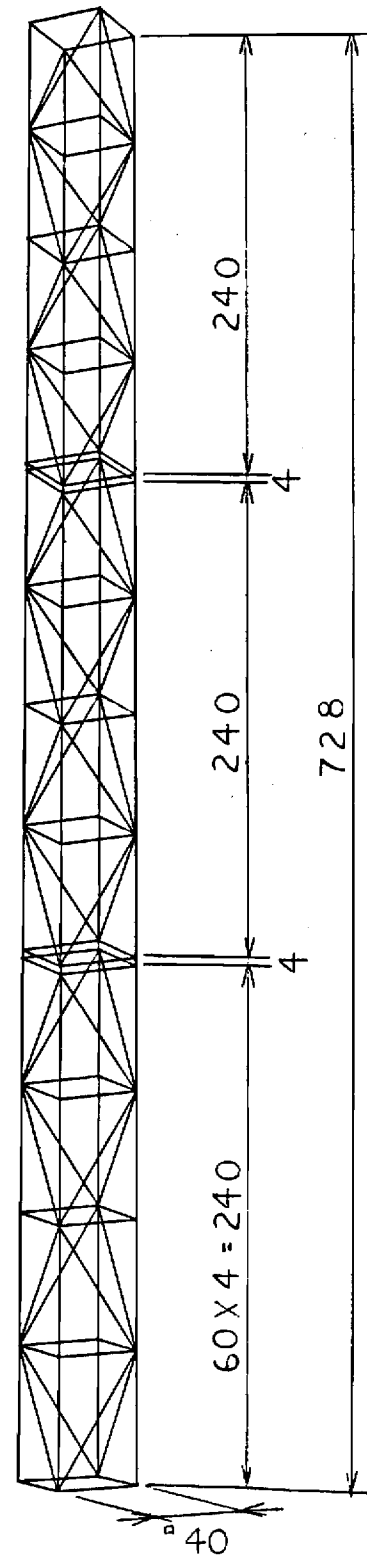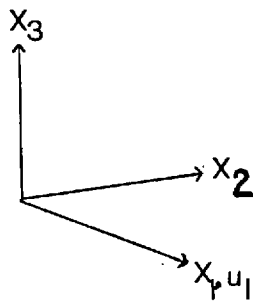| Longerons	Diagonal.Battens	Short Longerons	
7.08×10^6	2.70×10^5	1.65×10^8	lb
2.16×10^6	6.43×10^4	2.20×10^8	lb in^2
1.63×10^6	4.77×10^4	1.40×10^8	lb in^2

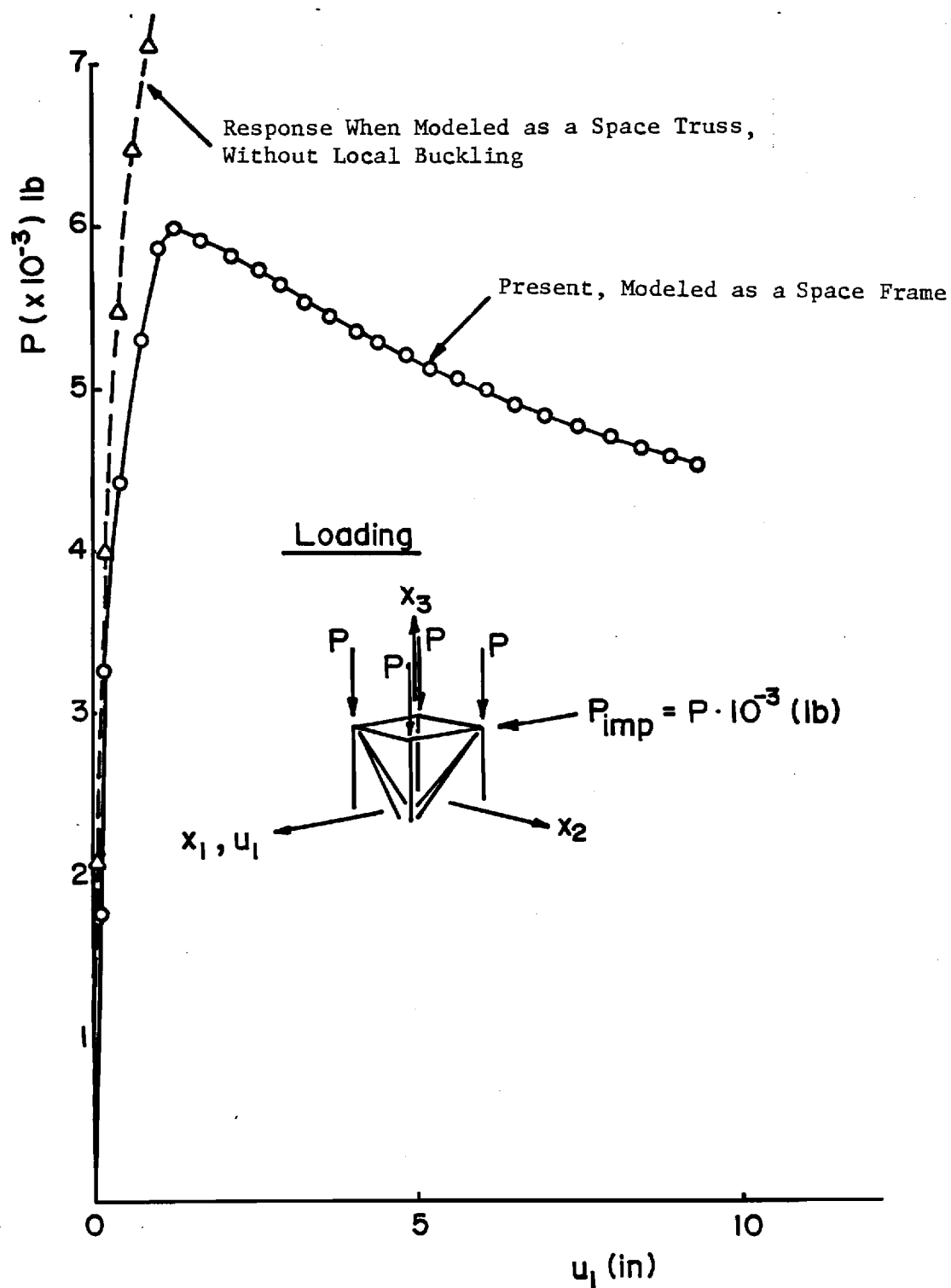Fig. 40. Schematic of a Twelve-Bay Space Frame

163

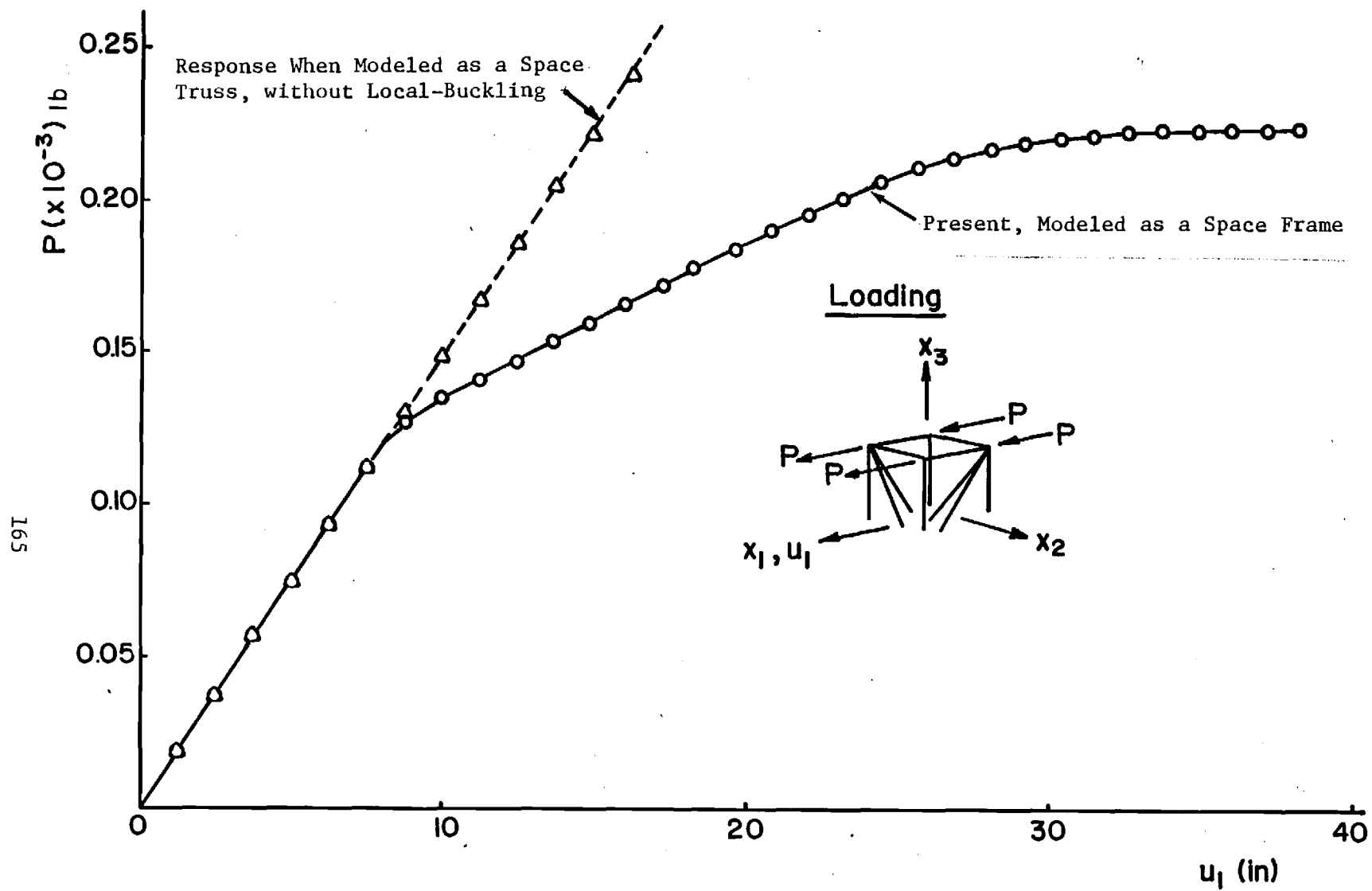Fig. 41. Deflections at Free End under Axial Loads

164

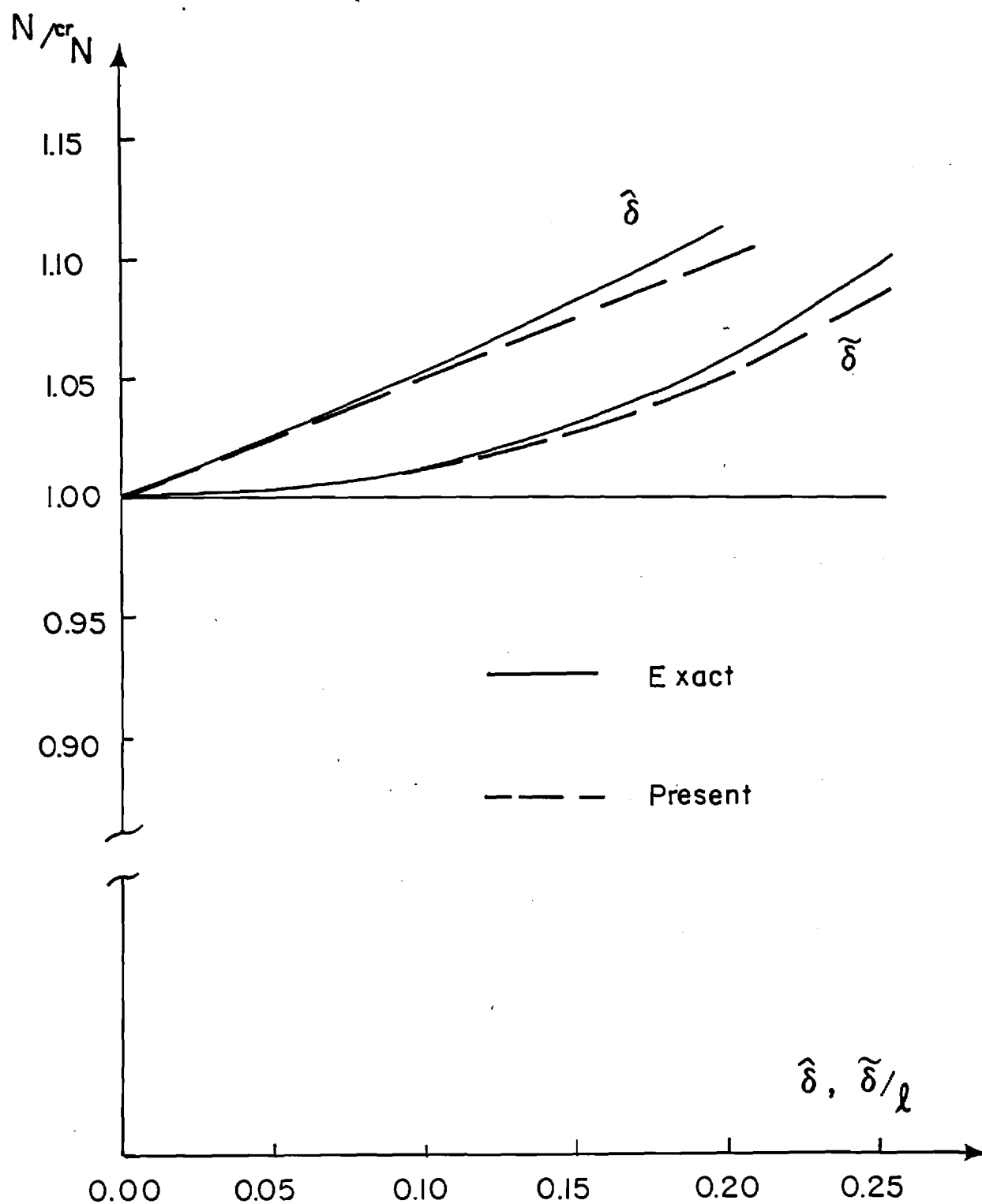Fig. 42. Deflections at the Free End under Bending Loads

Fig. 43. Axial Stretches and Lateral Deflections (at the center of the span of the member) in the Post-Buckled Range under an Axial Force
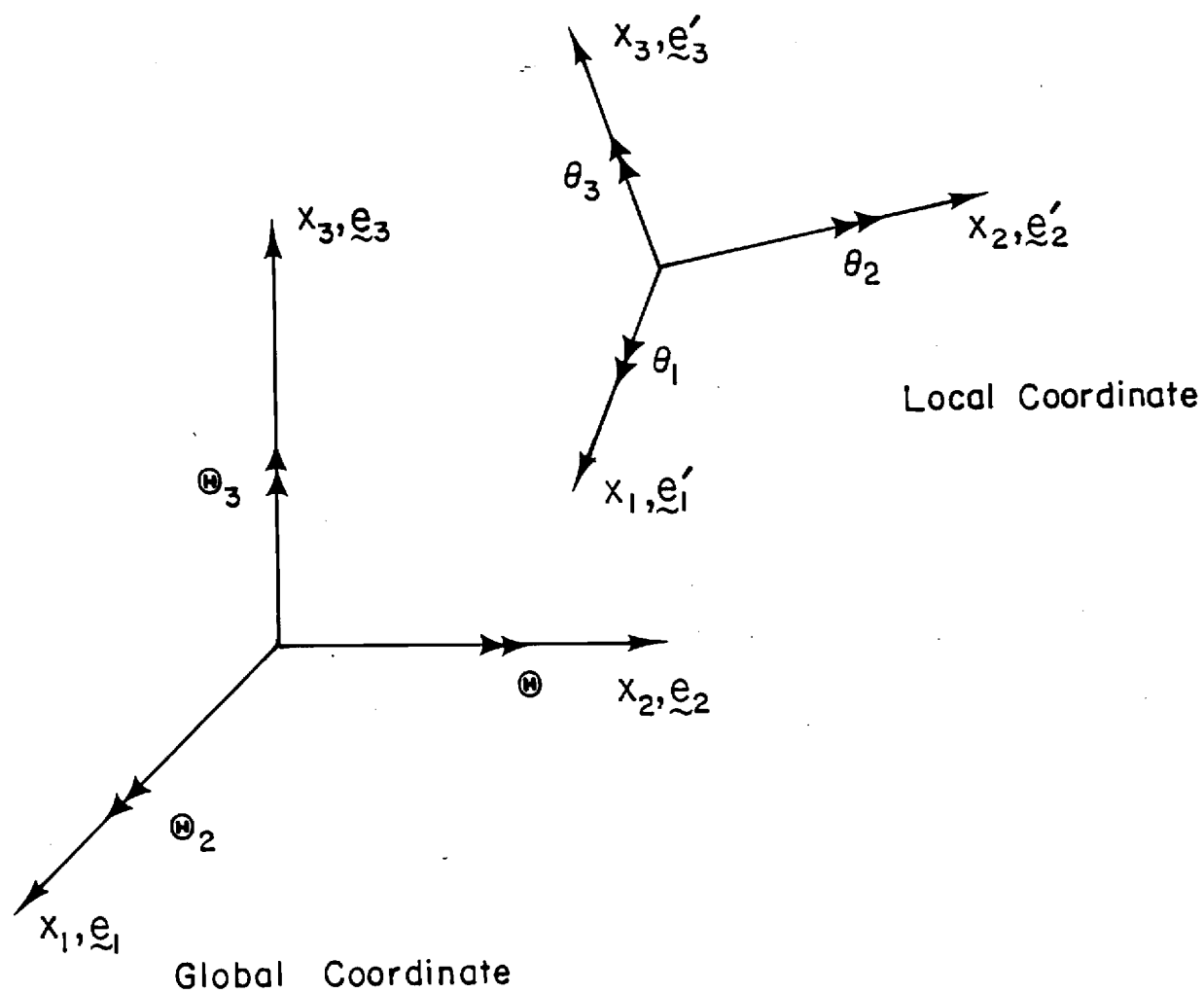
Fig. 44. Nomenclature for Coordinate Transformation of Rotations

BIBLIOGRAPHY

1. R. H. Gallagher, "Finite Element Analysis of Geometrically Nonlinear Problems" in Theory and Practice in Finite Element Structural Analysis (Eds: Y. Yamada and R. H. Gallagher), University of Tokyo Press, 1973, pp. 109-123.

2. Y. Hangai and S. Kawamata, "Perturbation Method in the Analysis of Geometrically Nonlinear and Stability Problems" in Advancement in Computational Mechanics in Structural Mechanics and Design (Eds: J.T. Oden, R. W. Clough, and Y. Yamamoto), UAH Press, Huntsville, Alabama, 1972, pp. 473-489.

3. R. H. Gallagher, "Finite Element Method for Instability Analysis" in Handbook of Finite Elements (Eds: H. Kardestuncer, F. Brezzi, S.N. Atluri, D. Norrie, and W. Pilkey), McGraw-Hill (In Press).

4. J.M.T. Thompson and G.W. Hunt, A General Theory of Elastic Stability, J. Wiley & Sons, 1973.

5. O.C. Zienkiewicz, The Finite Element Method, 3rd Edition, McGraw-Hill, 1977.

6. G. Horrigmoe and P. Bergan, "Nonlinear Analysis of Free Form Flat Shells by Flat Finite Elements", Comp. Meth. Appl. Mech. Engng., Vol. 11, 1977, pp. 97-131.

7. A.K. Noor and J.M. Peters, "Recent Advances in Reduction Methods for Instability Analysis of Structures", Comp. & Struct., Vol. 16, 1983, pp. 67-80.

8. H. Murakawa and S.N. Atluri, "Finite Elasticity Solutions Using Hybrid Finite Elements Based on a Complementary Energy Principle", Trans. ASME J. Appl. Mech., Vol. 45, 1978, pp. 539-547.

9. H. Murakawa, K.W. Reed, S.N. Atluri, and R. Rubinstein, "Stability Analysis of Structures via a New Complementary Energy Method", Comp. & Struct., Vol. 13, 1981, pp. 11-18.

10. Y. Yoshida, T. Nomura, and N. Masuda, "A Formulation and Solution Procedure for Post-Buckling of Thin-Walled Structures", Comp. Meth. Appl. Mech. Engng., Vol. 32, 1982, pp. 285-309.

11. W.E. Haisler and J.A. Stricklin, "Displacement Incrementation in Nonlinear Structural Analysis", Int. J. Num. Meth. Engng., Vol. 11, 1977, p. 3.

12. G. Powell and J. Simons, "Improved Iteration Strategy for Nonlinear Structures", Int. J. Num. Meth. Engng., Vol. 17, 1981, pp. 1455-1467.

13. E. Ramm, "Strategies for Tracing the Nonlinear Response Near Limit Points" in Nonlinear Finite Element Analysis in Structural Mechanics (Eds: W. Wunderlich, E. Stein, and K.G. Bath), Springer-Verlag, New York, 1981, pp. 63-89.

14. P.G. Bergan and T.H. Soreide, "Solution of Large Displacement and Instability Problems Using the Current Stiffness Parameter" in Finite Elements in Nonlinear Mechanics (Eds: P.G. Bergan, P.K. Larsen, H. Peterson, A. Samuelssen, T.H. Soreide, and N.K. Weiberg), Tapir Press, Norwegian Institute of Technology, 1977, pp. 647-669.

15. P.G. Bergan, G. Horrigmoe, B. Krakeland, and T.H. Soreide, "Solution Techniques for Nonlinear Finite Element Problems" Int. J. Num. Meth. Engng., Vol. 12, 1978, pp. 1677-1696.

16. E. Riks, "The Application of Newton's Method to the Problem of Elastic Stability", J. Appl. Mech., Vol. 39, 1972, pp. 1060-1066.

17. E. Riks, "An Incremental Approach to the Solution of Snapping and Buckling Problems", Int. J. Solids Struct., Vol. 15, 1979, pp. 529-551.

18. G.A. Wempner, "Discrete Approximations Related to Nonlinear Theories of Solids", Int. J. Solids Struct., Vol. 7, 1971, pp. 1581-1599.

19. M.A. Chrisfield, "A Fast Incremental/Iterative Solution Procedure that Handles Snap-through", Comp. & Struct., Vol. 13, 1981, pp. 55-62.

20. M.A. Chrisfield, "An Arch-Length Method Including Line Searches and Acceleration", Int. J. Num. Meth. Engng., Vol. 19, 1983, pp. 1269-1289.

21. K. Kondoh and S.N. Atluri, "Influence of Local Bucking on Global Instability: Simplified, Large Deformation, Post-Buckling Analyses of Plane Trusses", Comp. & Struct., 1984 (In Press).

22. K. Kondoh and S.N. Atluri, "A Simplified Finite Element Method for Large Deformation, Post-Buckling Analyses of Large Frame Structures, Using Explicitly Derived Tangent Stiffness Matrices", Int. J. Num. Meth. Engng., 1984 (In Press).

23. A. Rosen and L.A. Schmit, "Design Oriented Analysis of Imperfect Truss Structures", UCLA-ENG-7764, 1977. See also "Design Oriented Analysis of Imperfect Truss Structures Part I (Accurate Analysis) and Part 2 (Approximate Analysis)", Int. J. Num. Meth. Engng., Vol. 14, 1979, pp. 1309-1321 and Vol. 15, 1980, pp. 483-494.

24. J.H. Argyris, P.C. Dunne, and D.W. Scharpf, "On Large Displacement-Small Strain Analysis of Structures with Rotational Degrees of Freedom", Comp. Meth. Appl. Mech. Engng., Vol. 14, 1978, pp. 401-451.

25. J.H. Argyris, "An Excursion into Large Rotations", Comp. Meth. App. Mech. Engng., Vol. 32, 1982, pp. 85-155.

26. A.C. Eringen, Nonlinear Theory of Continuous Media, McGraw-Hill, New York, 1962.

27. S.N. Atluri, Lecture Note in Computational Mechanics, 1984-1985.

28. S.P. Timoshenko and J. M. Gere, Theory of Elastic Stability, 2nd Edition, McGraw-Hill, New York, 1961, pp. 76-82.

29. S.J. Britvec and A.H. Chilver, "Elastic Bucking of Rigidly-Jointed Braced Frames", J. Engng. Mech. Div., Proc. ASCE, EM6, 1963, pp. 217-255.

30. S.J. Britvec, The Stability of Elastic Systems, Pergamon Press, New York, 1973.

31. S.N. Atluri, "On Some New General and Complementary Energy Theorems for the Rate Problems in Finite Strain, Classical Elastoplasticity", J. Struct. Mech., Vol. 8, No. 1, 1980, pp. 61-92.

32. A.K. Noor and J.M. Peters, "Instability Analysis of Space Trusses", Comp. Meth. Appl. Mech. Engng., Vol. 40, 1983, pp. 199-218.

33. K.J. Bathe and S. Bolourchi, "Large Displacement Analysis of Three-Dimensional Beam Structures", Int. J. Num. Meth. Engng., Vol. 14, 1979, pp. 961-986.

34. H.O. Newboult, Analytical Method in Dynamics, Oxford University Press, London, 1946, pp. 26-29.

35. R.F. Byrd and M.D. Friedman, Handbook of Elliptic Integrals for Engineers and Scientists, Springer-Verlag, Berlin, 1971.

36. S.J. Britvec, The Stability of Elastic Systems, Pergamon Press, New York, 1973, pp. 196-248.

37. J.M.T. Thompson and G.W. Hunt, A General Theory of Elastic Stability, J. Wiley & Sons, 1973.

38. F.W. Williams, "An Approach to the Nonlinear Behaviour of Members of a Rigid Jointed Plane Framework with Finite Deflections", Quart. J. Mech. Appl. Math., Vol. 17, No. 4, 1964, pp. 451-469.

39. R.D. Wood and O.C. Zienkiewicz, "Geometrically Nonlinear Finite Element Analysis of Beams, Frames, Arches, and Axisymmetric Shells", Comp. & Struct., Vol. 7, 1977, pp. 725-735.

40. D. Karamanlidis, A. Honecker, and K. Knothe, "Large Deflection Finite Element Analysis of Pre- and Post-Critical Response of Thin Elastic Frames" in Nonlinear Finite Element Analysis in Structural Mechanics (Eds: W. Wunderlich, E. Stein, and K.J. Bathe), Springer-Verlag, New York. 1981, pp. 217-235.

41. J. Roorda, "Stability of Structures with Small Imperfections", J. Engng. Mech. Div., Proc. ASCE, EM1, 1965, pp. 87-106.

42. W.T. Koiter, "Post-Buckling Analysis of a Simple Two-Bar Frame" in Recent Progress in Applied Mechanics, The Folke Odquist Volume (Eds: B. Broberg, J. Hult, and F. Niordson), Admquist & Wiksell, Stockholm, 1962, pp. 337-354.

43. J.H. Argyris and P.C. Dunne, "On the Application of the Natural Mode Technique to Small Strain Large Displacement Problems", Proc. World Congress on Finite Element Methods in Structural Mechanics, Bournemouth, England, 1975.

44. S.-L. Lee, F.S. Manuel, and E.C. Rossow, "Large Deflections and Stability of Elastic Frames", J. Engng. Mech. Div., Proc. ASCE, EM2, 1968, pp. 521-547.

45. A.N. Kerr, "Large Deflections of a Square Frame", Quart. J. Mech. Appl. Math., Vol. 17, 1964, pp. 23-38.